Permanent densification behaviors of various glasses by high-pressure treatments

宮宇地，晃一

博士論文

Permanent Densification Behaviors of Various Glasses

by High-Pressure Treatments

（超高圧印加による種々のガラスの永久高密度化挙動）

平成 15 年 1 月

神戸大学大学院自然科学研究科

宮宇地　晃一

Contents

General Introduction

It has been of interest what kinds of phenomena happen when pressure and/or temperature become extremely high and/or low because pressure as well as temperature is an important parameter that governs some natural phenomena. Pressure effect means a decrease of volume in other word and it is the effect that shortens the distances between molecules or atoms forming materials from the microscopic viewpoint. When the distances between molecules decrease, the changes of interaction and state of aggregation occur and then they are appeared as the structure, property, and changes of reactivity. Therefore, pressure effect helps us to reveal the state of aggregation and physical reactivity. It also can be available for the synthesis of new materials. The synthesis of diamond by high-pressure and high-temperature treatments is one of the famous examples.

The decrease of volume is accomplished by cooling, and it is said that the cooling to zero Kelvin is match for the compression under 1.2 GPa. However, the usage of high-pressure is significant because cooling accompanies not only the decreases of distance between molecules but also the change of the state of vibration. Needless to say, a high-pressure apparatus is needed to obtain the adequate pressure effects and the special techniques are required to generate high pressure. Many kinds of apparatuses are developed, improved, and used for various experiments [1–31]. These high-pressure apparatuses are divided into two different types, the one is an isostatic-type apparatus [1–25], and the other is a shock-wave-type apparatus, which is compressed by bombarding [26–31]. Bridgman made a development of the former type apparatus in the early days [1,3] and the apparatuses we use today are developed based on his design. Nowadays, the progress of high-pressure techniques has enabled us to carry out the

1

experiments under about half a million GPa [21–25]. The shock-wave method can generate the high-pressure of more than several million GPa [30,31], though it is an instantaneous compression.

The experimental and theoretical investigations of substances and/or materials under high-pressure were also undertaken by Bridgman [32]. So far, a number of data related to the compression rate of substance [33–37], the high-pressure phase [38–40], the structure of non-crystalline solids [41–46], transport phenomenon such as diffusion and electrical conduction [47–50], optical properties [51–56], magnetism [50,57–59], and mechanical properties [33,60,61] has been accumulated. In recent years, the experimental results in these fields are conspicuous with the progress of techniques of measurements under high pressure and the increase of the number of the researchers studying in the field.

The high-pressure experiments concerned with glasses have also reported in plenty until now. Bridgman and Simon made a first report in 1953 [62]. In the report, they systematically investigated the high-pressure effect on two simple oxide glasses such as SiO_2 and B_2O_3, and several silicate glasses by measuring the densities, dimensions, and X-ray diffraction patterns. In the study, disc-shaped glasses (diameter: 5 – 8 mm, thickness: 0.15 – 0.25 mm) were compressed by uniaxial-pressing at room temperature. The densities of compacted glasses increased by 6 – 8% with pressure treatment up to 10 – 20 GPa. This fact is now known as "permanent densification phenomenon of glass", which is observed only for glassy materials due to their structural freedom. They also investigated the thermal annealing effects of densified glasses and then determined the activation energies of thermal relaxation.

Cohen and Roy [63], on the other hand, investigated the applied pressure dependence of refractive index of SiO_2 glass, which was powdered sample with particle size of 40 – 80 µm. They obtained a quite different result from Bridgman and Simon

2

[62], that is, the rates of increase in densities in the powdered samples are larger than those of bulk samples, and the threshold pressure for permanent densification (plastic deformation) becomes low (bulk: ~10 GPa, powder: ~2 GPa). Furthermore, the increased refractive index by high-pressure treatment is stable and the decrease is observed by the thermal annealing at 600°C at atmospheric pressure. Afterward, Mackenzie [64], however, examined the pressure effects of densities of SiO_2 glass with a piston-cylinder-type high-pressure apparatus, which was a different type apparatus from Roy's. In the study, he confirmed the decrease of densities of densified glass due to thermal annealing and explained the several different results as follows. In the high-pressure treatments by Roy et al., the applied pressure was released during the heating treatment and then the temperature was returned to room temperature. In the result, the pressure effect became weak by annealing effect, therefore, no decrease of refractive index was observed on densified glass due to thermal annealing at atmospheric pressure. Afterward, Sakka and Mackenzie [65] made an experiment with the same high-pressure apparatus as Roy's, and obtained the similar results to Mackenzie's. From these investigations performed in the early years, it is widely known that the applied pressure should be released after the temperature is returned to room temperature.

Another important point, which we have to keep in mind when we investigate the high-pressure effects, is whether the generated pressure field is hydrostatic or not. That depends on the methods of compression. Generally, hydrostatic pressure field is obtained by using gases or liquids as a pressure-transmission medium [66–68], and non-hydrostatic pressure field, which is involved with share-stress, is obtained by using a solid substance such as powder as a pressure-transmission medium [62–64]. The rate of increase of densities compressed with non-hydrostatic pressure field is larger than that of hydrostatic pressure field, and, because of the share-stress, the local structure inside the glass has large distortion and results in fragile. Furthermore, because the difference

3

in the pressure field influences the density, structure, and physicochemical properties of glass, it is necessary to take it into account in discussion.

Many kinds of pressure effects such as densities [62–68], mechanical properties [60,61], optical properties [55,69–71], chemical properties [72–74], and the relaxation behavior due to thermal annealing [64,75–77] on densified glasses have been investigated so far. From these investigations, the permanent densification phenomenon of glass is of great interest from the viewpoint of glass technology because the physicochemical properties of glass can be changed largely without changing glass composition. The phenomenon is also of interest from the viewpoint of glass science because a part of changed structure is permanently kept even after removal of the applied pressure. The developments of high-pressure experimental methods have enabled us to investigate the structures of densified glasses and even those of the glasses under high pressures.

More recently, materials processing technology by using femtosecond laser irradiation has attracted tremendous interest from both the scientific and technological communities. In particular, the use of femtosecond laser processing to write three-dimensional structures in transparent materials is technologically attractive for applications such as optical waveguides [78,79]. The refractive index changes can be induced within various kinds of glasses such as silica, borate, phosphate, fluoride, and chalcogenide glasses, by irradiating the glass with femtosecond laser pulses [80]. Although the mechanism of change in refractive index has not been cleared yet, densification of materials by irradiating is considered to be one of the causes. Therefore, the elucidation of the mechanism of densification by high-pressure treatment is helpful and should be paid attention in order to clarify the irradiation effects in the materials.

Many kinds of studies on the structural analysis have been carried out for SiO_2 glass and two-components silicate glasses because of their simple compositions

4

and chemical stabilities. Raman scattering and infrared absorption are observed by the change of polarizability and the vibration and rotation of molecules, respectively. So these measurements are often used for investigating the glass structure because the combined state can be revealed by these spectra (several hundred to several thousand cm^{-1}). In the case of SiO_2 glass, whose structure has three-dimensional random structure composed of SiO_4 tetrahedra, the structural changes by applying high-pressure are revealed as follows by *in-situ* Raman scattering spectroscopy and *in-situ* infrared spectroscopy. At first, the Si–O–Si bond angle decreases, keeping the SiO_4 tetrahedron unit, with increasing the applied-pressure [42,44]. Then the ring-structures composed of 5 – 8 members SiO_4 tetrahedra change into smaller ring-structures composed of 3 – 4 members SiO_4 tetrahedra [42,81]. Further increasing applied pressure, the increase of O coordination number of Si from 4 to 5 – 6 occurs [82]. The threshold pressure of irreversible structural changes is around 8 GPa [82].

The number of studies for ionic glasses is not so many in comparison with the covalent glasses such as silicate glasses. Park and Uhlmann made an experiment on aluminate glass, which is an ionic glass and has less directional nature in the bonds between the constituent elements than silicate glasses. From the results, they reported that densification of glass is not affected by the difference in chemical bond [83]. Aasland et al. investigated the formation of fluorozirconate glasses under high pressures. In the study they made measurements of Raman scattering spectra and infrared spectra on fluorozirconate glasses under high pressure and reported that the F^- coordination number increases with increasing applied-pressure [84]. In general, the structure between the glass under high pressure and densified glass obtained by high-pressure treatment is different. However, it has not been investigated on ionic glasses such as fluorozirconate glasses in that viewpoint.

It has already passed about fifty years since the discovery of permanent

densification phenomenon of glass. However, the structural studies of densified glasses are limited to oxide glasses and the densification mechanism has not been clarified enough. In the present study, therefore, I investigate the permanent densification phenomenon of several glasses with different chemical structures. The objectives of this study are to discuss the densification behaviors in the viewpoint of chemical structures of glasses and to elucidate the mechanism of permanent densification of the respective glasses. Glasses employed in this study are fluoride, silicate, and chalcogenide glasses.

Fluorozirconate glass is one of the fluoride glasses and was discovered by Poulain et al. during an investigation of crystalline laser host materials in 1975 [85]. Since then, intensive researches have been carried out in order to examine the structure and properties of the glass. Fluorozirconate glass is highly ionic materials in the chemical bonds between constituent ions and the packing density is extremely high (~60%). The structural unit of the glass is ZrF_n ($n = 7 - 8$) polyhedron and these ZrF_n polyhedra construct three-dimensional random network structure. Recently, fluorozirconate glasses are paid much attention as a host glass for optical device because of their high efficiency of emission of rare-earth ions doped in glass matrix and their high refractive index.

Trap and Stevels have reported that some silicate systems such as the SiO_2–K_2O–CaO–SrO and SiO_2–K_2O–CaO–BaO systems are easily vitrified even in compositions below 50 mol% SiO_2 contents [86]. They demonstrated the dependences of physicochemical properties such as dielectric and mechanical losses, viscosity, and thermal expansion coefficient in these glasses. They presumed an inversion in the structure role of glass-network modifying cations around 50 mol% SiO_2 contents and they termed the silicate glasses containing less than 50 mol% SiO_2 contents as "invert glass". The conventional silicate glasses are characterized by a random network structure composed of SiO_4 tetrahedra, in the interstices of which a number of network

modifier ions are situated. The physicochemical properties of these glasses are mainly determined by the behavior of this network. However, with going to a rather low silica content, the coherence of these glasses and their physicochemical properties can no longer be determined by the spatial SiO_4 tetrahedra network, because of the short SiO_4 tetrahedra chains. The cations determine the behavior of the glass. Because these systems can be vitrified in wide composition ranges, the chemical bond between glass constituent ions can be changed widely.

Germanium disulfide, GeS_2, glass is one of the single component compounds which can be vitrified. Kawamoto and Tsuchihashi examined this Ge–S system glasses in 1969 for the first time [87]. In the study, they investigated the structures and physicochemical properties of this system with several techniques. The structure of GeS_2 glass is similar to that of SiO_2 glass, however, they are much different each other in the chemical bond between the glass constituent ions. That is, the chemical bond between Ge and S is strongly covalent compared to SiO_2 glass. Furthermore, the radius of glass constituent anion, S, is larger than that of O.

The present studies are concerned with the permanent densification phenomenon of various glasses with different chemical structures. The thesis consists of two parts. In Part I (Chapters from 1 to 4), I describe the investigations of peculiar high-pressure behavior in permanent densification, which was found for the first time in the present studies. In Part II (Chapters from 5 to 8), I examined the permanent densification behavior of GeS_2 glass by structural analyses using several spectroscopic methods. The contents of the respective chapters are as follows.

In Chapters 1 and 2, I describe the peculiar high-pressure behavior in permanent densification observed in fluorozirconate glasses. I examine the local structures around glass-constituent cations in the undensified and densifid fluorozirconate glasses by means of Raman scattering spectroscopy, Eu^{3+} fluorescence

spectroscopy, and EXAFS spectroscopy. Then I propose the mechanism of peculiar high-pressure behavior based on the results of the structural analyses.

In Chapter 3, I describe the permanent densification experiment in SiO_2–K_2O–CaO–SrO silicate glasses. At first, I clarify the structures of invert-composition glasses, whose structure has not been cleared yet, by ^{29}Si MAS NMR spectroscopy. Then I investigate the composition dependence of the densification behavior. Finally, I make an attempt to disclose the skeleton structure composed of SiO_4 tetrahedra in order to interpret of densification behavior on each glass.

In Chapter 4, I discuss the densification behavior of glasses having different chemical-bond properties and structures. For the discussion, I employ ionic ZrF_4-based fluoride glasses, mixed ionic and covalent SiO_2-based oxide glasses, and a covalent GeS_2 sulfide glass as densification experiments. The discussion of permanent densification phenomenon of glass from this standpoint is a first report.

In Chapters 5 and 6, I clarify the structure of densified GeS_2 glasses by means of Raman scattering spectroscopy, XAFS spectroscopy, and X-ray radial distribution analysis. I propose the densification mechanism based on the structures of GeS_2 polymorphous and structural-changes in GeS_2 glass with densification. I also discuss the change of the bandgap energy with densification.

In Chapter 7, I investigate the local structural-change around Ge in GeS_2 glass through compression and decompression processes, i.e., densification process, by an *in-situ* EXAFS method. I believe that investigating the structure of glass under high pressures is important for an elucidation of mechanism of permanent densification. From this measurement, I clarify the change of structural unit, GeS_4 tetrahedron, in GeS_2 glass through densification process.

In Chapter 8, I describe the thermal relaxation behavior of densified GeS_2 glass. The analyses of thermal relaxation give some information of densified glasses. I

clarify the presence of two types of relaxation processes, that is, the fast and slow processes, in the thermal relaxation in densified GeS_2 glass. Then, I estimate the activation energies of each relaxation process. I also examine the structural relaxation during both processes by the measurements of Raman scattering spectra and EXAFS spectra. Finally, I discuss the relationship between the red shift of visible absorption edge and the structural change through thermal relaxation.

References

[1] P. W. Bridgman, *Phys. Rev.*, **48**, 893 (1935).

[2] F. R. Boyd and J. L. England, *Year Book Carnegie Inst.*, **57**, 170 (1958).

[3] P. W. Bridgman, *Phys. Rev.*, **48**, 825 (1935).

[4] A. S. Balchan and H. G. Drickamer, *Rev. Sci. Instr.*, **32**, 308 (1961).

[5] A. Jayaraman, W. Klement Jr., R. C. Newton and G. C. Kennedy, *J. Phys. Chem. Solids*, **24**, 7 (1963).

[6] H. T. Hall, *Rev. Sci. Instr.*, **31**, 125 (1960).

[7] F. P. Bundy, *J. Chem. Phys.*, **38**, 631 (1963).

[8] W. B. Daniels and M. T. Jones, *Rev. Sci. Instr.*, **32**, 885 (1961).

[9] W. B. Wilson, *Rev. Sci. Instr.*, **31**, 331 (1960).

[10] H. T. Hall. *Rev. Sci. Instr.*, **29**, 267 (1958).

[11] H. T. Hall, *Rev. Sci. Instr.*, **33**, 1278 (1962).

[12] H. T. Hall, *Rev. Phys. Chem. Jpn*, **37**, 63 (1967).

[13] A. Zeitlin, *Mech. Eng.*, **83**, 37 (1961).

[14] E. C. Lloyd, U. O. Hutton and D. P. Johnson, *J. Res. Natl. Bur. Std.*, **63C**, 59 (1959).

[15] J. Osugi, K. Shimizu, K. Inoue and K. Yasunami, *Rev. Phys. Chem. Japan*, **34**, 1 (1964).

[16] K. F. Forsgren and H. G. Drickamer, *Rev. Sci. Instr.*, **36**, 1709 (1965).

[17] N. Kawai, M. Togaya and A. Onodera, *Proc. Jpn. Acad.*, **46**, 623 (1973).

[18] G. J. Piermarini and S. Block, *Rev. Sci. Instr.*, **46**, 973 (1973).

[19] G. Fasol and J. C. Schilling, *Rev. Sci. Instr.*, **49**, 1722 (1978).

[20] K. Syasen and W. B. Holzapfel, *Phys. Rev. B*, **18**, 5826 (1978).

[21] F. P. Buddy and K. J. Dunn, *Rev. Sci. Instr.*, **51**, 753 (1980).

[22] A. Jayaraman, *Rev. Modern Phys.*, **55**, 65 (1983).

[23] T. H. Lin and K. J. Dunn, *Phys. Rev. B*, **33**, 807 (1986).

[24] T. Yagi, W. Utsumi, M. Yamakawa and O. Shimomura, *Phys. Rev. B*, **46**, 6031 (1991).

[25] Y. Akahama, M. Kobayashi, H. Kawamura and S. Endo, *Rev. Sci. Instr.*, **64**, 1979 (1993).

[26] M. H. Rice, R. G. McQueen and J. M. Walsh, *Solid State Phys.*, **6**, 1 (1958).

[27] L. V. Altshuler, *Soviet Phys. – Uspekhi*, **8**, 52 (1965).

[28] R. G. McQueen, S. P. Marsh, J. W. Taylor, J. N. Fritz and W. J. Carter, *High velocity impact Phenomena*, 293, (1970).

[29] L. Davison and R. A. Graham, *Phys. Rep. (Phys. Lett. Sec. C)*, **55**, 256 (1979).

[30] E. N. Avrorin, B. K. Vodolaga, V. A. Simonenko and V. E. Fortov, *Soviet Phys. – Uspekhi*, **36**, 337 (1993).

[31] R. F. Trunin, *Soviet Phys. – Uspekhi*, **164**, 1215 (1994).

[32] P. W. Bridgman, in *"Collected Experimental Papers"*, (Harvard Univ. Press, Cambridge Ma., 1964), p. 1-7.

[33] P. W. Bridgman, in *"The Physics of High Pressure"*, (G. Bell & Sons, London, 1949), p. 149-188.

[34] C. A. Swenson, *Phys. Rev.*, **99**, 423 (1955).

[35] D. L. Decker, *J. Appl. Phys.*, **36**, 157 (1965); **37**, 5012 (1966).

[36] H. J. McSkimin, A. Jayaraman and P. Andreath Jr., *J. Appl. Phys.*, **38**, 2362 (1967).

[37] O. L. Anderson and P. Glynn, *J. Phys. Chem. Solids*, **26**, 1961 (1965).

[38] S. M. Stishov and S. V. Popova, *Geochemistry*, **10**, 923 (1961).

[39] K. F. Seifert, *Fortschr. Mineral.*, **45**, 214 (1968).

[40] H. Olojuyk and W. B. Holzapfel, *J. de Phys., Coll.*, **C8**, 153 (1884).

[41] J. Ferraro and M. Manghnani, *J. Appl. Phys.*, **43**, 4595 (1972).

[42] P. McMillan, B. Piriou and R. Couty, *J. Chem. Phys.*, **81**, 4234 (1984).

[43] D. P. Gosain, K. L. Bhatia, G. Parthasarathy and E. S. R. Gopal, *Phys. Rev. B*, **32**, 2727 (1985).

[44] B. Velde and R. Couty, *Chem. Geol.*, **62**, 35 (1987).

[45] C. Meade, R. J. Hemley and H. K. Mao, *Phys. Rev. Lett.*, **69**, 1387 (1992).

[46] N. Kitamura, K. Fukumi, H. Mizoguchi, M. Makihara, A. Higuchi, N. Ohino and T. Fukunaga, *J. Non-Cryst. Solids*, **274**, 244 (2000).

[47] P. W. Bridgman, *Proc. Am. Acad. Arts Sci.*, **81**, 165 (1952).

[48] W. Paul and D. M. Warschauer, *"Role of Pressure in Semiconductor Research"* in *"Solids under Pressure"*, (McGraw Hill, 1963), p. 179.

[49] J. Witting, *Z. Physik*, **195**, 228 (1966).

[50] J. S. Schillings, in *"Phys. Solids Under Press"*, (N. H. Pub., 1981), p. 345.

[51] H. L. Suchan, S. Wiederhorn and H. G. Drickamer, *J. Chem. Phys.*, **31**, 355 (1959).

[52] R. J. Swanson and G. E. Masek, *Rev. Sci. Instr.*, **32**, 212 (1961).

[53] H. K. Mao and P. M. Bell, *Science*, **200**, 1145 (1978).

[54] B. A. Weinstein, R. Zallen and M. L. Slade, *Phys. Rev. B*, **25**, 781 (1982).

[55] C. K. Jayasankar, P. Babu, Th. Tröster and W. B. Holzapfel, *J. Lumin.*, **91**, 33 (2000).

[56] A. Eiling, J. S. Schilling and H. Bach, in *"Physics of Solids Under Pressure"*, (Amsterdam, 1981), p. 385.

[57] S. Ramaseshan, G. Parthaarathy and E. S. R. Gopal, *J. Phys.*, **28**, 435 (1987).

[58] Y. A. Timofeev, *Instru. Experi. Tech.*, **35**, 900 (1992).

[59] M. H. Manghnani and W. M. Benzing, *J. Phys. Chem. Solids*, **30**, 2241 (1969).

[60] R. Ota and N. Soga, *J. Non-Cryst. Solids*, **56**, 105 (1983).

[61] M. P. Brassington, A. J. Miller and G. A. Saunders, *Phil. Mag. B*, **43**, 1049 (1981).

[62] P. W. Bridgman and I. Simon, *J. Appl. Phys.*, **24**, 405 (1953).

[63] H. M. Cohen and R. Roy, *J. Am. Ceram. Soc.*, **44**, 523 (1961).

[64] J. D. Mackenzie, *J. Am. Ceram. Soc.*, **46**, 461 (1961).

[65] S. Sakka and J. D. Mackenzie, *J. Non-Cryst. Solids*, **1**, 107 (1969).

[66] P. W. Bridgman, *Proc. Amer. Acad. Arts Sci.*, **84**, 111 (1955).

[67] J. A. Aboaf, *J. Am.Ceram. Soc.*, **46**, 296 (1963).

[68] H. M. Cohen and R. Roy, *J. Am. Ceram. Soc.*, **6**, 149 (1965).

[69] M. Fleet, C. Herzberg, G. Henderson, E. Crozier, M. Osborne and C. Scafe, *Geochim. Cosmochim. Acta*, **48**, 1455 (1984).

[70] A. Mierzejewski, G. Saunders, H. Sidek and B. Bridge, *J. Non-Cryst. Solids*, **104**, 323 (1988).

[71] C. H. Posky, K. H. Smith and G. H. Wolf, *J. Non-Cryst. Solids*, **248**, 159 (1999).

[72] D. Chakravorty and L. E. Cross, *J. Am. Ceram. Soc.*, **47**, 370 (1964).

[73] R. M. Biefeld, R. T. Johnson Jr. and R. J. Baughman, *J. Electrochem. Soc.*, **125**, 179 (1978).

[74] G. G. Wicks, W. C. Mosley, P. G. Whitkop and K. A. Saturday, *J. Non-Cryst. Solids*, **49**, 413 (1982).

[75] R. M. Kimmel and D. R. Uhlmann, *Phys. Chem. Glasses*, **10**, 12 (1969).

[76] J. Arndt, R. A. B. Devine and A. G. Revesz, *J. Non-Cryst. Solids*, **131-133**, 1206 (1991).

[77] N. Kitamura, K. Fukumi, M. Makihara and H. Yamashita, *Proc. Mat. Res. Soc. Symp.*, **407**, 179 (1996).

[78] K. Miura, J. Qiu, H. Inouye, T. Mitsuya and K. Hirao, *Appl. Phys. Lett.*, **71**, 3329 (1997).

[79] D. Homoelle, S. Wielandy and A. L. Gaeta, *Opt. Lett.*, **24**, 1311 (1999).

[80] K. M. Daivis, K. Miura, N. Sugimoto and K. Hirao, *Opt. Lett.*, **21**, 1729 (1996).

[81] Q. Williams and R. Jeanloz, *Science*, **239**, 902 (1988).

[82] R. Hemley, H. Mao, P. Bell and B. Mysen, *Phys. Rev. Lett.*, **57**, 747 (1986).

[83] J. R. Park and D. R. Uhlmann, *J. Non-cryst. Solids*, **7**, 438 (1970).

[84] S. Aasland, T. Grande, A. Grzechnik and P. F. McMillan, *J. Non-Cryst. Solids*, **195**, 180 (1996).

[85] M. Poulain, M. Poulain, J. Lucas and P. Brun, *Mat. Res. Bull.*, **10**, 243 (1975).

[86] H. J. L. trap and J. M. Stevel, *Glastechn. Ber.*, **32 K. VI**, 31 (1959).

[87] Y. Kawamoto and S. Tsuchihashi, *J. Am. Ceram. Soc.*, **52**, 626 (1969).

Part I

Peculiar High-Pressure Behavior in

Permanent Densification of Glass

Chapter 1

Peculiar High-Pressure Behavior in Permanent Densification of Fluorozirconate Glass

1.1. Introduction

In general, it has been well established that glasses subjected to high-pressure treatment undergo a significant increase in density that persists even after removal of the applied pressure. Bridgman and Simon demonstrated this permanent densification phenomenon of glass for the first time in 1953 [1]. Thus far this phenomenon has been investigated using various kinds of oxide and chalcogenide glasses [2,3]. These investigations have revealed that the permanent densification at a given temperature promotes with increasing applied-pressure, though the degree of densification is somewhat different, depending on both glass system and glass composition. The permanent densification of glass is of interest from the viewpoint of glass science because the change in glass structure is permanently kept. Also, it is of importance from the viewpoint of glass technology because the optical, electrical, mechanical, and magnetic properties of glass are largely changed without changing glass composition.

Heavy metal fluoride glasses (HMFG), which are represented by fluorozirconate glasses, have the following structural features: The chemical bonds

16

between glass-constituting cations and fluoride ions have extremely high ionic character. As a result, the packing densities of glass-constituting ions in HMFG reach about 65%, compared with 20 – 40% in oxide glasses. The permanent densification in HMFG is of much interest from the phenomenological point of view. Nevertheless, there have been no reports except for a study on "formation of fluorozirconate glasses under high pressures" [4]. However, even this study is not concerned with the permanent densification of fluorozirconate glasses.

In this chapter, a permanent densification experiment on a fluorozirconate glass is carried out and a peculiar behavior of permanent densification, which has not been observed in any other glasses so far, is reported.

1.2. Experimental Procedure

A fluorozirconate glass employed for the permanent densification experiment was a $60ZrF_4 \cdot 30BaF_2 \cdot 10EuF_3$ glass (ZBE glass). The glass was prepared from high-purity ZrF_4, BaF_2, and EuF_3 as starting materials. A batch of 5 g of the mixture with a small amount of $NH_4F \cdot HF$ added as a fluoridizing reagent was placed in a Pt crucible and melted at 450°C for 15min and then at 900°C for 15 min in an Ar gas atmosphere. The glass was obtained by pouring the melt into a brass mold maintained at about 200°C and then it was annealed at the glass-transition temperature for several hours. The obtained glass was cut into a plate of $8 \times 8 \times 2$ mm^3 in size.

The high-pressure and high-temperature treatment of the ZBE glass was carried out with a 6–8 multi-anvil-type high-pressure apparatus [5]. The sample was compressed up to desired high pressures, i.e., 1.5, 3.0, 4.5, 6.0, and 9.0 GPa, with a 0.033 GPa·min^{-1} ascending rate at room temperature. Then the sample was heated up to

250°C within 5 min under each pressure and then it was kept at this temperature for 30 min. After the heating treatment, the sample was cooled to room temperature within 5 min and then the applied pressure was released with a 0.033 GPa·min^{-1} descending rate.

Densities of the glasses were measured by the Archimedes method using CCl_4 as an immersion liquid.

Raman scattering measurements were performed in the wavenumber range of 250 – 1000 cm^{-1} at room temperature with a Perkin-Elmer 2000NIR FT-Raman spectrometer. A Nd:YAG laser ($\lambda_{emission}$ = 1064 nm) with 500 mW power was used as an excitation source.

Fluorescence spectra of Eu^{3+} were measured in the wavelength range of 570 – 670 nm at room temperature with a HITACHI F-3020 fluorescence spectrophotometer. The wavelength of excitation light was 395 nm of a Xe lamp.

1.3. Results and Discussion

1.3.1. Densities

In Figure 1.1, the densities of ZBE glasses before and after high-pressure treatment are plotted against the applied pressure, together with the experimental error bars. It can be seen from the figure that the density steeply increases with increasing applied-pressure up to 3.0 GPa, and shows a maximum value at 3.0 GPa, then gradually decreases with further increasing applied-pressure. Such a density variation with pressure is a very strange behavior, which has not been reported previously. In order to ascertain whether this strange behavior is due to a mistake in experimental procedures or not, the experiments were conducted several times. The observed density-pressure variations were almost the same as shown in Figure 1.1. Furthermore, no crystallization

was confirmed for the densified glasses in the X-ray diffraction measurements.
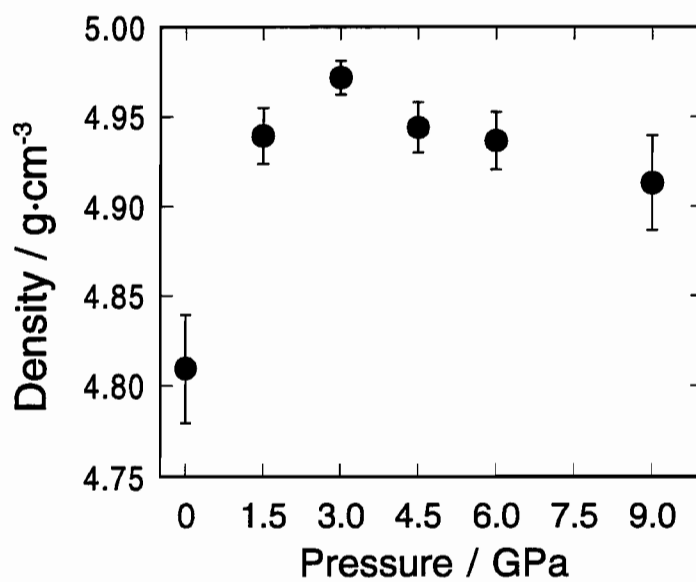
Figure 1.1   Pressure dependence of density of 60 $ZrF_4 \cdot 30BaF_2 \cdot 10EuF_3$ glass.

1.3.2. Raman Scattering Spectra

Figure 1.2 shows the Raman scattering spectra of the undensified and permanently densified ZBE glasses. The band at about 580 cm^{-1} is assigned to the totally symmetric stretching vibration of ZrF$_n$ polyhedra ($n = 7$ or 8) [6]. Figure 1.3 shows the pressure dependence of the peak position (the center of gravity in band area) of the bands. As can be seen from the figure, the peak position shifted linearly to lower energies up to 3.0 GPa with increasing applied-pressure. However, the peak positions are approximate the same values with further increasing applied-pressure. Aasland et al. [4] have mentioned that the low energy shift of the ~580cm^{-1} Raman band is due to an increase in the F$^-$ coordination number of Zr^{4+}. Therefore, the Raman band shift observed for permanently densified ZBE glasses indicates that, though the F$^-$ coordination number of Zr^{4+} increases up to 3.0 GPa, no subsequent increase in F$^-$ coordination number takes place in glasses densified under pressures above 3.0 GPa. However, an additional interpretation might be given. As the linkage manner of ZrF$_n$ polyhedra connection, there exists corner-sharing and edge-sharing [6]. Thus, the discontinuity at 3.0 GPa could be due to a change the linkage manner in ZrF$_n$ polyhedral connectivity.
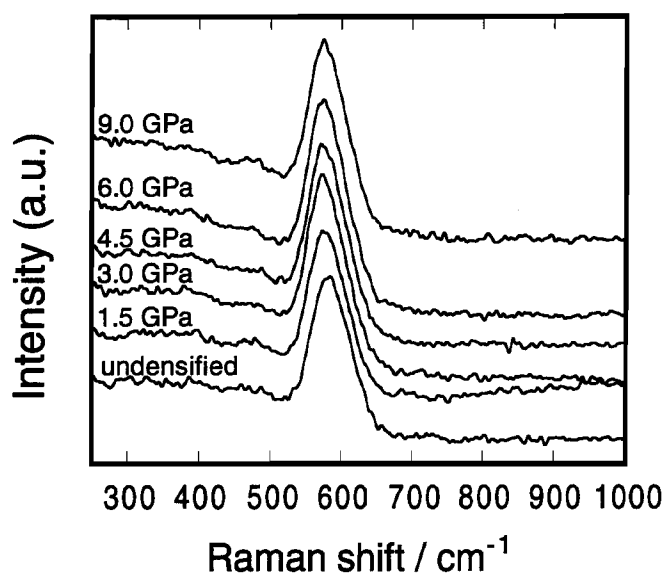
Figure 1.2   Raman scattering spectra of undensified and permanently densified 60 $ZrF_4 \cdot 30BaF_2 \cdot 10EuF_3$ glasses.
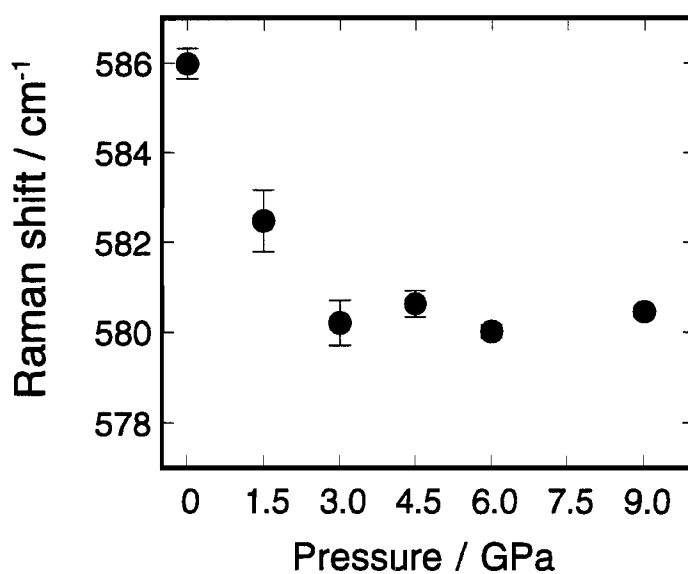
Figure 1.3   Pressure dependence of peak position of totally symmetric stretching vibration ZrF_n polyhedra ($n = 7$ or 8) in undensified and permanently densified 60 $ZrF_4 \cdot 30BaF_2 \cdot 10EuF_3$ glasses.

1.3.3. Fluorescence Spectra of Eu^{3+}

The Eu^{3+} fluorescence spectra of the undensified and permanently densified ZBE glasses are shown in Figure 1.4. In the spectra, the $^5D_0 \rightarrow {}^7F_J$ (J = 0, 1, and 2) bands give information about the F$^-$ coordination environments around Eu^{3+} [7,8]. The peak position and the full width at half maximum (FWHM) of the $^5D_0 \rightarrow {}^7F_0$ band give the F$^-$ ligand field strength for Eu^{3+} and the degree of a variety of Eu^{3+} sites, respectively. On the other hand, a ratio of the integrated intensity of the $^5D_0 \rightarrow {}^7F_2$ band to that of the $^5D_0 \rightarrow {}^7F_1$ band informs the degree of a deviation from inversion symmetry in the F$^-$ coordination around Eu^{3+}. As can be seen from the figure, the $^5D_1 \rightarrow {}^7F_3$ band overlaps the $^5D_0 \rightarrow {}^7F_J$ (J = 0, 1, and 2) bands. Therefore, the separation of the $^5D_1 \rightarrow {}^7F_3$ band from the $^5D_0 \rightarrow {}^7F_J$ bands was performed by curve fitting with a Gaussian-type function, as indicated in the figure. In Figure 1.5, the peak positions and the FWHM of the $^5D_0 \rightarrow {}^7F_0$ bands in the undensified and permanently densified ZBE glasses are plotted against applied pressure. The figure indicates that both the F$^-$ ligand field strength around Eu^{3+} and the degree of a variety of Eu^{3+} sites reach maximum values at about 3.0 GPa and become constant values above about 3.0 GPa. On the other hand, the degree of deviation from inversion symmetry in the F$^-$ coordination around Eu^{3+} increases monotonically with increasing applied-pressure, as shown in Figure 1.6. The increase in the F$^-$ ligand field strength around Eu^{3+} is probably due to an increase in the F$^-$ coordination number of Eu^{3+}, though there is no definitive evidence at present. To obtain information about the F$^-$ coordination environments around Eu^{3+} under high pressures, a molecular dynamics simulation has been performed. The result revealed that, when high pressures are applied to the ZBE glass, the Eu^{3+}–F$^-$ inter-ionic bond length barely changes, but the average F$^-$ coordination number of Eu^{3+} increases under high pressures. In high EuF$_3$ content of 10 mol%, Eu^{3+} may play an ambivalent role, i.e., that of a glass-forming ion and a glass-modifying ion. A change in the role under high

pressures might be related to the pressure dependence of Eu^{3+} fluorescence in Figures 1.5 and 1.6.
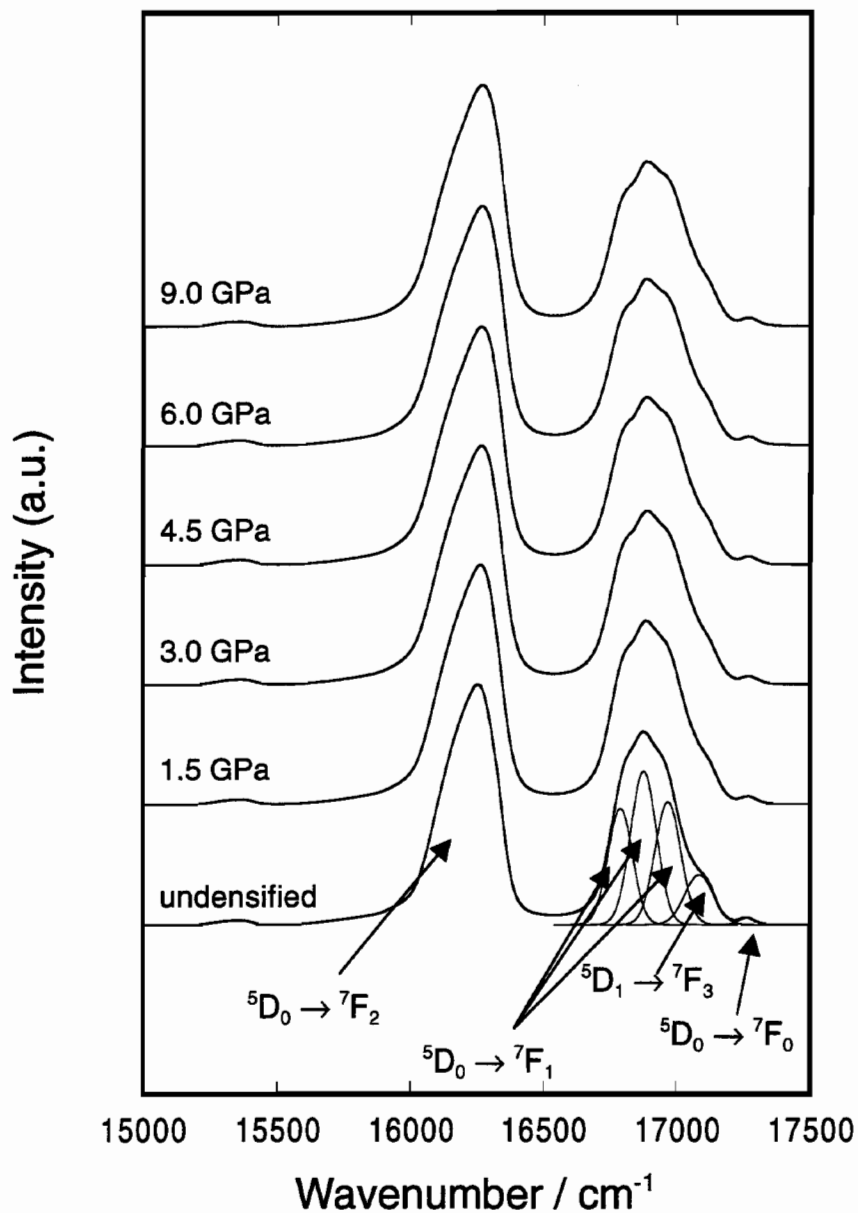
Figure 1.4   Fluorescence spectra of Eu^{3+} in undensified and permanently densified 60 $ZrF_4 \cdot 30BaF_2 \cdot 10EuF_3$ glasses.
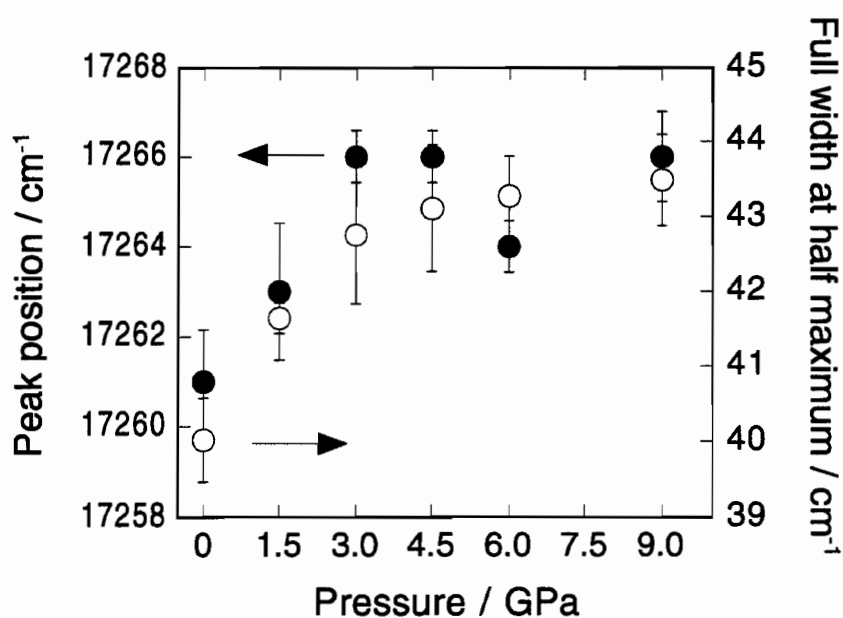
Figure 1.5 Peak positions (closed circles) and full width at half maximum (open circles) of $^5D_0 \rightarrow {}^7F_0$ bands in undensified and permanently densified 60 $ZrF_4 \cdot 30BaF_2 \cdot 10EuF_3$ glasses.
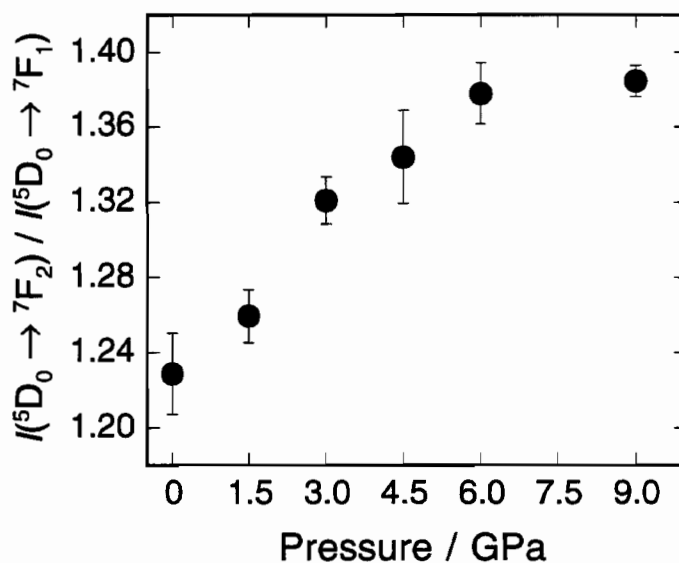
Figure 1.6 Degree of deviation from inversion symmetry in F^- coordination around Eu^{3+} in undensified and permanently densified 60 $ZrF_4 \cdot 30BaF_2 \cdot 10EuF_3$ glasses.

1.3.4. Mechanism of Peculiar Permanent Densification Behavior

The following is postulated to explain the peculiar pressure-density variation observed in permanently densified ZBE glass, namely, a maximum density at about 3.0 GPa and then a gradually decreased density above about 3.0 GPa. The schematic diagram in Figure 1.7 gives an interpretation, although speculative, for the peculiar pressure-density variation. Pressure dependences of the density of ZBE glass and the F^- coordination environments around Zr^{4+}, Eu^{3+}, and Ba^{2+} in the densified glass are depicted in this figure. In the diagram, solid lines represent the observed pressure dependences, broken lines represent the hypothetical pressure dependences, and a dotted line represents the pressure dependence that should be observed for Ba^{2+}. As can be seen from the figure, the densification for F^- coordination around Ba^{2+} exhibits a maximum value at about 3.0 GPa and progressively decreases above 3.0 GPa. By assuming such a densification behavior of the F^- coordination around Ba^{2+}, the permanent densification behavior observed for the ZBE glass may be explained. To ascertain the densification behavior assumed for the F^- coordination around Ba^{2+}, XAFS experiments of Ba^{2+} are planned.

The peculiar permanent densification behavior observed for the 60 $ZrF_4 \cdot 30BaF_2 \cdot 10EuF_3$ glass may be attributed to a spontaneous structural-relaxation of the F^- coordination environments around Zr^{4+}, Eu^{3+}, and Ba^{2+}, which takes place instantaneously when the applied pressure returns to atmospheric pressure. The fact that more than three-quarters of the glass volume are occupied by F^- and, therefore, the F^- coordination geometry is of major importance should be kept in mind.
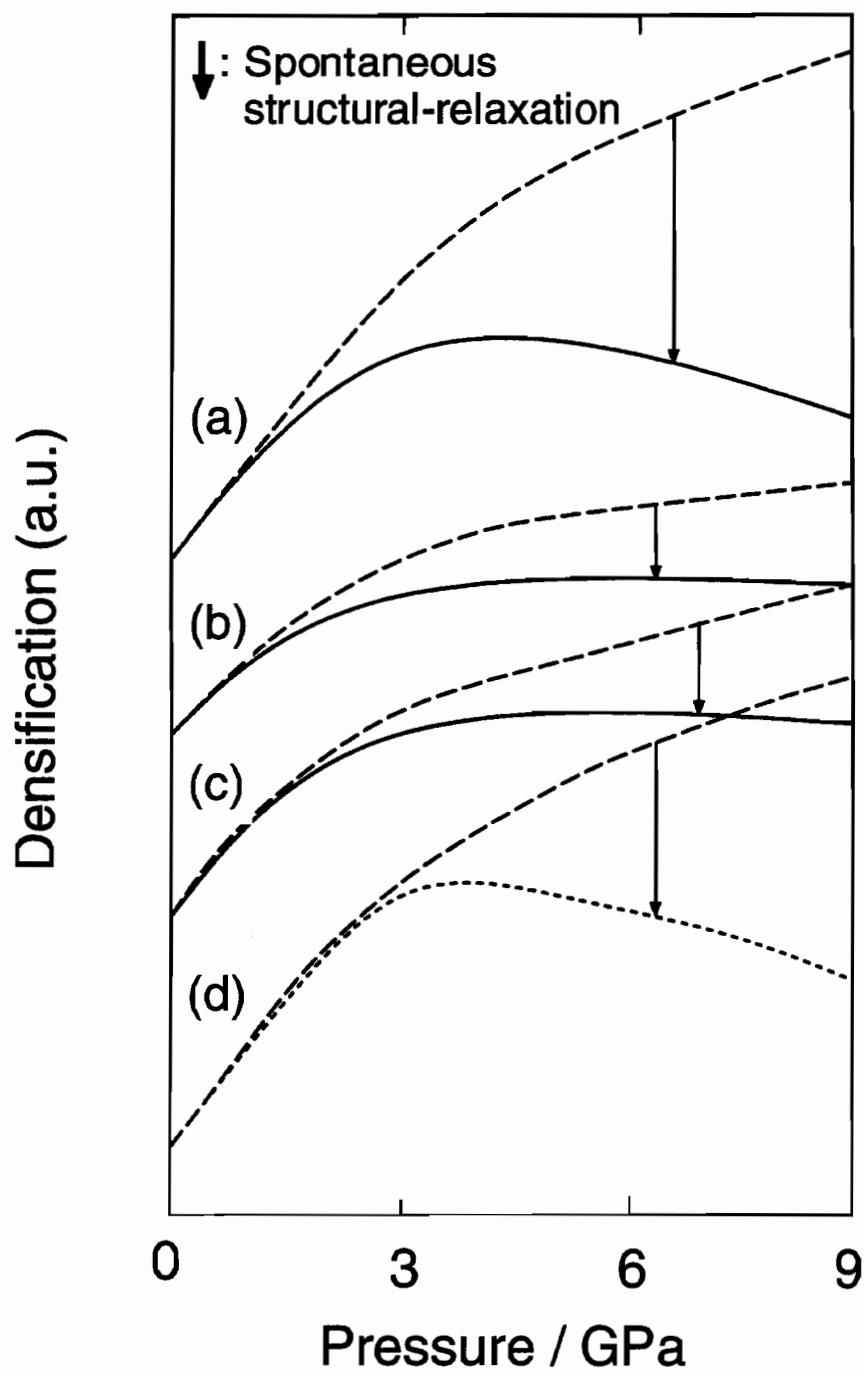
Figure 1.7   Schematic diagram showing pressure dependences of density of 60 $ZrF_4 \cdot 30BaF_2 \cdot 10EuF_3$ glass (a) and densification in F^- coordination around Zr^{4+} (b), Eu^{3+} (c), and Ba^{2+} (d) in the glass.

1.4. Conclusion

A $60ZrF_4 \cdot 30BaF_2 \cdot 10EuF_3$ glass was densified under 1.5, 3.0, 4.5, 6.0, and 9.0 GPa at 250°C with a 6–8 multi-anvil-type high-pressure apparatus. The densities of permanently densified ZBE glasses exhibit a maximum value at the 3.0 GPa treatment and then a marked decrease with increasing applied-pressure.

The local structural-changes around Zr^{4+} and Eu^{3+} ions were examined by means of Raman scattering spectroscopy and Eu^{3+} fluorescence spectroscopy.

In Raman scattering spectra, the peak position of totally symmetric stretching vibration of ZrF_n (n = 7 or 8) shifted linearly toward lower energies up to 3.0 GPa with increasing applied-pressure. Above 3.0 GPa, however, the peak positions are approximate a constant value. This fact indicates that the F^- coordination number around Zr^{4+} increases up to 3.0 GPa, and that the discontinuity in the change of ZrF_n polyhedron connectivity occurs at 3.0 GPa.

The Eu^{3+} fluorescence spectroscopy revealed the following facts: The F^- ligand field strength around Eu^{3+} and the degree of a variety of Eu^{3+} sites reach maximum values at about 3.0 GPa and become constant values above 3.0 GPa. An increase in F^- ligand field strength is due to an increase in the F^- coordination number around Eu^{3+}. The degree of deviation from inversion symmetry in the F^- coordination around Eu^{3+} monotonically increases with increasing applied-pressure.

The spontaneous structural-relaxation, which takes place when the applied pressure is released, is considered as a cause of a peculiar permanent densification behavior observed for a $60ZrF_4 \cdot 30BaF_2 \cdot 10EuF_3$ glass.

References

[1] P. W. Bridgman and I. Simon, *J. Appl. Phys.*, **24**, 405 (1953).

[2] S. Sakka and J. D. Mackenzie, *J. Non-Cryst. Solids*, **1**, 107 (1969).

[3] G. Parthasarathy and E. S. R. Gopal, *Bull. Mater. Sci.*, **3&4**, 271 (1985).

[4] S. Aasland, T. Grande, A. Grzechnik and P. F. McMillan, *J. Non-Cryst. Solids*, **195**, 180 (1996).

[5] N. Kawai, M. Togaya and A. Onodera, *Proc. Jpn. Acad.*, **49**, 623 (1973).

[6] Y. Kawamoto, T. Horisaka, K. Hirao and N. Soga, *J. Chem. Phys.*, **83**, 2398 (1985).

[7] P. K. Gallagher, C. R. Kurkjian and P. M. Bridenbaugh, *Phys. Chem. Glasses*, **6**, 95 (1965).

[8] G. Blasse, A. Bril and W. C. Nieuwpoort, *Phys. Chem. Solids*, **27**, 1587 (1965).

Chapter 2

Structural Study on Peculiar High-Pressure Behavior of Fluorozirconate Glass in Permanent Densification

2.1. Introduction

When glasses are treated under high pressures at ambient or high temperatures, significant increase in density is observed. The increase in density permanently remains even after removal of the applied pressure. Bridgman and Simon demonstrated this permanent densification of glass for the first time in 1953 [1]. Thus far, this phenomenon has been investigated on various kinds of oxide and chalcogenide glasses [2–5]. This phenomenon is of great interest from the viewpoint of both science and glass technology because the densified structure is permanently kept, and consequently the optical, electrical, mechanical, and magnetic properties of glass are largely changed without changing glass composition.

The permanent densification in heavy metal fluoride glasses is of great interest from the phenomenological point of view, since these glasses have a highly ionic bond character. Nevertheless, the study is limited to only one, that is, a formation of fluorozirconate (ZrF_4-based) glasses, which has been examined under high pressures [6]. Even this study, however, has not concerned with the permanent densification of

fluorozirconate glass. Recently the present author et al. found a peculiar high-pressure behavior in the permanent densification of a fluorozirconate glass of a $60ZrF_4 \cdot 30BaF_2 \cdot 10EuF_3$ composition in mol%, as described in Chapter 1. That is, the density of glass increased with applied pressure until exhibiting a maximum value around 3.0 GPa and then gradually decreased with further increasing applied-pressure [7]. In the study, it was postulated that the peculiar high-pressure behavior is attributed to the structural changes around a glass network-modifying Ba^{2+} ion during the release of applied pressure. Later, such a peculiar high-pressure behavior was found to occur more remarkably in a $55ZrF_4 \cdot 17BaF_2 \cdot 23NaF \cdot 5EuF_3$ fluorozirconate glass.

In the present study, therefore, the local structures around Zr^{4+}, Eu^{3+}, and Ba^{2+} in the $55ZrF_4 \cdot 17BaF_2 \cdot 23NaF \cdot 5EuF_3$ glass, permanently densified under high pressures up to 9.0 GPa, are examined by means of Raman scattering spectroscopy, Eu^{3+} fluorescence spectroscopy, and Zr–K, Eu–L_{III}, and Ba–L_{III} EXAFS spectroscopies. Then the structural-changes, which may be a cause of the peculiar high-pressure behavior in permanent densification, are clarified based on these experimental results.

2.2. Experimental Procedures

2.2.1. Sample Preparation

A $55ZrF_4 \cdot 17BaF_2 \cdot 23NaF \cdot 5EuF_3$ glass (ZBNE glass) in mol% was prepared by using high purity reagents of ZrF_4, BaF_2, NaF, and EuF_3 as starting materials. A 5-g batch of the starting materials was melted in a Pt crucible at 900°C for 15min in an Ar gas atmosphere. A small amount of a fluoridizing agent $NH_4F \cdot HF$ was added to the batch in order to remove residual water and also to convert very slight inclusions such as oxides and oxyfluorides into fluorides. The glass was obtained by pouring the melt

into a brass mold maintained at about 200°C and then annealed at the glass-transition temperature (250°C) determined by DTA. The prepared glass was cut into pieces of 8 × 8 × 2 mm^3 in size.

2.2.2. High-Pressure and High-Temperature Treatments

High-pressure and high-temperature treatments of the ZBNE glass were carried out with a 6–8 multi-anvil-type high-pressure apparatus [8] using a high-pressure cell, as shown in Figure 2.1. The ZBNE glass sample was wrapped with platinum foil and then embedded in powder of boron nitride, which works as a pressure-transmission medium. A platinum thin plate was used as a heater. The temperature was measured with a chromel-alumel thermocouple. The samples were compressed up to desired pressures, i.e., 1.5, 3.0, 4.5, 6.0, and 9.0 GPa, with a 0.033 GPa·min^{-1} ascending rate at room temperature. Subsequently, these glasses were heated up to 250°C within 5 min under each pressure and they were kept at this temperature for 30 min. After the heating treatment, the samples were cooled to room temperature within 5 min and then the applied pressure was released with a 0.033 GPa·min^{-1} descending rate.

2.2.3. Density Measurements

Densities of ZBNE glasses before and after high-pressure treatments were measured by the Archimedes method using CCl$_4$ as an immersion liquid. The experimental error in density measurements was about ±0.025 g·cm^{-3}.
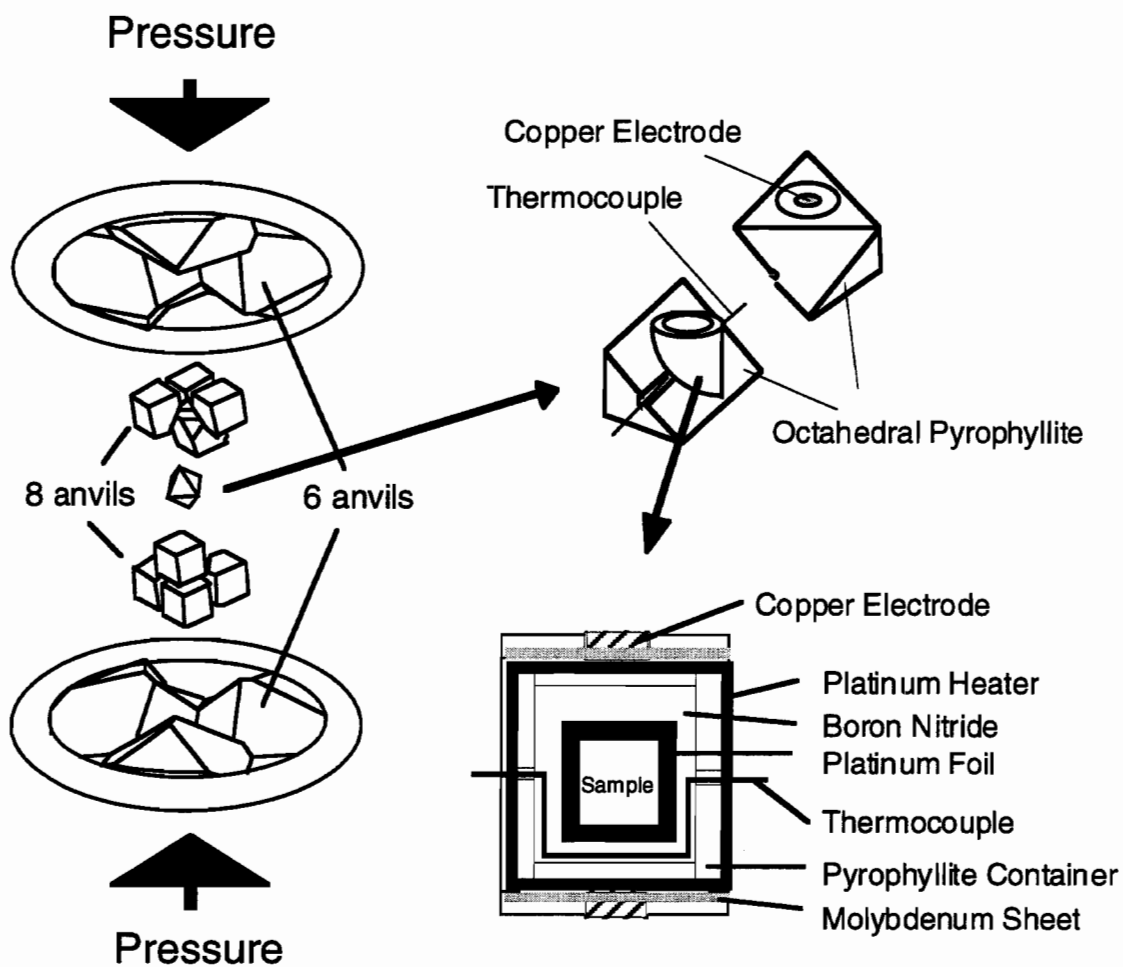
Figure 2.1 Schematic illustration of 6–8 multi-anvil-type high-pressure apparatus and high-pressure cell assembly.

2.2.4. Raman Scattering Measurements

Raman scattering spectra of the undensified and densified ZBNE glasses were measured in the wavenumber range of $250 - 1000$ cm^{-1} at room temperature with a Perkin-Elmer 2000NIR FT-Raman spectrometer. An Nd:YAG laser ($\lambda_{emission} = 1064$ nm) with 500 mW power was used as an excitation source.

2.2.5. Eu^{3+} Fluorescence Measurements

The fluorescence spectra of the $^5D_0 \rightarrow {}^7F_J$ ($J = 0$, 1, and 2) transitions of Eu^{3+} in the undensified and densified ZBE glasses were measured in the wavelength range of $570 - 670$ nm with a HITACHI F-3010 fluorescence spectrophotometer at room temperature. A 395 nm light of a Xe lamp was used as an excitation source.

2.2.6. $Zr–K$, $Eu–L_{III}$, and $Ba–L_{III}$ EXAFS Measurements

The EXAFS measurements in this work were performed under the approval of Photon Factory Program Advisory Committee (PF-PAC Proposal No. 97G046).

The measurements were carried out on the undensified and densified ZBNE glasses, and also on the β-$BaZrF_6$ and $EuZrF_7$ reference crystals, which were synthesized according to the procedures described in Refs. 9 and 10, respectively. For the measurements the undensified and densified glasses, and the synthesized β-$BaZrF_6$ and $EuZrF_7$ crystals were finely powdered under an Ar atmosphere in a glove box. These powders were thinly and homogeneously sandwiched between polyethylene thin films.

The EXAFS measurements of $Zr–K$, $Eu–L_{III}$, and $Ba–L_{III}$ were performed at BL-10B at Photon Factory in The National Laboratory for High Energy Physics (Tsukuba). The electron energy and the ring current of the storage ring were 2.5 GeV

and 250 – 400 mA, respectively. The monochromators of channel-cut Si(311) and Si(111) were used for Zr–K and for Eu–L_{III} and Ba–L_{III}, respectively. The incident and transmitted X-ray beam intensities were monitored by ionization chambers with flowing gases of 100% Ar and (75% N_2 + 25% Ar), 100% N_2 and 100% N_2, and (15% Ar + 85% N_2) and 100% N_2, respectively. The measurements were made at room temperature. The Zr–K, Eu–L_{III}, and Ba–L_{III} absorption data were collected in the energy ranges of 17 649 – 19049 eV, 6623 – 7603 eV, and 4897 – 5619 eV, respectively.

2.3. Results

2.3.1. Densities

Figure 2.2 shows the densities of undensified and densified ZBNE glasses, which were plotted against the applied pressures, together with the experimental error bars. In the figure, the previous result of a $60ZrF_4 \cdot 30BaF_2 \cdot 10EuF_3$ glass is also shown. It can be seen from the figure that the density increases with increasing applied-pressure until 3.0 GPa, shows a maximum value around 3.0 GPa, and then decreases with further increasing applied-pressure.
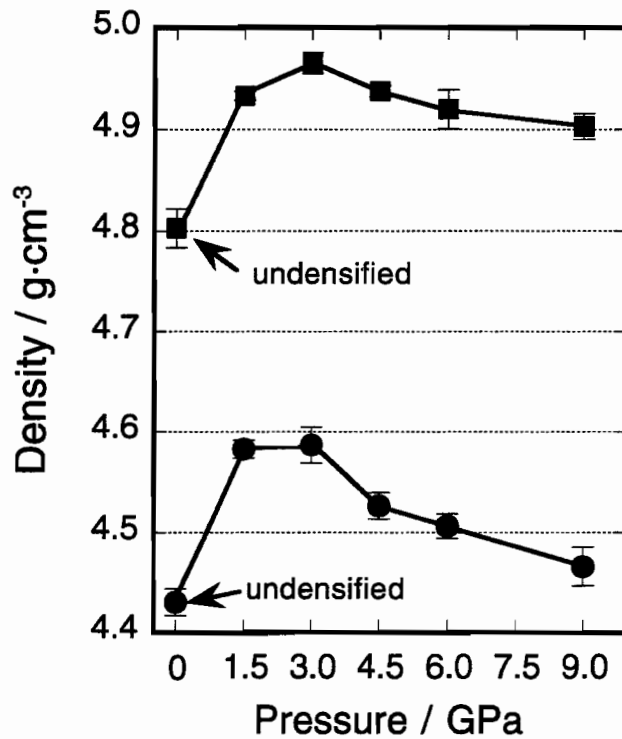
Figure 2.2   Pressure dependences of densities of permanently densified $55ZrF_4 \cdot 17BaF_2 \cdot 23NaF \cdot 5EuF_3$ (closed circles) and $60ZrF_4 \cdot 30BaF_2 \cdot 10EuF_3$ (closed squares) glasses. Lines are drawn between data symbols as guides for eyes.

2.3.2. Raman Scattering Spectra

Raman scattering spectra of the undensified and densified ZBNE glasses are shown in Figure 2.3. The peaks at about $580cm^{-1}$ are attributed to the totally symmetric stretching vibration of ZrF_n polyhedra ($n = 7$ or 8) [11]. In Figure 2.4, the peak positions (the center of gravity in peak area) are plotted against the applied pressure, together with the experimental error bars.
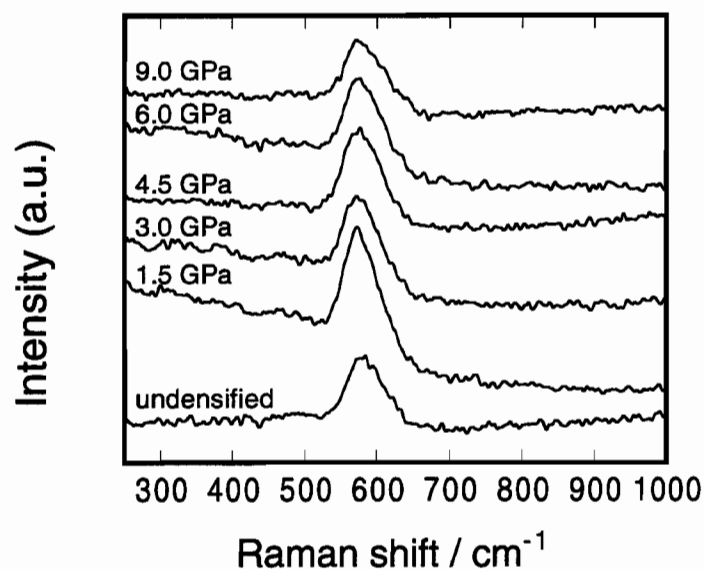
Figure 2.3   Raman   scattering   spectra   of   undensified   and   densified $55ZrF_4 \cdot 17BaF_2 \cdot 23NaF \cdot 5EuF_3$ glasses.
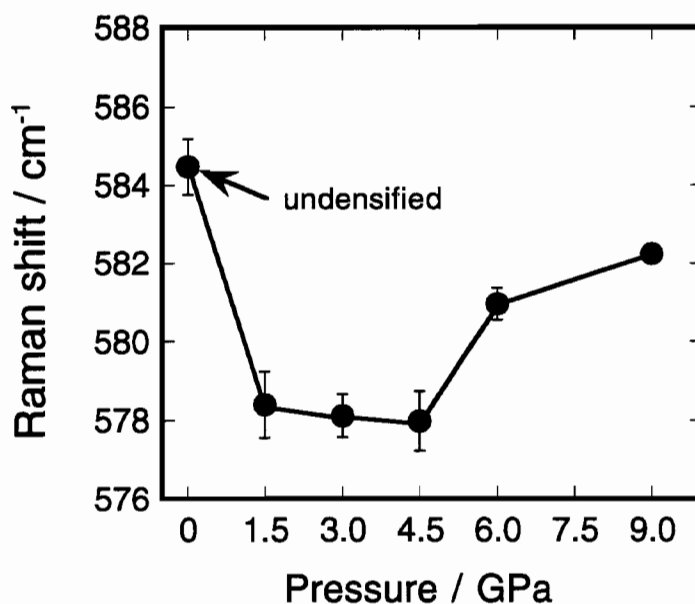
Figure 2.4   Pressure dependence of Raman peak positions of totally symmetric stretching vibration in undensified and densified $55ZrF_4 \cdot 17BaF_2 \cdot 23NaF \cdot 5EuF_3$ glasses. Line is drawn between data symbols as guide for eyes.

37

2.3.3. Fluorescence Spectra of Eu^{3+}

The Eu^{3+} fluorescence spectra of the undensified and densified ZBNE glasses are shown in Figure 2.5(a). As can be seen from the figure, $^5D_0 \rightarrow {}^7F_0$, $^5D_1 \rightarrow {}^7F_3$, and $^5D_0 \rightarrow {}^7F_1$ emission bands overlap each other. Thus, the deconvolution of each band was necessary in order to obtain the peak position and the full width at half maximum (FWHM) of $^5D_0 \rightarrow {}^7F_0$ emission and also to calculate the intensity ratio of the $^5D_0 \rightarrow {}^7F_2$ emission to the $^5D_0 \rightarrow {}^7F_1$ emission. The deconvolution was performed with a Gaussian-type function by using a curve-fitting program of the least squares method. As an example, the deconvolution features for the undensified glass are shown in Figure 2.5(b).

2.3.4. Zr–K, Eu–L$_{III}$, and Ba–L$_{III}$ EXAFS Analyses

The Zr–K, Eu–L$_{III}$, and Ba–L$_{III}$ EXAFS oscillation curves, $|f(k, \pi)|^{-1}|\chi(k)|$, of the undensified and densified ZBNE glasses are shown in Figure 2.6(a–c), together with those of the β-BaZrF$_6$ and EuZrF$_7$ reference crystals. The EXAFS data were analyzed by using a "Xanadu" program [12]. Detailed procedures of the data analyses are described in Chapter 7. The Fourier transform magnitude curves, $|\phi(r)|$, of the undensified and densified ZBNE glasses, which were obtained from EXAFS oscillation curves, are shown in Figure 2.7(a–c), together with those of the β-BaZrF$_6$ and EuZrF$_7$ reference crystals.

In Figure 2.8(a–c), the F$^-$ coordination environments around Zr^{4+}, Eu^{3+}, and Ba^{2+} (the Zr^{4+}–F$^-$, Eu^{3+}–F$^-$, and Ba^{2+}–F$^-$ bond lengths and the F$^-$ coordination numbers of Zr^{4+}, Eu^{3+}, and Ba^{2+}) in the respective glasses are plotted against the applied pressure, together with the experimental error bars.
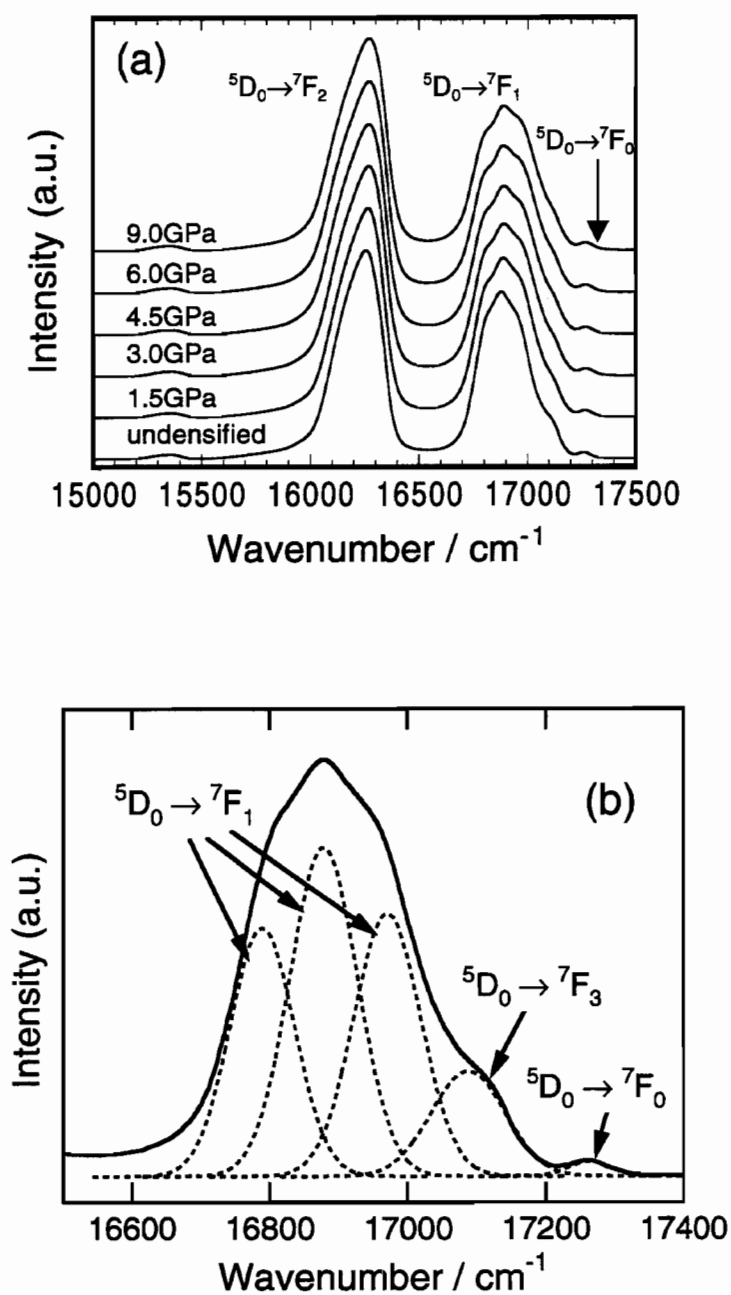
Figure 2.5 Eu^{3+} fluorescence spectra of undensified and densified $55ZrF_4 \cdot 17BaF_2 \cdot 23NaF \cdot 5EuF_3$ glasses (a) and deconvolution features of Eu^{3+} fluorescence spectrum of undensified glass (b).
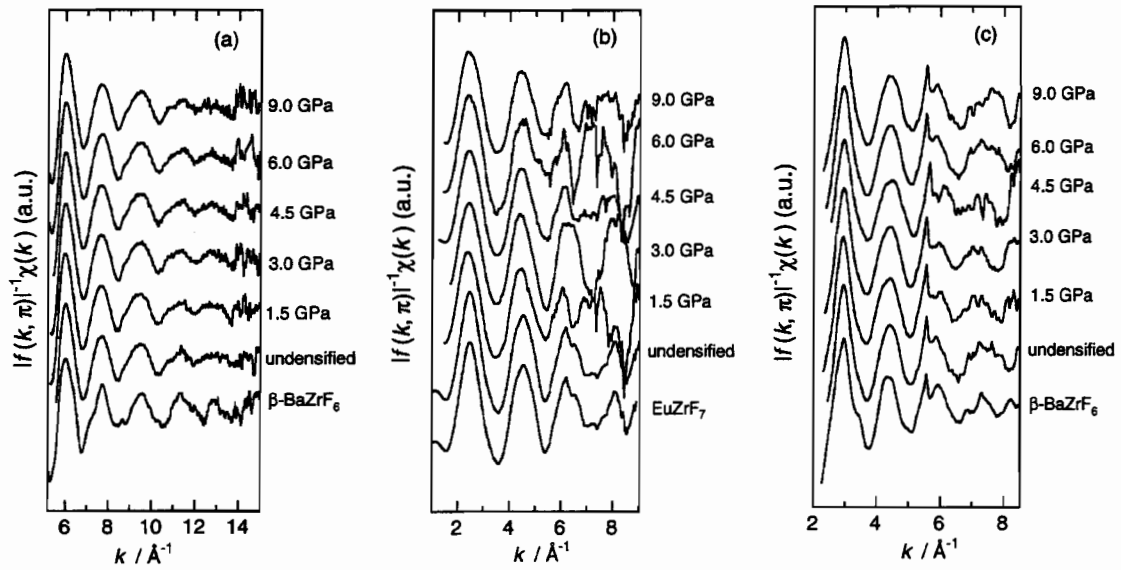
Figure 2.6 Zr–K (a), Eu–L$_{III}$ (b), and Ba–L$_{III}$ (c) EXAFS oscillation curves, $|f(k, \pi)^{-1}|\chi(k)$, of undensified and densified 55ZrF$_4$·17BaF$_2$·23NaF·5EuF$_3$ glasses, and β-BaZrF$_6$ and EuZrF$_7$ reference crystals.
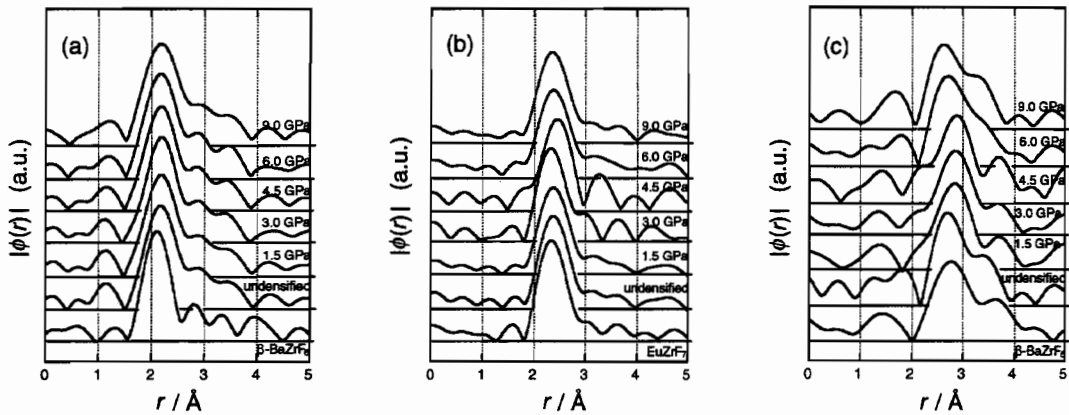
Figure 2.7 Fourier transform magnitude curves, $|\phi(r)|$, of Zr (a), Eu (b), and Ba(c) in undensified and densified 55ZrF$_4$·17BaF$_2$·23NaF·5EuF$_3$ glasses, and β-BaZrF$_6$ and EuZrF$_7$ reference crystals.
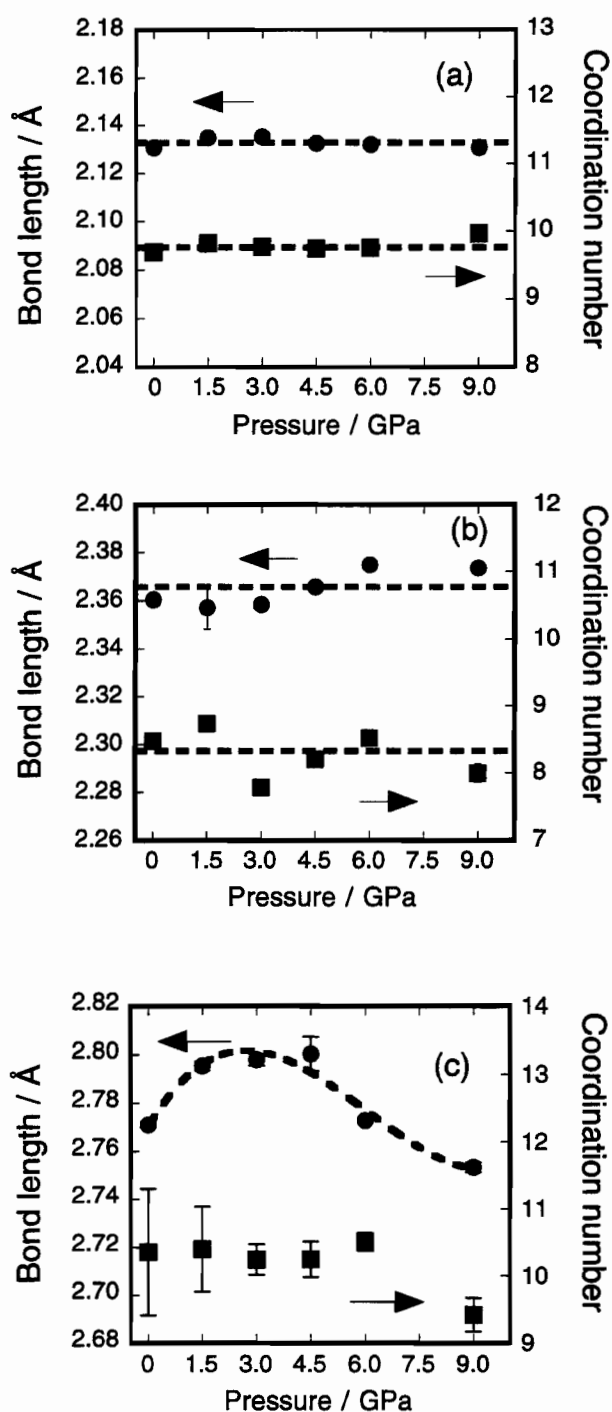
Figure 2.8   Pressure dependences of Zr^{4+}–F^- bond length and F^- coordination number of Zr^{4+} (a), Eu^{3+}–F^- bond length and F^- coordination number of Eu^{3+} (b), and Ba^{2+}–F^- bond length and F^- coordination number of Ba^{2+} (c) in undensified and densified $55ZrF_4 \cdot 17BaF_2 \cdot 23NaF \cdot 5EuF_3$ glasses, and β-$BaZrF_6$ and $EuZrF_7$ reference crystals. Lines are drawn as guides for eyes.

2.4. Discussion

2.4.1. Local Structural-Change around Zr^{4+}

The local structures around Zr^{4+} in the undensified and densified ZBNE glasses were examined by analyzing the totally symmetric stretching vibration peaks of Raman scattering spectra and the Zr–K EXAFS spectra. As can be seen from Figure 2.4, the positions of the totally symmetric stretching vibration peaks shifted toward lower energies with increasing applied-pressure until 3.0 – 4.5 GPa, exhibited a minimum value around these pressures and then gradually shifted toward higher energies with further increasing applied-pressure. The peak position of totally symmetric stretching vibration is related to the force constant between Zr^{4+} and F^-. Therefore, it is assumed that the energy shift of the peak position is due to a change in the Zr^{4+}–F^- bond length. As can be seen from Figure 2.8(a), the Zr^{4+}–F^- bond length shows a very slight increase (about 0.005 Å) in the pressure range of 1.5 – 4.5 GPa and then decreases beyond these pressures. The ionic radii of Zr^{4+} at ambient pressure are 0.86, 0.92, and 0.98 Å as the coordination number increases from 6 to 7 and 8, respectively; the ionic radius of F^- is considered to be constant (1.33 Å) [13]. If these values are referred to the present Zr–K EXAFS results, an increase of about 0.005 Å in the Zr^{4+}–F^- bond length corresponds to an increase of about 0.1 in the F^- coordination of Zr^{4+}, being almost negligible. Therefore, the pressure dependence of the peak position of totally symmetric stretching vibration implies that, in the glasses permanently densified under 1.5 – 4.5 GPa, glass network-modifying Ba^{2+} and Na^+ ions locate near the ZrF_n polyhedra, causing a very slight elongation of the Zr^{4+}–F^- bond length. As a result, a decrease in the force constant of the Zr^{4+}–F^- bond leads to a low energy shift of Raman peak. On the other hand, the Ba^{2+} and Na^+ ions in the glasses densified under pressures above 4.5 GPa become slightly more distant from the ZrF_n polyhedra, causing a recovery of the Zr^{4+}–F^- bond

42

length and a high energy shift of Raman peak.

2.4.2. Local Structural-Change around Eu^{3+}

The local structures around Eu^{3+} in the undensified and densified ZBNE glasses were examined by analyzing the Eu^{3+} fluorescence spectra and the $Eu-L_{III}$ EXAFS spectra. In the Eu^{3+} fluorescence spectra, the $^5D_0 \rightarrow {}^7F_J$ ($J = 0$, 1, and 2) peaks give information about the F^- coordination environments around Eu^{3+}. The ratio of the integrated intensity of the $^5D_0 \rightarrow {}^7F_2$ peak to that of the $^5D_0 \rightarrow {}^7F_1$ peak, $I(^5D_0 \rightarrow {}^7F_2)/I(^5D_0 \rightarrow {}^7F_1)$, informs the degree of the deviation from inversion symmetry in the F^- coordination around Eu^{3+} [14]. The pressure dependence of the $I(^5D_0 \rightarrow {}^7F_2)/I(^5D_0 \rightarrow {}^7F_1)$ value is shown in Figure 2.9, together with the experimental error bars. The $I(^5D_0 \rightarrow {}^7F_2)/I(^5D_0 \rightarrow {}^7F_1)$ value increased with applied pressure, indicating that the degree of a deviation from the inversion symmetry monotonously increases with pressure. On the other hand, the ligand field strength around Eu^{3+} and the inhomogeneous line-width of Eu^{3+} fluorescence can be estimated from the spectral profile of $^5D_0 \rightarrow {}^7F_0$ transition [15]. Peak position and full width at half maximum (FWHM) of the emission line of $^5D_0 \rightarrow {}^7F_0$ transition represent ligand field strength and inhomogeneous line-width, respectively. The pressure dependences of the position and FWHM of the $^5D_0 \rightarrow {}^7F_0$ emission peak are shown in Figure 2.10, together with the experimental error bars. The ligand field strength around Eu^{3+} increases with increasing applied-pressure until about 3.0 GPa and then exhibits a maximum value around 3.0 GPa. However, it decreases with further increasing applied-pressure. As can be seen from the figure, on the other hand, the FWHM of $^5D_0 \rightarrow {}^7F_0$ emission peak increases with applied pressure until 3.0 GPa and then becomes roughly constant with further increasing applied-pressure. This indicates that the degree of a variety of the Eu^{3+} site becomes constant around 3.0 GPa and keeps the constant value above 3.0 GPa. As can

be seen from Figure 2.8(b), however, changes in the Eu^{3+}–F^- bond length and the F^- coordination number of Eu^{3+} are within experimental errors, meaning that no definitive changes take place. Therefore, it is deduced that changes in the F^- coordination environments around Eu^{3+} may be some distortion of the F^- coordination polyhedra of Eu^{3+}.
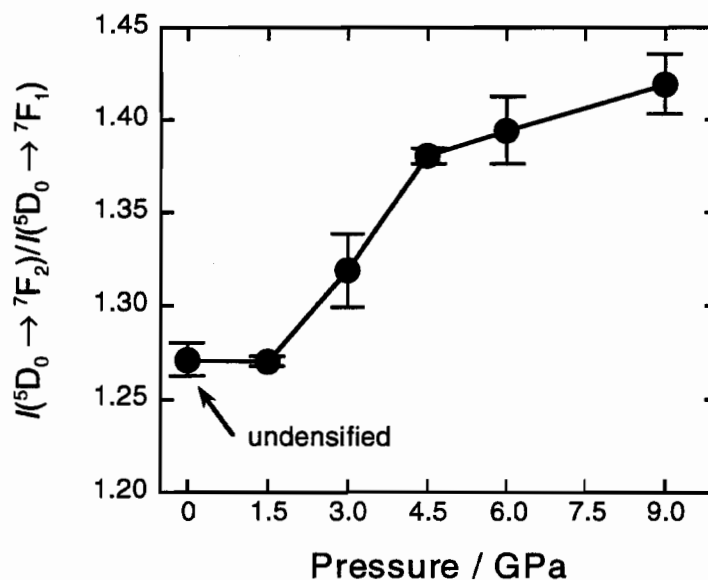
Figure 2.9 Pressure dependence of $(^5D_0 \rightarrow {}^7F_2)/(^5D_0 \rightarrow {}^7F_1)$ intensity ratio of Eu^{3+}, $I(^5D_0 \rightarrow {}^7F_2)/I(^5D_0 \rightarrow {}^7F_1)$, in in undensified and densified $55ZrF_4 \cdot 17BaF_2 \cdot 23NaF \cdot 5EuF_3$ glasses. Line is drawn between data symbols as guide for eyes.
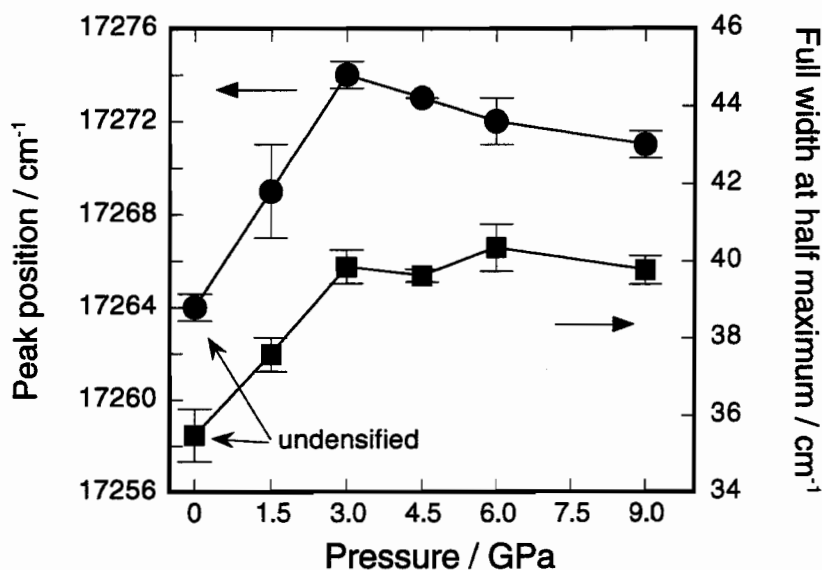
Figure 2.10 Pressure dependences of peak position (filled circles) and full width at half maximum (FWHM) (filled squares) of Eu^{3+}: $^5D_0 \rightarrow {}^7F_0$ emission peak in in undensified and densified $55ZrF_4 \cdot 17BaF_2 \cdot 23NaF \cdot 5EuF_3$ glasses. Lines are drawn between data symbols as guides for eyes.

2.4.3. Local Structural-Change around Ba^{2+}

The local structures around Ba^{2+} in the undensified and densified ZBNE glasses were revealed from Ba–L_{III} EXAFS spectra. As can be seen from Figure 2.8(c), the Ba^{2+}–F^- bond length largely changed with applied-pressure, compared with those of Zr^{4+} and Eu^{3+}. The Ba^{2+}–F^- bond length exhibited a remarkable increase of about 0.03 Å in the pressure range of 1.5 – 4.5 GPa and then a large decrease in the pressure range above 4.5 GPa. The ionic radii of Ba^{2+} at ambient pressure are 1.36, 1.42, 1.47, 1.52,

45

and 1.60, as the coordination number increases from 6 to 7, 8, 9, 10, and 12, respectively; the ionic radius of F^- is considered to be constant (1.33 Å) [13]. If these values are referred to the present Ba–L_{III} EXAFS results, an increase of about 0.03 Å in the Ba^{2+}–F^- bond length corresponds to an increase of on the average 0.5 – 0.6 in the F^- coordination of Ba^{2+}. It has been clarified that crystalline BaF_2 with a cubic fluorite-type structure at ambient pressure transforms to the orthorhombic cotunnite ($PbCl_2$) structure above 3.5 GPa, and then to the Ni_2In-type structure above 12 GPa. These high-pressure phases transformed by high pressure are quenchable at ambient pressure [16]. In the first- and second-phase transitions, the Ba^{2+}–F^- bond length increases (0.07 Å and 0.10 Å, respectively) and the F^- coordination number of Ba^{2+} increases from 8 to 9 and then 11, accompanying an increase in the density. The following fact should be noted here: In the present EXAFS result of the F^- coordination number of Ba^{2+}, no observation of the corresponding pressure dependence may be due to a difficulty in obtaining accurate coordination number in an EXAFS analysis. The reason is because $|\phi(r)|$ was so very wavy and heavily overlapped, as can be seen from Figure 2.7(c).

In order to investigate the local structure around Na^+ in the undensified and densified ZBNE glasses, the Na–K EXAFS measurements were performed. The EXAFS spectra, however, overlapped with Eu–M_v EXAFS oscillation. Regrettably, therefore, no information about the local structures around Na^+ was obtained.

2.4.4. Mechanism of Peculiar Permanent Densification Behavior

From a comparison of the local environments of Zr^{4+}, Eu^{3+}, and Ba^{2+} ions in the present ZBNE glasses, the local structures around a glass network-modifying Ba^{2+} ion are more influenced by high-pressure treatments than glass network-forming Zr^{4+} and Eu^{3+} ions. Therefore, the peculiar densification behavior observed for the ZBNE

glass may be attributed to the structural changes around glass network-modifying Ba^{2+} and Na^+ ions. That is, the following facts may be speculated. When high pressures are applied to the ZBNE glass, changes in the F^- coordination environments around Zr^{4+}, Eu^{3+}, Ba^{2+}, and Na^+, and also the distortion of ZrF_n and EuF_n polyhedra occur at the same time. Consequently, the *in-situ* densities are increased. As soon as the applied pressures are released, however, a recovery of the F^- coordination environments around Zr^{4+} and Eu^{3+} and the distortion of ZrF_n and EuF_n polyhedra take place somewhat. However, the structural relaxation in the F^- local structures around Ba^{2+} and Na^+ largely occurs, and consequently, the densities are remarkably decreased. In such a case, the driving force of relaxation is proportional to the magnitude of applied pressure in densification, so that the glasses treated under high pressures relax in higher magnitude than those treated under lower pressures. As a result, a peculiar high-pressure behavior in permanent densification is observed.

In closing, the following is mention. Tamai and Kawamoto [17–19] have performed molecular dynamics (MD) simulation studies on the permanent densification of a ZBNE glass. A peculiar high-pressure behavior observed for the real ZBNE glass has been satisfactorily reproduced. From the MD simulation analyses, a mechanism of a peculiar high-pressure behavior has been clarified on an atomic scale. For example, changes in the F^- coordination environments around Zr^{4+}, Eu^{3+}, Ba^{2+}, and Na^+ ions and the connectivity of glass network-forming ZrF_n and EuF_n polyhedra with compression and decompression processes have been examined in detail. Consequently, the same mechanism as that mentioned in the present discussion has been proposed.

2.5. Conclusion

A $55ZrF_4 \cdot 17BaF_2 \cdot 23NaF \cdot 5EuF_3$ glass was densified under 1.5, 3.0, 4.5, 6.0, and 9.0 GPa at 280°C with a 6–8 multi-anvil-type high-pressure apparatus. The densities of permanently densified glasses increased until 3.0 GPa, reached a maximum value around 3.0 GPa, and then decreased with further increasing applied-pressure.

The local structures around Zr^{4+}, Eu^{3+}, and Ba^{2+} ions of the undensified and permanently densified glasses were examined by means of Raman scattering spectroscopy, Eu^{3+} fluorescence spectroscopy, and Zr–K, Eu–L_{III}, and Ba–L_{III} EXAFS spectroscopies.

In Raman scattering spectra, the peak position of totally symmetric stretching vibration of ZrF_n (n = 7 or 8) polyhedra shifts toward lower energies with increasing applied-pressure. This fact indicates that the force constant of Zr^{4+}–F^- bond decreases because of a slight elongation of the Zr^{4+}–F^- bond length. The Eu^{3+} fluorescence spectroscopy revealed the following three facts: (1) The degree of a deviation from the inversion symmetry in EuF_n polyhedra monotonously increases with pressure. (2) The ligand field strength around Eu^{3+} increases with increasing pressure until 3.0 GPa and then decreases with further increasing applied-pressure. (3) The degree of a variety of Eu^{3+} site reaches a maximum around 3.0 GPa and becomes constant above about 3.0 GPa.

The Zr–K and Ba–L_{III} EXAFS analyses gave a fact that the F^- coordination environment around Ba^{2+} exhibits a very large change in the pressure range of 1.5 – 4.5 GPa and that around ZrF^{4+} exhibits a slight change with densification.

As a cause of a peculiar high-pressure behavior observed in the $55ZrF_4 \cdot 17BaF_2 \cdot 23NaF \cdot 5EuF_3$ glass, a spontaneous structural relaxation in the F^- coordination environments around Ba^{2+} while releasing applied-pressure is considered.

48

References

[1] P. W. Bridgman and I. Simon, *J. Appl. Phys.*, **24**, 405 (1953).

[2] H. M. Cohen and R. Roy, *J. Am. Ceram. Soc.*, **44**, 523 (1961).

[3] J. D. Mackenzie, *J. Am. Ceram. Soc.*, **46**, 461 (1963).

[4] S. Sakka and J. D. Mackenzie, *J. Non-Cryst. Solids*, **1**, 107 (1969).

[5] G. Parthasarathy and E. S. R. Gopal, *Bull. Mater. Sci.*, **3&4**, 271 (1985).

[6] S. Aasland, T. Grande, A. Grzechnik and P. E. McMillan, *J. Non-Cryst. Solids*, **195**, 180 (1996).

[7] K. Miyauchi, J. Qiu, M Shojiya, Y. Kawamoto and N. Kitamura, *Mater. Res. Bull.*, **34**, 1383 (1999).

[8] N. Kawai, M. Togaya and A. Onodera, *Proc. Jpn. Acad.*, **46**, 623 (1973).

[9] B. Mehlhorn and R. Hoppe, *Z. anorg. allg. Chem.*, **425**, 180 (1976).

[10] M. Poulain, M. Poulain and J. Lucas, *J. Solid State Chem.*, **8**, 132 (1973).

[11] Y. Kawamoto, T. Hoshisaka, K. Hirao and N. Soga, *J. Chem. Phys.*, **83**, 2398 (1985).

[12] H. Sakane, T. Miyanaga, I. Watanabe, N. Matsubayashi, S. Ikeda and Y. Yokoyama, *Jpn. J. Appl. Phys.*, **32**, 4641 (1993).

[13] R. D. Shannon and C. T. Prewitt, *Acta Crystallogr.*, **B25**, 925 (1969).

[14] P. K. Gallagher, C. R. Kurkjian and P. M. Bridenbaugh, *Phys. Chem. Glasses*, **6**, 95 (1965).

[15] N. Motegi and S. Shionoya, *J. Lumin.*, **8**, 1 (1973).

[16] J. M. Leger, J. Haines, A. Atouf and O. Schulte, *Phys. Rev. B*, **52**, 13247 (1995).

[17] Y. Tamai and Y. Kawamoto, *Chem. Phys. Lett.*, **302**, 15 (1999).

[18] Y. Tamai and Y. Kawamoto, *J. Chem. Phys.*, **112**, 3875 (2000).

[19] Y. Tamai and Y. Kawamoto, *Phys. Rev. B*, **62**, 865 (2000).

Chapter 3

Permanent Densification Behavior and ^{29}Si MAS NMR of SiO$_2$–K$_2$O–CaO–SrO Glasses

3.1. Introduction

Trap and Stevels [1] have reported that some silicate systems such as the SiO$_2$–K$_2$O–CaO–SrO and SiO$_2$–K$_2$O–CaO–BaO systems are easily vitrified even in compositions below 50 mol% SiO$_2$. They have demonstrated that, in these glasses, the dependences of physicochemical properties such as dielectric and mechanical losses, viscosity, and thermal expansion coefficient on the SiO$_2$-content reverse in going across the 50 mol% SiO$_2$ composition. They have presumed an inversion in the structural role of glass network modifying cations around about 50 mol% SiO$_2$ and termed the silicate glasses containing less than 50 mol% SiO$_2$ as an 'invert glass' [1]. According to their argument, glass network modifying cations in compositions above 50 mol% break glass-network composed of SiO$_4$ tetrahedra, while the cations in compositions below 50 mol% SiO$_2$ stabilize the glass structure by ionic bonds between glass network modifying cations and anions composed of small group of an SiO$_4$ tetrahedron. Although Trap and Stevels have proposed a schematic structure-model of such an 'invert glass', no structural studies of the invert glasses have been performed so far.

In the permanent densification study of xSiO$_2$·0.4(100 − x)K$_2$O·0.4(100 − x)CaO·0.2(100 − x)SrO glasses (x = 42.1, 47.1, 50.0, 57.1, and 66.7) in mol%, more

50

recently, the present author et al. found a peculiar behavior for the glasses of x below 50.

[29]Si magic angle spinning (MAS) NMR spectroscopy for silicate glasses is an appropriate method to reveal the local structures around a Si nucleus. That is, five types of SiO_4 tetrahedra with the bridging-oxygen number n, Q_n ($n = 0 - 4$), can be discriminated from the isotropic chemical shifts and, moreover, the Q_n fractions can be estimated from the respective peak areas. Owing to these advantages the structures of many silicate glasses have been studied. For example, binary alkali-silicate glasses have been examined by this technique by Maekawa et al. [2] and Grimmer et al. [3].

In the present work, ^{29}Si MAS NMR spectra are measured for undensified $xSiO_2 \cdot 0.4(100 - x)K_2O \cdot 0.4(100 - x)CaO \cdot 0.2(100 - x)SrO$ glasses ($x = 41.2 - 66.7$) in mol% and the glasses of $x = 42.1, 47.1$, and 57.1, which were permanently densified under 3 and 6 GPa. At first, the skeleton structures composed of SiO_4 units in the undensified glasses are discussed and then the structures of the densified glasses are discussed in comparison of those of the undensified glasses. The present glasses are easily vitrified even in $x = 41.2$ and also are not hygroscopic, so that the NMR data are probably more reliable than those of Na_2O-SiO_2 glasses which are hygroscopic in compositions with low SiO_2 contents. On the other hand, ^{29}Si MAS NMR studies of permanently densified silicate-glasses have not been performed so far to our knowledge.

3.2. Experimental Procedures

3.2.1. Glass Preparation

Glasses prepared in the present study have the compositions of xSiO$_2$·0.4(100 $- x$)K$_2$O·0.4(100 $- x$)CaO·0.2(100 $- x$)SrO, where the x values are 41.2, 42.1, 43.0, 44.4, 47.1, 50.0, 57.1, and 66.7 and the molar ratio of K$_2$O:CaO:SrO is fixed to 2:2:1.

Trap and Stevels [1] introduced a parameter 'Y' that means the average number of bridging-oxygen ions per a SiO$_4$ tetrahedron. The parameter Y can be calculated from

$$Y = 6 - 200 / x \qquad (3.1)$$

where x is SiO$_2$ mol%. Equation 3.1 means that the Y is independent of the kinds of the glass network modifying ions. In the prepared glasses, the x-values of 41.2, 42.1, 43.0, 44.4, 47.1, 50.0, 57.1, and 66.7 correspond to the Y-values of 1.15, 1.25, 1.35, 1.5, 1.75, 2.0, 2.5, and 3.0, respectively. Hereafter, therefore, these glasses are abbreviated as the 1.15, 1.25, 1.35, 1.5, 1.75, 2.0, 2.5, and 3.0 glasses by using their Y-values.

In the present glasses, 0.2 mol% Fe$_2$O$_3$ was added in order to shorten the relaxation time of a Si nucleus with $I = 1/2$. Reagent-grade SiO$_2$, K$_2$O$_3$, CaCO$_3$, SrCO$_3$, and Fe$_2$O$_3$ were used as starting materials. The 4-g batches of well-mixed reagents were heated in a 95%Pt–5%Rh crucibles at 750°C for 15 min and then melted at 1400 – 1550°C for 1 h. The melts were quenched by immersing the bottom of the crucible into ice water. All the prepared glasses were annealed at the respective glass-transition temperatures for 5 h.

3.2.2. Permanent Densification Treatments

Permanent densification treatments of the 1.25, 1.75, 2.0, 2.5, and 3.0 glasses were carried out with a 6–8 multi-anvil-type high-pressure apparatus [4]. The procedure is the followings: At first the glasses were compressed up to desired high pressures, i.e. 3 and 6 GPa, with a 0.033 GPa·min^{-1} ascending rate at room temperature. Then these glasses were heated up to temperatures of three-quarters of the glass-transition temperatures in Kelvin within 5 min under each pressure. Then these glasses were kept at these temperatures for 30 min. After the heating treatment the glasses were cooled to room temperature and then the applied pressures were released with a 0.033 GPa·min^{-1} descending rate.

3.2.3. Density Measurements

Densities of the undensified and densified glasses were measured by the Archimedes method using CCl$_4$ as an immersion liquid. The experimental error in density measurements was about ±0.005 g·cm^{-3}.

3.2.4. NMR Measurements

^{29}Si MAS NMR spectra were measured on powder glasses at 79.463 MHz (9.4 T) with a Varian UNITY INOVA 400 MAS FT-NMR spectrometer. A single pulse sequence was used; a pulse length of 5 μs, the accumulation of 1000 – 4000 scans and a pulse delay of 1.0 s. A cylindrical zirconia rotor in which a glass sample was put was rated at a speed of about 5 – 6 kHz. Polydimethylsilane was used as a secondary standard whose chemical shift was $\delta = -34.5$ ppm from TMS.

3.3. Results

3.3.1. Densities

The densities of undensified and densified 1.25, 1.75, 2.0, 2.5, and 3.0 glasses are shown in Figure 3.1. The densities of the 2.5 and 3.0 glasses increased with increasing applied-pressure, while the 1.25, 1.75, and 2.0 glasses exhibited the maximum values at 3 GPa and then gave the decreased values at 6 GPa. The permanent densification behaviors observed for the latter glasses are peculiar and observed here for the first time for silicate glasses to the best of our knowledge. These behaviors are assumed to result from the structural characteristics of these glasses.

3.3.2. NMR Spectra

Figure 3.2 shows the ^{29}Si MAS NMR spectra of the undensified 1.15, 1.25, 1.35, 1.5, 1.75, 2.0, 2.5, and 3.0 glasses. All the spectra consist of one broad peak with no splitting in the range from –60 to –110 ppm. The peak positions shifted to higher magnetic field with increasing Y-value (increasing SiO_2-content).

All the spectra were satisfactorily reproduced by three to five peaks with Gaussian functions. Peak deconvolution for the 1.15 and 3.0 glasses are shown in Figure 3.3. The fractions of structural units were estimated from the areas of the respective peaks. The results of peak separation are given in Table 3.1. For the 1.15, 1.25, and 1.35 glasses the peak deconvolution of Q_2 was performed by assuming that the Q_2 consists of different two types of Q_2' and Q_2'', since the spectra of these glasses were not successfully reproduced by using only one Gaussian curve of Q_2. As can be seen from the Table 3.1, the isotropic chemical shifts δ_{iso} of Q_0, Q_1, Q_2', Q_2'', Q_3, and Q_4 are hardly shifted with Y-value. This fact suggests that each SiO_4 unit in the glasses is

definitely distinguished by the isotropic chemical shift and also that the isotropic chemical shifts corresponding to Q_2' and Q_2'' (about -78 and -83 ppm, respectively) reflect different structural states of Q_2. In the $1.5 - 3.0$ glasses, the spectra were satisfactorily reproduced by only one Gaussian curve of Q_2. The δ_{iso} values of Q_2 in the $1.5 - 3.0$ glasses shifted from -79.9 to -87.0 ppm with increasing Y-value. This shift is considered to be caused by a change in the Q_2' and Q_2'' fractions in Q_2. By assuming that one Gaussian curve of Q_2 in the $1.5 - 3.0$ glasses consists of two Gaussian curves of Q_2' and Q_2'', peak deconvolution of these glasses was performed. The results are also given in Table 3.1. Because the δ_{iso} values of Q_2 in the 2.5 and 3.0 glasses are smaller than those of Q_2'' in the other glasses, the Q_2's in the 2.5 and 3.0 glasses are concluded to be composed of Q_2'' alone.

As an example, simulated and experimental ^{29}Si MAS NMR spectra of the undensified 1.25 glasses are shown in Figure 3.4. The peaks of the glasses become shaper with increasing applied-pressure, whereas the peak positions are almost unchanged. All the spectra in this figure were well reproduced by five peaks with Gaussian functions. The peak deconvolution for the densified 1.75 and 2.5 glasses were also performed in a similar manner. The results are listed in Table 3.2.
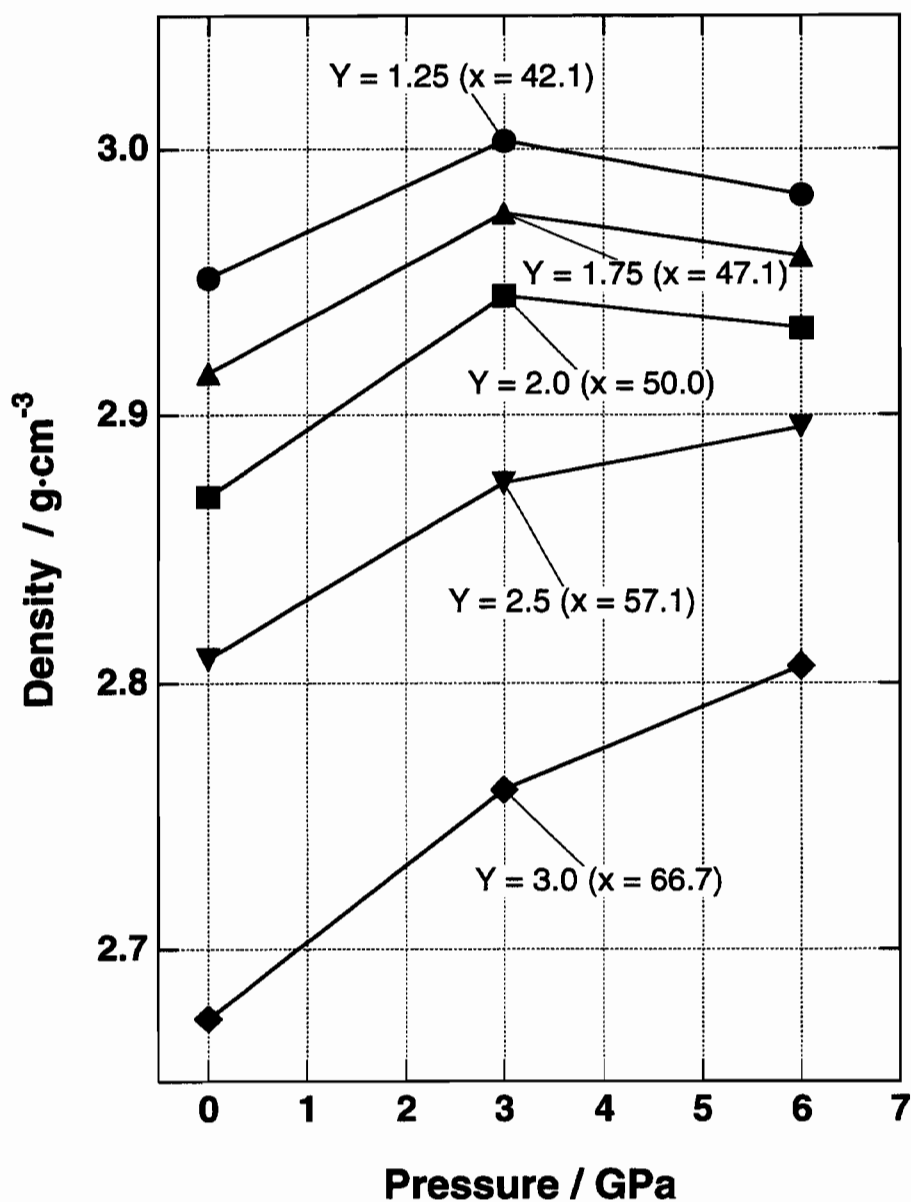
Figure 3.1   Densities of undensified and densified xSiO$_2$·0.4(100 − x)K$_2$O·0.4(100 − x)CaO·0.2(100 − x)SrO glasses of x = 42.1, 47.1, 50.0, 57.1, and 66.7 (i.e. Y = 1.25, 1.75, 2.0, 2.5, and 3.0, respectively). Lines are drawn between data symbols of each type as guides for eyes.
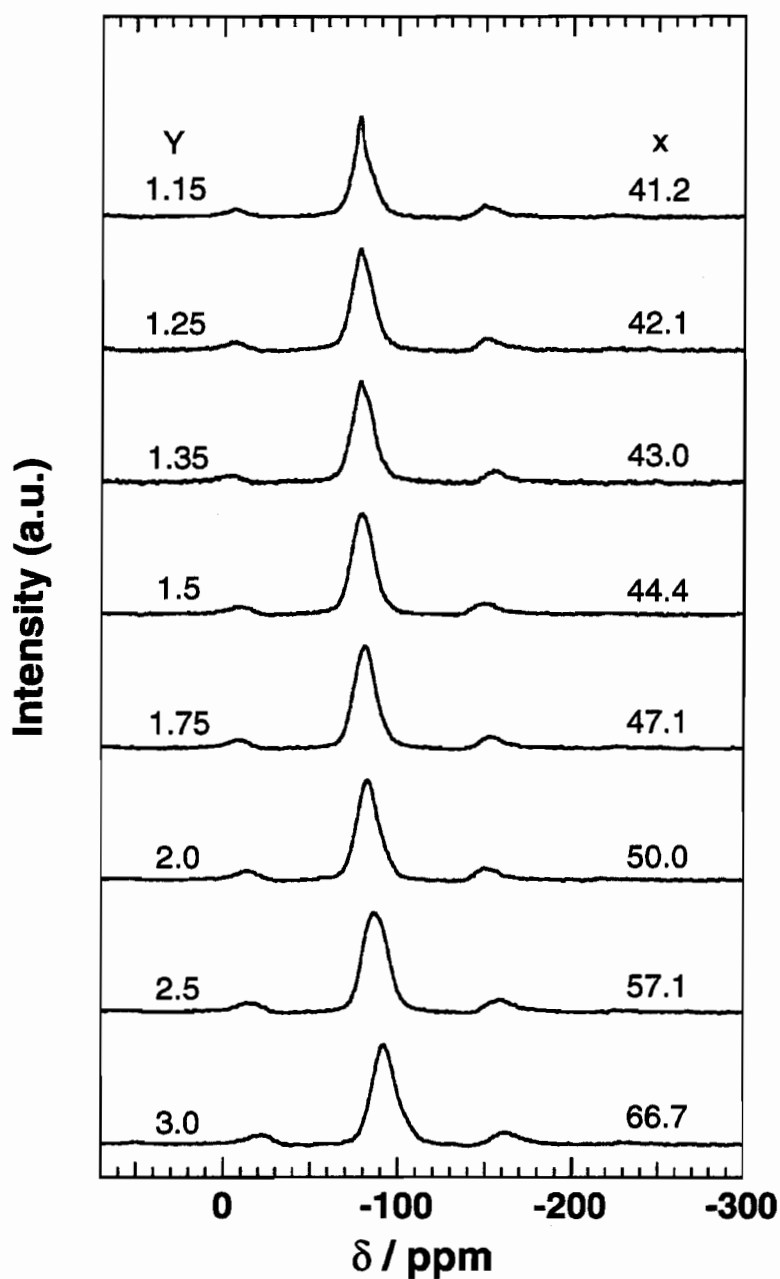
Figure 3.2 ^{29}Si MAS NMR spectra of undensified $x\text{SiO}_2{\cdot}0.4(100 - x)\text{K}_2\text{O}{\cdot}0.4(100 - x)\text{CaO}{\cdot}0.2(100 - x)\text{SrO}$ glasses of x = 41.2, 42.1, 43.0, 44.4, 47.1, 50.0, 57.1, and 66.7 (i.e. Y = 1.15, 1.25, 1.35, 1.5, 1.75, 2.0, 2.5, and 3.0, respectively).
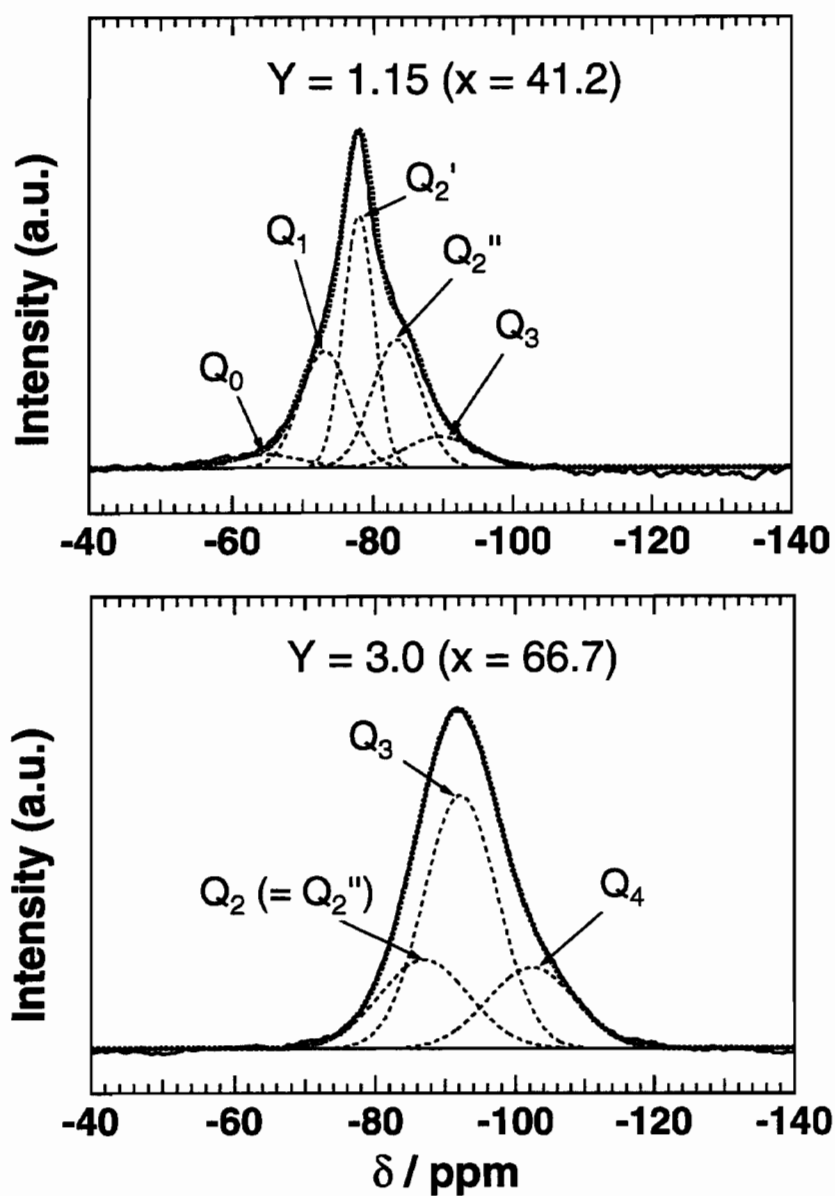
Figure 3.3   Peak deconvolution for $x\text{SiO}_2 \cdot 0.4(100 - x)\text{K}_2\text{O} \cdot 0.4(100 - x)\text{CaO} \cdot 0.2(100 - x)\text{SrO}$ glasses of $x = 41.2$ and 66.7 (i.e. $Y = 1.15$ and 3.0, respectively).

Table 3.1   Isotropic chemical shifts (δ_{iso}), full widths at half maxima (FWHM) and Q_n fractions determined from ^{29}Si MAS NMR spectra of xSiO$_2$·0.4(100 − x)K$_2$O·0.4(100 − x)CaO·0.2(100 − x)SrO glasses[a].

x	Y notation	Q_n	δ_{iso} / ppm	FWHM / ppm	Q_n fractions (%)
41.2	1.15	Q_0	−65.0	10.0	4.1
		Q_1	−73.0	6.9	24.7
		Q_2	−	−	61.5
		Q_2'	−77.9	4.4	34.0
		Q_2''	−83.3	7.0	27.5
		Q_3	−89.5	10.0	9.7
42.1	1.25	Q_0	−65.0	10.0	2.8
		Q_1	−72.9	7.8	23.1
		Q_2	−	−	63.4
		Q_2'	−77.8	5.8	34.6
		Q_2''	−83.5	6.8	28.8
		Q_3	−89.5	10.0	10.7
43.0	1.35	Q_0	−65.0	10.0	2.2
		Q_1	−72.9	7.8	20.8
		Q_2	−	−	65.3
		Q_2'	−77.9	5.9	34.4
		Q_2''	−83.5	6.8	30.9
		Q_3	−89.5	10.0	11.7
44.4	1.5	Q_0	−65.0	10.0	1.9
		Q_1	−73.6	9.5	15.6
		Q_2	−79.9	9.7	68.3
		Q_2'	−77.2	7.8	34.8
		Q_2''	−82.6	7.6	33.5
		Q_3	−89.2	9.6	14.2
47.1	1.75	Q_1	−72.4	11.0	9.1
		Q_2	−80.6	10.0	73.2
		Q_2'	−78.0	7.9	36.6
		Q_2''	−83.3	7.8	36.6
		Q_3	−89.6	10.0	16.4
		Q_4	−101.0	15.9	1.3
50.0	2.0	Q_1	−72.0	13.0	7.5
		Q_2	−81.6	10.0	67.5
		Q_2'	−77.9	7.7	23.0
		Q_2''	−83.4	8.5	44.5
		Q_3	−90.1	10.0	22.0
		Q_4	−101.0	15.9	3.0
57.1	2.5	Q_1	−72.0	14.3	3.6
		Q_2 (Q_2'')	−83.6	9.9	49.4
		Q_3	−91.5	9.9	39.7
		Q_4	−101.7	15.9	7.3
66.7	3.0	Q_2 (Q_2'')	−87.0	12.7	23.5
		Q_3	−92.2	10.5	55.4
		Q_4	−102.3	12.5	21.1

[a]Errors in Q_n fractions are ±2%
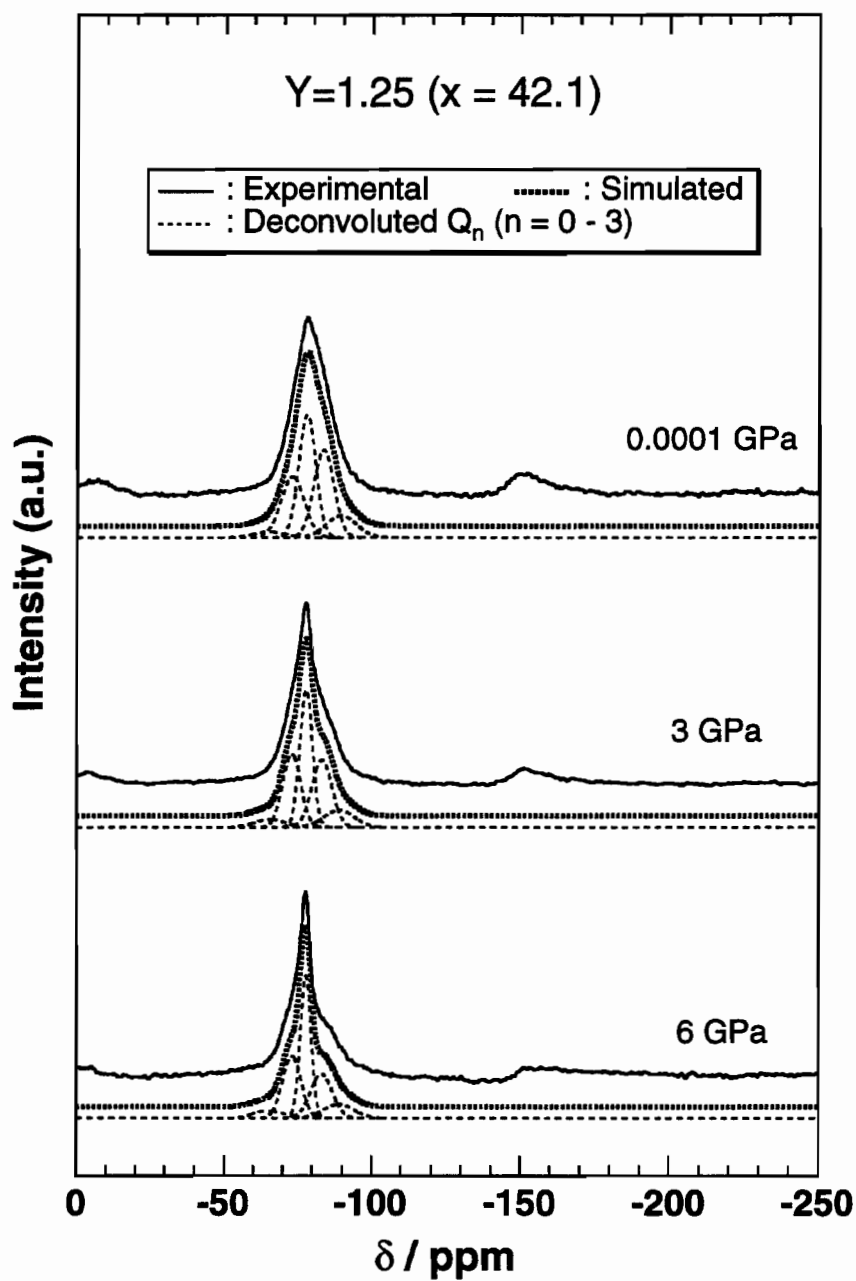
Figure 3.4   Simulated and experimental ^{29}Si MAS NMR spectra of xSiO$_2$·0.4(100 − x)K$_2$O·0.4(100 − x)CaO·0.2(100 − x)SrO glasses of x = 42.1 (i.e. Y = 1.25).

Table 3.2 Isotropic chemical shifts (δ_{iso}), full widths at half maxima (FWHM) and Q_n fractions determined from ^{29}Si MAS NMR spectra of $xSiO_2 \cdot 0.4(100-x)K_2O \cdot 0.4(100-x)CaO \cdot 0.2(100-x)SrO$ glasses undensified and densified under 3 and 6 GPa.

x	Y notation	Q_n	δ_{iso} / ppm			FWHM / ppm			Q_n fractions (%)		
			undensified	3GPa	6GPa	undensified	3GPa	6GPa	undensified	3GPa	6GPa
42.1	1.25	Q_0	−65.0	−65.5	−65.2	10.0	10.0	10.0	2.8	4.5	5.2
		Q_1	−72.9	−72.8	−73.0	7.8	6.0	6.2	23.1	25.3	26.5
		Q_2	–	–	–	–	–	–	63.4	60.1	58.4
		Q_2'	−77.8	−77.7	−77.7	5.8	4.3	3.7	34.6	33.9	36.0
		Q_2''	−83.5	−83.1	−83.1	6.8	6.8	7.4	28.8	26.2	22.4
		Q_3	−89.5	−89.0	−89.0	10.0	10.0	10.2	10.7	10.1	9.9
47.1	1.75	Q_1	−72.4	−72.3	−72.2	11.0	11.0	11.0	9.1	11.0	13.1
		Q_2	−80.6	−80.5	−80.5	10.0	10.0	10.0	73.2	72.2	71.0
		Q_2'	−78.0	−78.0	−77.9	7.9	8.1	8.2	36.6	38.0	38.7
		Q_2''	−83.3	−83.3	−83.2	7.8	8.0	8.0	36.6	34.2	32.3
		Q_3	−89.6	−89.6	−89.6	10.0	10.0	10.0	16.4	15.8	15.1
		Q_4	−101.0	−101.0	−101.0	15.9	13.0	13.0	1.3	1.0	0.8
57.1	2.50	Q_1	−72.0	−72.0	−72.0	14.3	14.3	14.0	3.6	3.8	4.1
		$Q_2(Q_2'')$	−83.6	−83.4	−83.5	9.9	9.9	9.7	49.4	49.6	50.1
		Q_3	−91.5	−91.4	−91.4	9.9	9.9	9.5	39.7	39.7	39.0
		Q_4	−101.7	−101.7	−101.7	15.9	12.5	12.0	7.3	6.9	6.8

3.4. Discussion

At first the structures of SiO_4 units, which reflect $Q_2{}'$ and $Q_2{}''$, are considered. The SiO_4 tetrahedra in both α-$CaSiO_3$ (pseudo-wollastonite) and β-$CaSiO_3$ (β-wollastinite) crystals belong to Q_2 [5,6]. Three-ring silicate ions in α-$CaSiO_3$ (Si–O–Si bond angle = 130°) [5] exhibit the δ_{iso} value of –83.5 ppm [7], whereas chain silicate ions in β-$CaSiO_3$ (Si–O–Si bond angle = 143°) [6] exhibit the δ_{iso} value of –89.0 ppm [7]. The SiO_4 tetrahedra in these two $CaSiO_3$ polymorphs have very similar Si–O bond length. Therefore, a difference in the Si–O–Si bond angle between these two SiO_4 tetrahedra is one of main factors that affect the ^{29}Si chemical shifts. The influences of Si–O–Si bond angle on ^{29}Si chemical shifts have been already discussed [8–10]. Based on these experimental facts, a difference in δ_{iso} between $Q_2{}'$ and $Q_2{}''$ in the present glasses may be considered to be mainly caused by the Si–O–Si bond angle. Since Q_2's in the 2.5 and 3.0 glasses containing more than 50 mol% SiO_2 is $Q_2{}''$, $Q_2{}''$ probably shows Q_2 which is for the Si–O–Si bond angle found in conventional silicate glasses and takes part in chain-formation seen in the β-$CaSiO_3$ crystal. Since the δ_{iso} value of $Q_2{}'$ is larger than that of $Q_2{}''$, on the other hand, the Si–O–Si bond angle of $Q_2{}'$ is considered to be smaller than that of $Q_2{}''$, suggesting that a part of $Q_2{}'$ takes part in ring-formation seen in the α-$CaSiO_3$ crystal. The peaks of the 1.15, 1.25, and 1.35 glasses in Figure 3.2 have shaper line-profiles than those of the other glasses, indicating that the Si–O–Si angles in both $Q_2{}'$ and $Q_2{}''$ in these glasses have a narrow distribution than those of the other glasses. This suggests that the flexibility of glass structure decreases with decreasing Y-value.

Plots of the fractions of Q_n ($n = 0 - 4$) against Y-value in the undensified SiO_2–K_2O–CaO–SrO glasses are shown in Figure 3.5, together with plots of the absolute quantities of Q_n. With decreasing Y-value, the fractions of Q_0 and Q_1 increase

and those of Q_3 and Q_4 decrease. The Q_2 fraction exhibits a maximum value at $Y = 1.75$ (i.e. 47.1 mol% SiO_2) and then decreases with decreasing Y-value. The Q_2' fraction is 0% in the 2.5 and 3.0 glasses (i.e. SiO_2 contents above 57.1 mol%). With a decrease in Y-value, the Q_2' fraction increases in Y-values of 2.5 − 1.75 and then slightly decreases in Y-value < 1.75. On the other hand, the Q_2'' fraction exhibits a maximum value at $Y = 2.5$ and then decreases with decreasing Y-value.
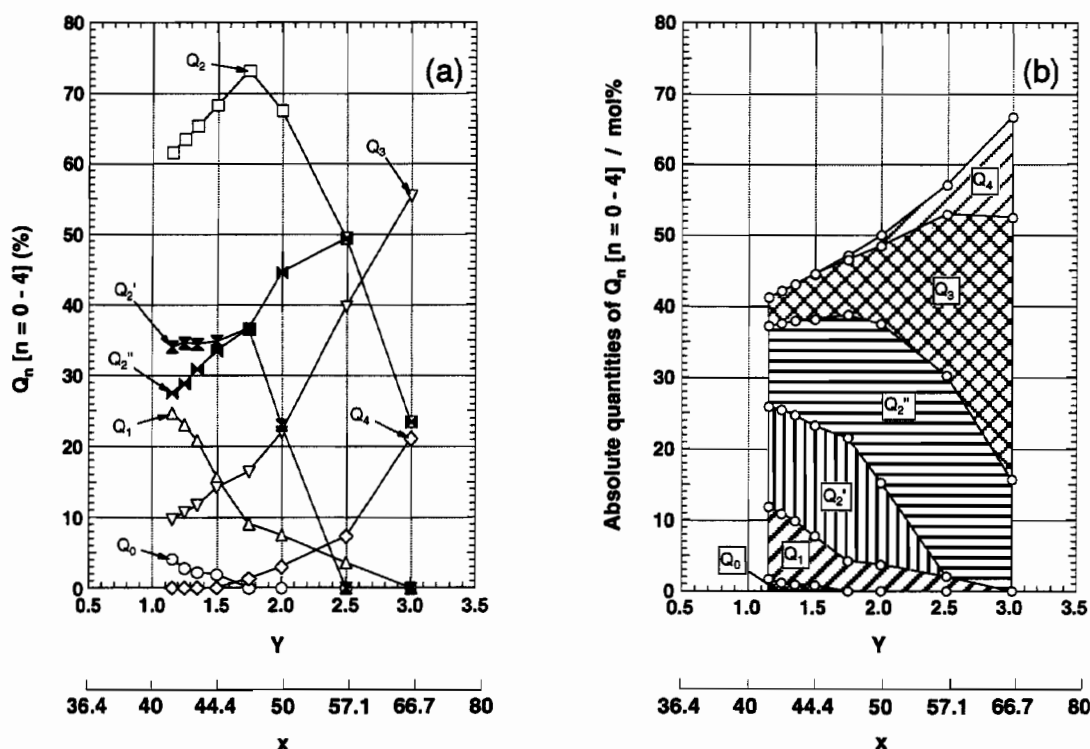
Figure 3.5 Plots of (a) Q_n fractions ($n = 0 − 4$) and (b) Q_n absolute quantities against $Y(x)$-value in undensified $xSiO_2 \cdot 0.4(100 − x)K_2O \cdot 0.4(100 − x)CaO \cdot 0.2(100 − x)SrO$ glasses.

In Y below 2.0 (i.e. 50 mol% SiO_2) the Q_2 fraction exceeds 60% and considerable amounts of Q_2' are present, indicating that the glasses of Y below 2.0 are mainly composed of Q_2 and consist of not only silicate-chains but also silicate-rings. The Q_2'' values in Y less than 1.75 decrease with decreasing Y-value, whereas the Q_2' values are almost constant. This suggests that a decrease in Y-value results in a decrease in the number and length of silicate chain, i.e. the formation of isolated and short silicate-chains and/or silicate-rings, and that the glass structures of Y below 2.0 approach the structure model proposed by Trap and Stevels.

Plots of the Q_n fractions in the 1.25, 1.75, and 2.5 glasses against the applied pressure are shown in Figure 3.6. In the 1.25 glass, the fractions of Q_0, Q_1, and Q_2' increased and those of Q_2, Q_2'', and Q_3 decreased with increasing applied-pressure. The Q_4 fractions were 0% for all the applied pressures. In the 1.75 glass, the fractions of Q_1 and Q_2' increased and those of Q_2, Q_2'', Q_3, and Q_4 decreased with increasing applied-pressure. The Q_0 fractions were 0% for all the applied pressures. In the 2.5 glass, the fractions of Q_1 and Q_2 (Q_2'') increased and those of Q_3 and Q_4 decreased with increasing applied-pressure. The Q_0 fractions were 0% for all the applied pressures. The fact that the fractions of Q_n with small n-values increase with an increase in the applied pressure as a whole indicates that a part of Si–O–Si bonds in the glasses is broken by the application of high-pressure. The changes are in the order of $Y = 1.25 > Y = 1.75 > Y = 2.5$, being proportional to the amounts of glass-network modifying cations in the glasses.

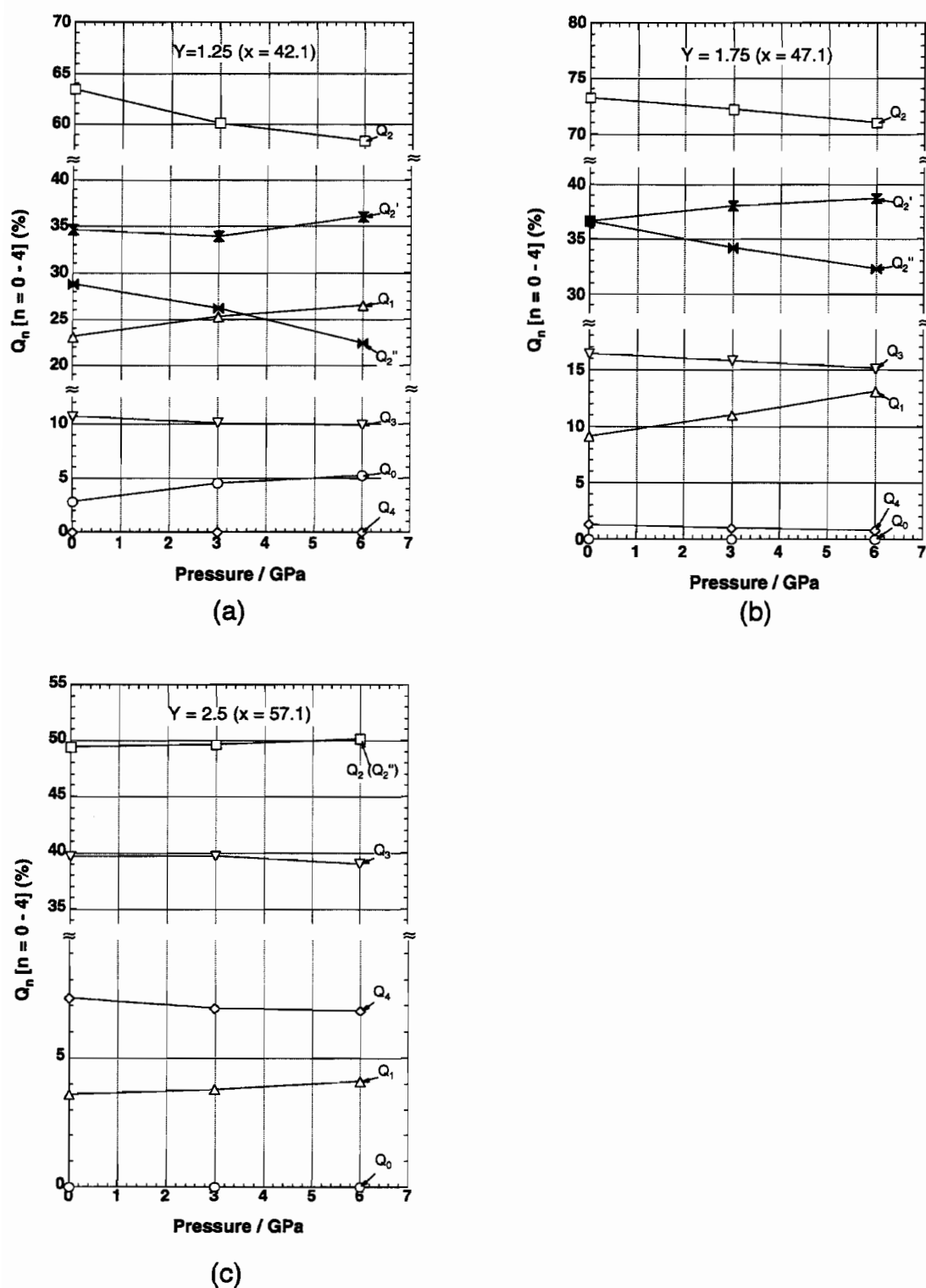Figure 3.6   Plots of Q_n fractions ($n = 0 - 4$) of $xSiO_2·0.4(100 - x)K_2O·0.4(100 - x)CaO·0.2(100 - x)SrO$ glasses of (a) $x = 42.1$ (i.e. $Y = 1.25$), (b) 47.1 (i.e. $Y = 1.75$), and (c) 57.1 (i.e. $Y = 2.5$) against applied pressure.

As can be seen from Figure 3.4, the peaks of the 1.25 glass become sharper with increasing applied-pressure, indicating that the distribution of Si–O–Si bond angles in silicate ions decreases with increasing applied-pressure. The Q_2'/Q_2 ratio increases with an increase in the applied pressure, indicating that Si–O–Si bond angles decrease with increasing applied-pressure. When high pressure is applied or released, therefore, the following structural changes are presumed for glasses: When high pressure is applied to the glasses, both the reduction of Si–O–Si bond angles and their distribution and the compression between glass-network modifying cations and silicate anions composed of SiO_4 tetrahedra occur at the same time. When the applied pressure is released, on the other hand, the Si–O–Si bond angles and their distribution are retained, but a spontaneous structure-relaxation between glass-network modifying cations and silicate anions takes place. That is to say, changes in the local structure around Si ions cannot be related to the peculiar behavior in permanent densification observed for the 1.25 – 2.0 glasses. Probably the peculiar behavior seems to be related to changes in the local structures around glass-network modifying cations. Thus, changes in the local structures around glass-network modifying cations with permanent densification should be elucidated. Such experiments are necessitated and are in plan in the near future.

3.5. Conclusion

Glasses of compositions $xSiO_2 \cdot 0.4(100 - x)K_2O \cdot 0.4(100 - x)CaO \cdot 0.2(100 - x)SrO$ glasses (x = 42.1, 47.1, 50.0, 57.1, and 66.7) in mol% were prepared. In these glasses the x values can be related to the Y parameter that means the average number of bridging-oxygen ions per an SiO_4 tetrahedron according to an equation $Y = 6 - 200/x$. Thus, glasses of the x values of 41.2, 42.1, 43.0, 44.4, 47.1, 50.0, 57.1, and 66.7

correspond to those of the Y-values of 1.15, 1.25, 1.35, 1.5, 1.75, 2.0, 2.5, and 3.0, respectively. The 1.25, 1.75, and 2.5 glasses were permanently densified by the 3 and 6 GPa high-pressure treatments. The following phenomenon was observed: The densities of the 2.5 and 3.0 glasses increased with increasing applied-pressure, while the 1.25, 1.75, and 2.0 glasses exhibited the maximum values at 3 GPa and then gave the decreased values at 6 GPa.

^{29}Si MAN NMR spectra were measured for the undensified and densified glasses. From ^{29}Si MAS NMR measurements of the undensified glasses the following two facts were found: (1) With decreasing Y-value the peaks become sharper, suggesting a decrease in the distribution of Si–O–Si bond angles and the flexibility of glass structure. (2) In glasses of the Y-values below 2.0 the Q_2 fraction exceeds 60% and considerable amounts of Q_2' are present, indicating that the glasses are mainly composed of Q_2 and consist of not only silicate-chains but also silicate-rings.

From ^{29}Si MAS NMR measurements of the densified glasses the following three facts were found: (1) The peaks of the glasses become sharper with increasing applied-pressure, indicating that the distribution of Si–O–Si bond angles becomes narrower with increasing applied-pressure. (2) As a whole the fractions of Q_n of small n-values increased with an increase in applied pressure, indicating that a part of Si–O–Si bonds is broken under the applied pressures. (3) When high pressure is applied or released, the following structural changes are considered: When high pressure is applied to the glasses, both the reduction of Si–O–Si bond angles and their distribution and the compression between glass-network modifying cations and silicate anions composed of SiO_4 tetrahedra occur at the same time. When the high pressure is released, Si–O–Si bond angles and their distribution are retained, but a spontaneous structural-relaxation between glass-network modifying cations and silicate anions takes place.

References

[1] H. J. L. Trap and J. M. Stevels, *Glastechn. Ber. 32K.*, **VI**, 31 (1959).

[2] H. Maekawa, T. Maekawa, K. Kawamura and T. Yokokawa, *J. Non-cryst. Solids*, **127**, 53 (1991).

[3] A. R. Grimmer, M. Mägi, M. Hähnert, H. Stade, A. Samoson, W. Wieker and E. Lippmaa, *Phys. Chem. Glasses*, **25**, 105 (1984).

[4] N. Kawai, M. Togaya and A. Onodera, *Proc. Jpn. Acad.*, **49**, 623 (1973).

[5] T. Yamanaka and H. Mori, *Acta Cryst.*, **B37**, 1010 (1981).

[6] M. J. Buerger and C. T. Prewitt, *Proc. Nat. Acad. Sci. USA*, **47**, 1884 (1961).

[7] M. Mägi, E. Lippmaa, A Samoson, G. Engelhardt and A. R. Grimmer, *J. Phys. Chem.*, **88**, 1518 (1984).

[8] J. M. Thomas, J. Klinowski, S. Ramdas, B. K. Hunter and D. T. B. Tennakoon, *Chem. Phys. Lett.*, **108**, 271 (1984).

[9] G. Engelhardt and R. Radeglia, *Chem. Phys. Lett.*, **108**, 271 (1984).

[10] J. V. Smith and C.S.Blackwell, *Nature*, **303**, 223 (1983).

Chapter 4

High-Pressure Densification of Fluoride, GeS$_2$, and Silicate Glasses

4.1. Introduction

Glasses subjected to high-pressure treatments increase their densities. The effect persists even after removal of the applied pressure [1–4]. This permanent densification of glass is of great interest from the viewpoint of glass science and technology because the changes in glass structure are permanently retained and consequently the optical, electrical, mechanical, and magnetic properties of the glass can be changed without changing glass composition.

Although permanent densification experiments have been performed on silicate and sulfide glasses [5,6], no experiments of fluorozirconate glasses have been reported. Especially there are no studies exist from the standpoint of the chemical-bond properties and packing density (defined as the fractional molar volume occupied by the ions assuming them to be perfect spheres) to our knowledge.

In fluorozirconate glasses the chemical bonds between cations and fluoride anions are ionic [7] and consequently the packing densities of the ions are over 60% [8]. On the other hand, the Ge and S atoms in GeS$_2$ glass that is a typical sulfide glass are covalently bonded. The packing density of Ge and S in the glass is about 20% (value calculated from the measured density and the covalent radii in Ref. 16). Silicate glasses

70

have both ionic and covalent bond-character and the packing densities of glass constituents range 20 – 50% (value calculated from the measured density and the covalent radii in Refs. 15 and 16) depending on the glass composition.

In the present study the permanent densification of ionic ZrF$_4$-based fluoride glasses, mixed ionic and covalent SiO$_2$-based oxide glasses, and a covalent GeS$_2$ glass are examined and discussed based on the chemical-bond characters and the packing densities.

4.2. Experimental Procedures

4.2.1. Glass Samples

Fluorozirconate glasses of the 60ZrF$_4$·30BaF$_2$·10EuF$_3$ (ZBE) and 55ZrF$_4$·17BaF$_2$·23NaF·5EuF$_3$ (ZBNE) compositions, silicate glasses of the xSiO$_2$·0.4(100 – x)K$_2$O·0.4(100 – x)CaO·0.2(100 – x)SrO composition (x = 42.1, 44.4, 47.1, 50.0, 57.1, and 66.7), and a sulfide glass of a GeS$_2$ composition were prepared and annealed at the respective glass-transition temperatures. The preparation procedures of the respective glass samples have been described in Chapters 1, 2, 3, and 5, respectively.

4.2.2. Permanent Densification Treatments

Densification of the glass samples was carried out with a 6–8 multi-anvil-type high-pressure apparatus [10]. Specimens were compressed up to desired pressures of 1.5, 3.0, 4.5, 6.0, and 9.0 GPa with a 0.033 GPa·min^{-1} ascending rate at room temperature. After that, the glasses were heated to temperatures of 270°C and 250°C for ZBE and ZBNE fluoride glasses, respectively, 355°C, 340°C, 355°C, 370°C, 386°C, and 422°C

for silicate glasses with 42.1, 44.4, 47.1, 50.0, 57.1, and 66.7 mol% SiO_2, respectively, and 270°C for a GeS_2 glass within 5 min under each pressure. Then the glasses were kept at these temperatures for 30 min. After the heating treatments the specimens were cooled to room temperature and then the applied pressure were released with a 0.033 $GPa \cdot min^{-1}$ descending rate. The experimental errors in the pressure and temperature regulation in densification treatments are $\pm 2.23 \times 10^{-8}$ GPa and ± 0.3°C, respectively.

4.2.3. Density Measurements

Densities of the undensified and densified glasses were measured by the Archimedes method using CCl_4 as an immersion liquid. The experimental error in density measurements was about ± 0.005 $g \cdot cm^{-3}$.

4.3. Results

In the present silicate glasses the average number of bridging-oxygen ions per SiO_4 tetrahedron, Y, can be calculated from an equation $Y = 6 - 200/x$, where x is a molar ratio of SiO_2 content [9]. Therefore, glasses of x = 42.1, 44.4, 47.1, 50.0, 57.1, and 66.7 mol% have Y's of 1.25, 1.5, 1.75, 2.0, 2.5, and 3.0, respectively. In the glasses with smaller Y's the connectivity of SiO_4 tetrahedron units is less. Hereafter, glasses with x = 42.1, 44.4, 47.1, 50.0, 57.1, and 66.7 are abbreviated as the 1.25, 1.5, 1.75, 2.0, 2.5, and 3.0 silicate glasses, respectively.

The densities of the ZBE and ZBNE fluoride glasses before and after densification are plotted against the applied pressure in Figure 4.1. The densities of the 1.25, 1.5, 1.75, 2.0, 2.5, and 3.0 silicate glasses before and after densification are plotted against the applied pressure in Figure 4.2. Changes in densities of the GeS_2 glass on

pressurization are shown in Figure 4.3. In the figure the densities of crystalline α-GeS$_2$ (high-temperature modification) [11], β-GeS$_2$ (low-temperature modification) [12], and II-GeS$_2$ (high-pressure modification) [13] are plotted for reference.
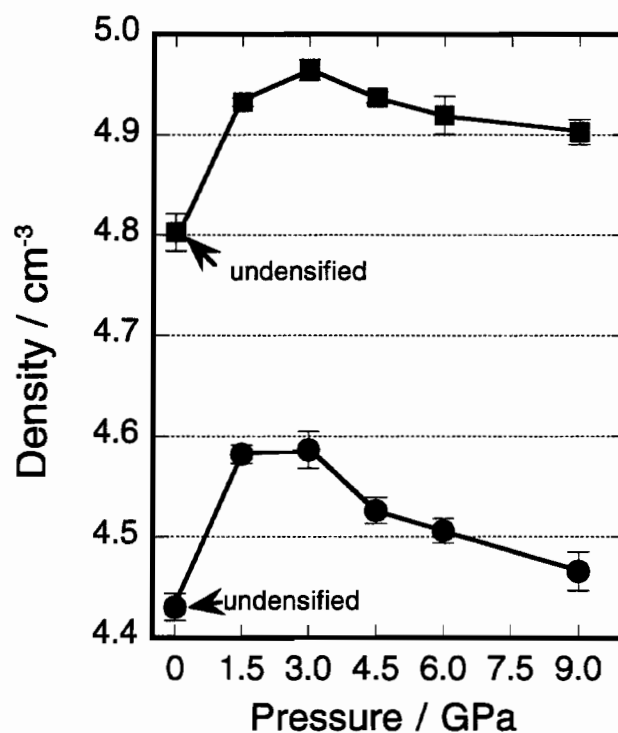
Figure 4.1   Pressure dependence of densities of undensified and densified ZBE (closed squares) and ZBNE (closed circles) fluoride glasses. Lines are drawn between data symbols as guides for eyes.
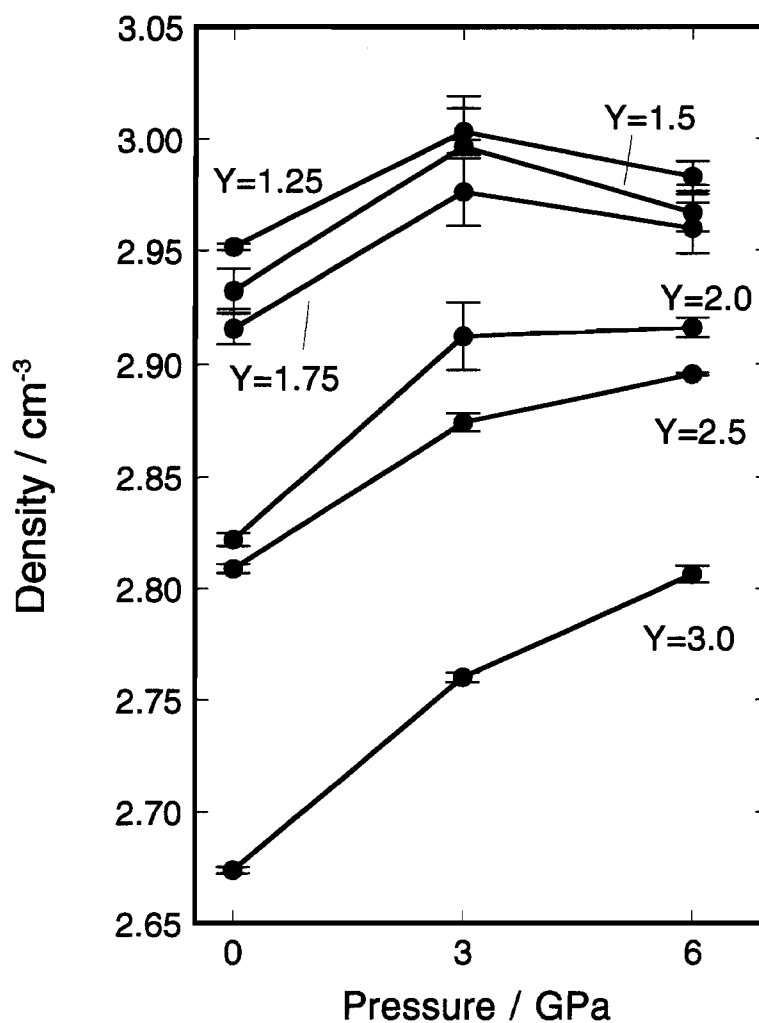
Figure 4.2   Pressure dependence of densities of undensified and densified silicate glasses of Y = 1.25, 1.5, 1.75, 2.0, 2.5, and 3.0. Lines are drawn between data symbols of each type as guides for eyes.
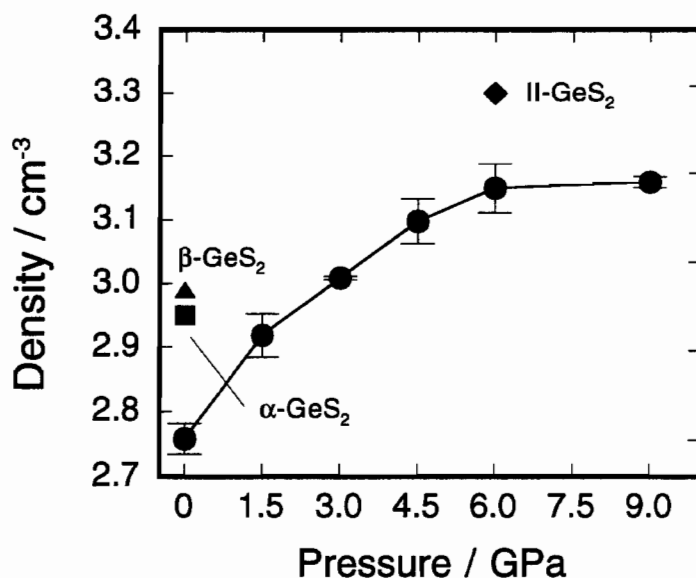
Figure 4.3   Pressure dependence of densities of undensified and densified GeS₂ glasses. Line is drawn between data symbols as guide for eyes.

4.4. Discussion

4.4.1. Densification of Respective Glass Systems

The followings can be observed in Figures 4.1, 4.2, and 4.3. The densities of a GeS₂ glass and the 2.0, 2.5, and 3.0 silicate glasses of higher contents than 50 mol% SiO₂ increase with increasing applied-pressure. In two fluoride glasses and the 1.25, 1.5, and 1.75 silicate glasses of lower contents than 50 mol% SiO₂, on the other hand, the densities increase until applied pressures of about 3.0 GPa, and then decrease with further increasing applied-pressure. Here it is noted that the pressure dependencies of densities observed in the latter glasses are a permanent densification that has not been reported so far to our knowledge.

Figure 4.4 shows the relationship between the ionicity and the packing density in the ZBE and ZBNE fluoride glasses, the 1.25, 1.5, 1.75, 2.0, 2.5, and 3.0 silicate glasses, and the GeS_2 glass. In the figure a SiO_2 glass is also given for reference. The ionicity in the respective glasses was calculated from a difference in electronegativity between two elements using the Pauling equation [14]. On the other hand, the packing densities of the fluoride, silicate, and GeS_2 glasses, which were obtained from the molar volumes calculated from the densities and the ionic [15] and/or covalent [16] radii of elements, are given in Table 4.1. From the ionicity and packing density relationship in the figure it is deduced that glasses with ionicity larger than 64% and with packing densities higher than 39% (a hatched area in the figure) have a different permanent densification behavior in the pressure-density relationship.
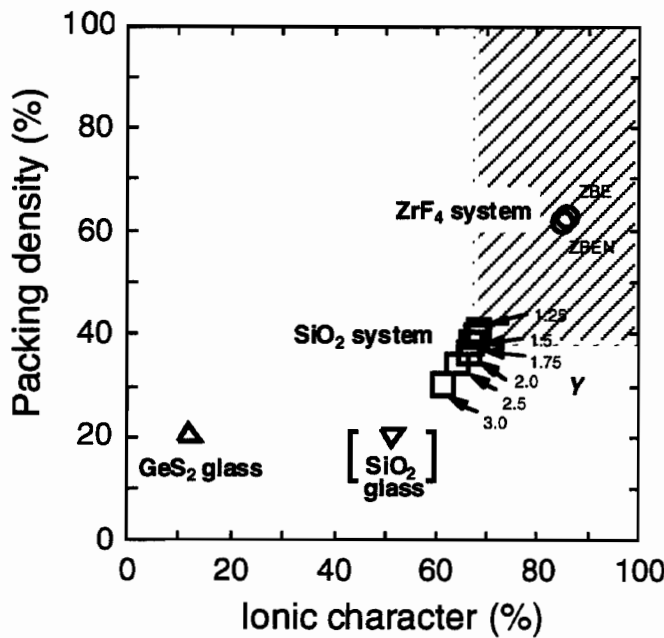
Figure 4.4   Relationship between ionicity and packing density in ZrF_4-based, SiO_2-based, and GeS_2 glasses.

Table 4.1   Ionic and/or covalent radii of elements in fluoride, silicate, and GeS_2 glasses [15,16].

Ionic radius / nm				Covalent radius / nm			
Fluoride glass		Silicate glass		Silicate glass		GeS_2 glass	
Zr^{4+}	0.084	K^+	0.137	Si	0.104	Ge	0122
Ba^{2+}	0.142	Ca^{2+}	0.100	O^a	0.066	S	0.104
Eu^{3+}	0.107	Sr^{2+}	0.118				
Na^+	0.116	$O^{2-, b}$	0.140				
F^-	0.133						

[a] O in SiO_2.

[b] O in K_2O, CaO, and SrO.

Figure 4.5 shows the relationship between the connectivity of glass-network forming tetrahedra and the packing density in the 1.25, 1.5, 1.75, 2.0, 2.5, and 3.0 silicate glasses and the GeS_2 glass. It is noted here that the ZBE and ZBNE fluoride glasses are composed of the ZrF_7 and/or ZrF_8 polyhedral units [17–19], so that this relationship is inapplicable. However, these polyhedra have ~100% ionicity. Tentatively, therefore, the connectivity of these polyhedra was assumed to be zero and plotted in Figure 4.6. The figure indicates that glasses with smaller connectivity of glass-network forming polyhedra have higher packing densities and that glasses with $Y < 2.0$ and packing densities > about 39% (a hatched area in the figure) have a different permanent densification dependence on pressure.
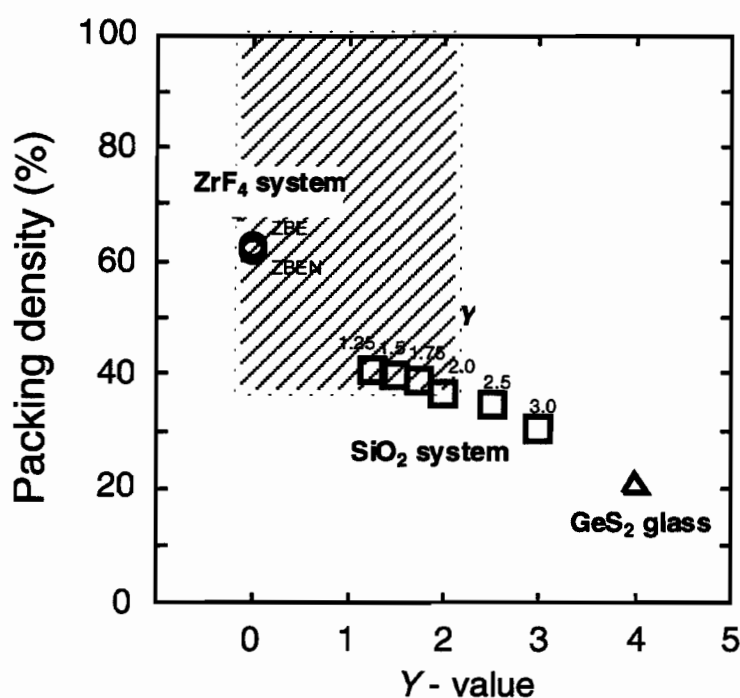
Figure 4.5   Relationship between connectivity of tetrahedron and packing density in ZrF$_4$-based, SiO$_2$-based, and GeS$_2$ glasses.

4.4.2. Structures of Permanently Densified Glasses

Changes in the F$^-$ coordination environments around Zr^{4+}, Eu^{3+}, and Ba^{2+} of the ZBE and ZBNE fluoride glasses with permanent densification have been examined by Raman and Eu^{3+}-fluorescence spectroscopies and extended X-ray absorption fine structure (EXAFS) analyses, as described in Chapters 1 and 2. In the 1.25, 1.75, and 2.5 silicate glasses, the changes in silicon-oxygen network structure with permanent densification have been examined by ^{29}Si magic-angle-spinning nuclear magnetic resonance (MAS NMR) spectroscopy, as described in Chapter 3. The structural studies of permanently densified GeS$_2$ sulfide glass have been performed by means of EXAFS

and Raman spectroscopies and an X-ray radial distribution (XRD) analysis, as will be described in Chapters 5 and 6. On the other hand, the reason for the pressure dependence of densification for a ZBNE fluoride glass has been also analyzed with a molecular dynamics (MD) simulation technique [20–22].

The MD simulations have revealed a mechanism for the densification as follows: Under pressures > 3.0 GPa the connectivity of the network-forming ZrF_n and EuF_n polyhedra partially transforms from corner-sharing type to edge-sharing one. The change in the connectivity causes a contraction of interstices around the network-modifying Ba^{2+} and Na^+ ions, around which the coordination numbers increase to those in the high-pressure polymorphs of the BaF_2 and NaF crystals [23,24]. After decompression the structural relaxation occurs in the ZBNE glass. The extent of the relaxation depends on temperature and pressure because of the 'fragility' of this glass [25]. The high-pressure network structures are fully or partially preserved after decompression at temperature < T_g. The partial preservation of the connectivity of network-forming polyhedra causes a maximum in the pressure dependence of structural relaxation in the F^- coordination environments around the network-modifying ions. This is responsible for the pressure dependence of permanent densification; the density maximum appears in the pressure dependence.

4.5. Conclusion

Permanent densifications was examined on ionic $60ZrF_4\cdot30BaF_2\cdot10EuF_3$ and $55ZrF_4\cdot17BaF_2\cdot23NaF\cdot5EuF_3$ fluoride glasses, mixed ionic and covalent $xSiO_2\cdot0.4(100 - x)K_2O\cdot0.4(100 - x)CaO\cdot0.2(100 - x)SrO$ silicate glasses (x = 42.1 – 66.7), and a covalent GeS_2 glass. The densified glasses were obtained by combined treatments of

heating at temperatures about three-quarters of their respective glass-transition temperatures and compression up to 9.0 GPa. In the GeS_2 glass and the SiO_2-based glasses of $x \geq 50$, which have higher covalency and lower packing densities, the densities increased with increasing applied-pressure. This pressure dependence of densification has been observed for a variety of glasses so far.

In the ZrF_4-based glasses and the SiO_2-based glasses of $x < 50$, which have a higher ionicity and higher packing densities, the densities showed the maximum values at a pressure of ~3.0 GPa. Such a pressure dependence of permanent densification is peculiar and a permanent densification that has not been reported to our knowledge.

References

[1] P. W. Bridgman and I. Simon, *J. Appl. Phys.*, **24**, 405 (1953).

[2] J. D. Mackenzie, *J. Am. Ceram. Soc.*, **46**, 470 (1963).

[3] H. Cohen and R. Roy, *Phys. Chem. Glasses*, **6**, 149 (1965).

[4] N. Mizouchi and A. Cooper Jr., *J. Am. Ceram. Soc.*, **56**, 320 (1973).

[5] S. Sakka and J. D. Mackenzie, *J. Non-Cryst. Solids*, **1**, 107 (1969).

[6] G. Parthasarathy and E. S. R. Gopal, *Bull. Mater. Sci.*, **3&4**, 271 (1985).

[7] Y. Kawamoto and I. Nohara, *Solid State Ionics*, **22**, 207 (1987).

[8] A. Konishi, H. Izumi, R. Kanno and Y. Kawamoto, *J. Mater. Sci.*, **29**, 1584 (1994).

[9] H. J. L. Trap and J. M. Stevels, *Glatech. Ber.*, **K 32 (6)**, 31 (1959).

[10] N. Kawai, M. Togaya and A. Onodera, *Proc. Jpn. Acad.*, **49**, 623 (1973).

[11] G. Dittmar and H. Schäfer, *Acta Crystallogr.*, **B32**, 1188 (1976).

[12] G. Dittmar and H. Schäfer, *Acta Crystallogr.*, **B31**, 2060 (1975).

[13] C. T. Prewitt and H. S. Young, *Science*, **149**, 535 (1965).

[14] L. Pauling, in *"The Nature of the Chemical Bond"*, 3rd Ed., (Cornell University, New York, 1960).

[15] R. D. Shannon and C. T. Prewitt, *Acta Crystallogr.*, **B25**, 925 (1969).

[16] L. Pauling and M. L. Huggins, *Z. Krist.*, **87**, 205 (1934).

[17] Y. Kawamoto and T. Horisaka, *J. Non-Cryst. Solids*, **56**, 39 (1983).

[18] Y. Kawamoto, T. Horisaka, K. Hirao and N. Soga, *J. Chem. Phys.*, **83**, 2398 (1985).

[19] Y. Kawamoto, in *Materials Science Forum*, vol. **6**, (TransTech, Aedermannsdorf, Switzerland, 1985), p. 767.

[20] Y. Tamai and Y. Kawamoto, *Chem. Phys. Lett.*, **302**, 15 (1999).

[21] Y. Tamai and Y. Kawamoto, *J. Chem. Phys.*, **112**, 3875 (2000).

[22] Y. Tamai and Y. Kawamoto, *Phys. Rev. B*, **62**, 865 (2000).

[23] D. P. Dandekar and J. C. Jamieson, *Trans. Am. Crystallogr. Assoc.*, **5**, 19 (1969).

[24] Y. Sato-Sorensen, *J. Geophys. Res.*, **88**, 3543 (1983).

[25] C. A. Angell, *J. Non-Cryst. Solids*, **73**, 1 (1985).

Part II

Permanent Densification Behavior

of GeS$_2$ Glass

Chapter 5

Structural Study of GeS$_2$ Glasses Permanently Densified under High Pressures up to 9 GPa

5.1. Introduction

In general it has been well established that glasses subjected to high-pressure treatments undergo a significant increase in density that persists even after removal of the applied pressure. Bridgman and Simon demonstrated this permanent densification phenomenon of glass for the first time in 1953 [1]. Thus far this phenomenon has been investigated on various kinds of oxide and chalcogenide glasses [2,3]. The permanent densification of glass is of great interest from the viewpoint of glass science and technology because the changes in glass structure are permanently kept and consequently because the optical, electrical, mechanical, and magnetic properties of the glass can be largely changed without changing glass composition.

On chalcogenide glasses the high-pressure effects on the various properties have been extensively investigated and the results have been reviewed in Ref. 3 in detail. However, almost no structural study of permanently densified chalcogenide glasses has been performed. On the structure of densified GeS$_2$ glass there is only one report [4], in which the presumed structure is based only on a change of the optical absorption-edges

measured *in-situ* under high-pressures.

On the structure of GeS$_2$ glass at atmospheric pressure, i.e. undensified GeS$_2$ glass, a number of studies have been reported so far. The first contribution to the structure of GeS$_2$ glass was made by Kawamoto and Tsuchihashi who have examined the detailed glass-forming regions in the Ge–S system and various physicochemical properties of the glasses [5]. However the structure proposed by them was a schematic one based on the structure of a GeS$_2$ crystal that has been known as only one modification at that time [6]. Later Rowland et al. [7], Lucovsky et al. [8], Kawamoto et al. [9,10], and Ibanez et al. [11] have investigated the structure of GeS$_2$ glass by using various experimental techniques such as an X-ray radial distribution analysis, Raman spectroscopy, a reverse Monte-Carlo simulation, and an EXAFS analysis.

On the polymorphism of GeS$_2$ crystal, on the other hand, three modifications have been found so far and their crystal structures have been determined; II-GeS$_2$ (a high-pressure modification) [12], α-GeS$_2$ (a high-temperature modification) [13], and β-GeS$_2$ (a low temperature modification) [14].

In the present study the structures of GeS$_2$ glasses permanently densified under high pressures up to 9.0 GPa are examined by means of Raman spectroscopy, an X-ray radial distribution analysis, EXAFS and XANES spectroscopies, and optical absorption spectroscopy. Then the structural changes with permanent densification are discussed based on the structures of α-, β-, and II-GeS$_2$ crystals.

5.2. Experimental Procedures

5.2.1. Sample Preparation

Germanium disulfide glass, GeS_2, was prepared from metallic Ge (5N purity) and elementary S (JIS special reagent grade) as starting materials. A 5-g batch was melted in an evacuated silica ampoule at 1000°C for 10 h using a rocking furnace and then it was rapidly quenched in air. Detailed procedure was described in Ref. 5. The prepared glass was annealed at the glass-transition temperature (about 490°C) determined by a DTA analysis.

Crystalline α-GeS_2 was obtained by the crystallization of GeS_2 glass by heat-treating it in an evacuated silica ampoule at about 700°C for 5 d. Crystalline β-GeS_2 was synthesized from crystalline GeS (5N purity) and elementary S according to the procedure reported by Viaene and Moh [15].

The X-ray powder diffraction pattern of the GeS_2 glass proved no inclusion of GeS_2 crystals. The diffraction patterns of the synthesized α- and β-GeS_2 crystals agree entirely with those reported by Viaene and Moh [15].

5.2.2. Permanent Densification Treatments

Permanent densification of the GeS_2 glass was carried out with a 6–8 multi-anvil-type high-pressure apparatus [16]. The specimens were compressed up to desired high pressures, i.e. 1.5, 3.0, 4.5, 6.0, and 9.0 GPa, with a 0.033 GPa·min⁻¹ ascending rate at room temperature. Subsequently these were heated up to 270°C within 5 min under each pressure and were kept at this temperature for 30 min under each pressure. After the heating treatment the specimens were cooled to room temperature and then the applied pressure was released with a 0.033 GPa·min⁻¹ descending rate.

5.2.3. Density Measurements

Densities of the undensified and densified GeS_2 glasses were measured by the Archimedes method, using CCl_4 as an immersion liquid. The experimental error in density measurements was about ± 0.013 g·cm^{-3}.

5.2.4. Measurements of X-ray Absorption Spectra

The X-ray absorption measurements were performed under the approval of the Photon Factory Program Advisory Committee (Proposal No. 99G054) and the Joint Studies Program of the Institute for Molecular Science (Proposal No. 11-553).

In order to obtain the EXAFS and XANES spectra of Ge–K and S–K, the X-ray absorption-edge spectra of Ge–K and S–K were measured at Beam Line 10B in Photon Factory, the National Laboratory for High Energy Physics (Tsukuba) and at Beam Line 7A in UVSOR Facility, the Institute for Molecular Science (Okazaki), respectively. In the former measurements, two flat channel-cut Si (311) monochromators were used and absorption data were collected in the energy range of 10859 to 12409 eV. In the latter measurements, a Ge (111) monochromator was used and absorption data were collected in the energy range of 2102 to 3457 eV. The measurements were made for the undensified and densified GeS_2 glasses and also for the α-GeS_2 and β-GeS_2 crystals as references. The measurements were carried out three times for the respective specimens in order to evaluate experimental errors. These measurements were carried out at room temperature.

5.2.5. X-ray Diffraction Measurements

In order to obtain X-ray radial distribution functions of the undensified and densified GeS$_2$ glasses, X-ray diffraction measurements were performed on the undensified glass and the glasses densified under pressures of 1.5 and 6.0 GPa at room temperature. Detailed procedures of the measurements have been described elsewhere [10].

5.2.6. Raman Scattering Measurements

Raman scattering spectra of the undensified and densified GeS$_2$ glasses were measured in the wavenumber range of 200 to 600 cm^{-1} at room temperature with a Perkin-Elmer 2000NIR FT-Raman spectrometer. A Nd:YAG laser (λ $_{emission}$ = 1064 nm) with 500 mW power was used as an excitation source.

5.2.7. Optical Absorption Measurements

Optical absorption spectra of the undensified and densified GeS$_2$ glasses were measured in the wavelength range of 400 to 800 nm at room temperature with a HITACHI U-3500 spectrophotometer. For the measurements each specimen was polished into optical finish and then the thickness was measured.

5.3. Results and Discussion

5.3.1. Densities

Figure 5.1 shows the treated-pressure dependence of density of GeS_2 glass, together with those of α-GeS_2 [13], β-GeS_2 [14], and II-GeS_2 [12]. The density value of II-GeS_2 is that reported for a sample, which was synthesized at 1100°C under 6 to 6.5 GPa for 2 to 3 h. In the figure the rates of increase in density are also shown.

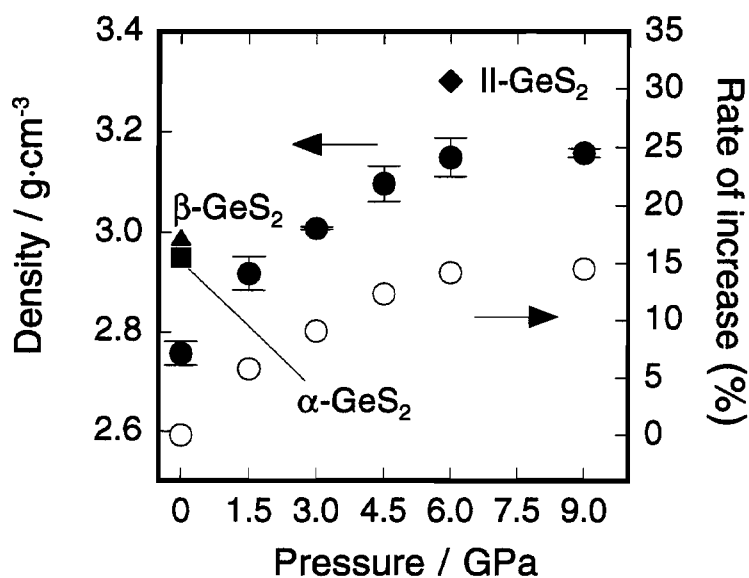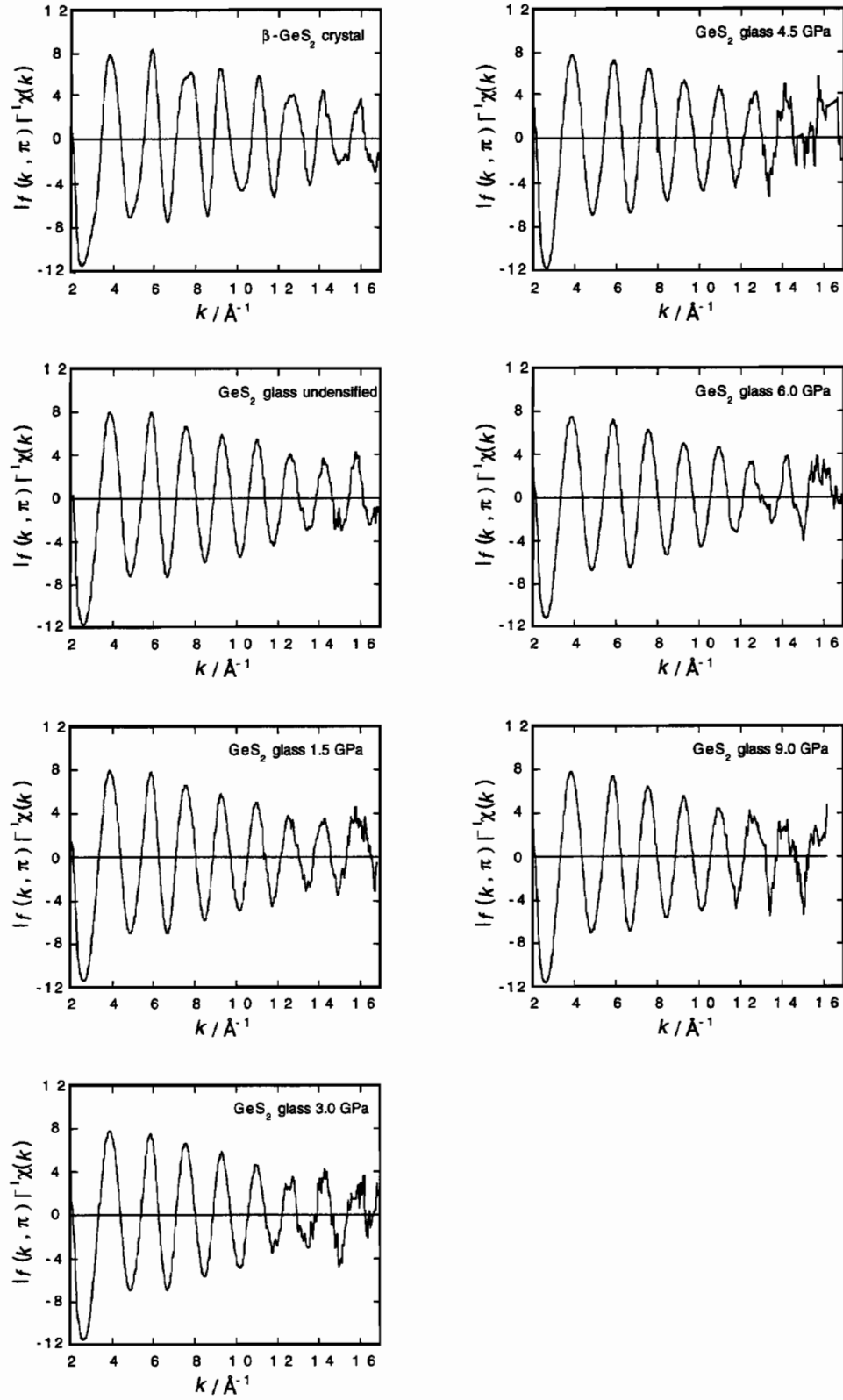Figure 5.1   Pressure dependence of density of GeS_2 glass in permanent densification.

89

Figure 5.2 Ge-K EXAFS oscillation curves of undensified and densified GeS$_2$ glasses and β-GeS$_2$ reference crystal.
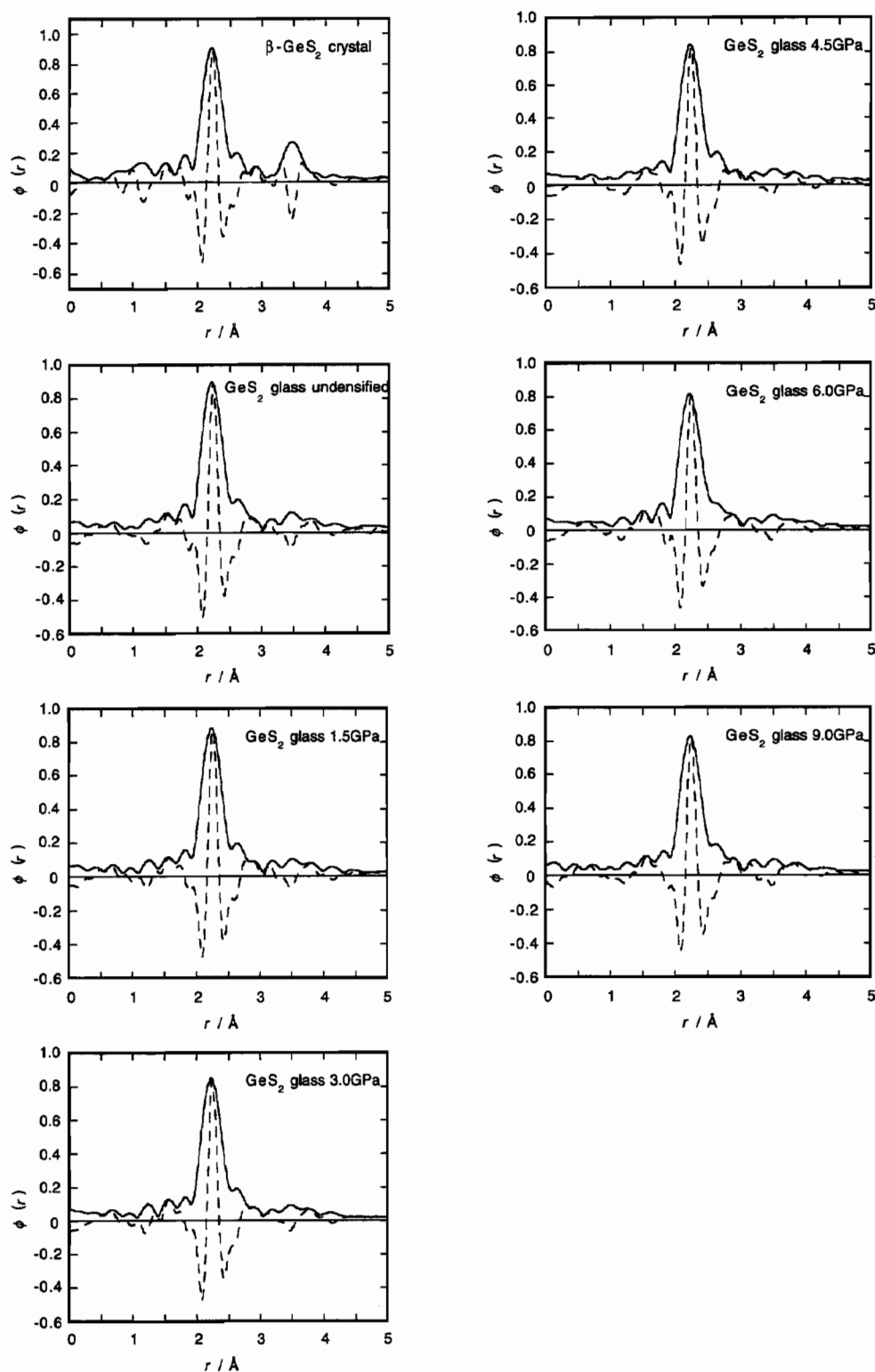
Figure 5.3   Absolute (solid lines) and imaginary (broken lines) parts of Fourier transforms of Ge–K EXAFS oscillation curves of undensified and densified GeS₂ glasses and β-GeS₂ reference crystal.

5.3.2. EXAFS Spectra and Analyses

Figures 5.2 and 5.3 show the Ge–K EXAFS oscillation curves and the absolute and imaginary parts of the Fourier transforms of the undensified and densified GeS$_2$ glasses, together with those of a β-GeS$_2$ reference crystal. The Ge–EXAFS data were analyzed by using a 'Xanadu' program [17]. Detailed procedures of the data analyses will be described in Chapter 7.

The S coordination environments around Ge in the respective glasses, i.e. the Ge–S bond length and the S coordination number of Ge, obtained for the respective glasses are plotted against the applied pressures in Figure 5.4.

Figure 5.4   Pressure dependences of Ge–S bond length (closed circles) and S coordination number of Ge (closed squares) in GeS$_2$ glasses

5.3.3. XANES Spectra

Figure 5.5 shows the S–K XANES spectra of the undensified and densified GeS$_2$ glasses and those of α- and β-GeS$_2$ reference crystals. The combined S–K XANES s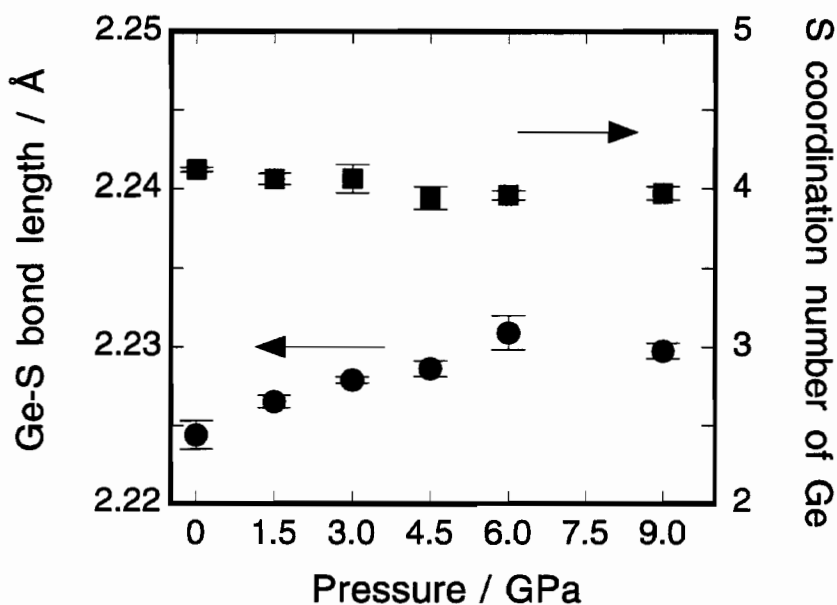pectra of α- and β-GeS$_2$ with given ratios are also shown in order to compare the spectra of undensified and densified GeS$_2$ glasses with those of α- and β-GeS$_2$ reference crystals. In the figure, the combined S-K XANES spectra of α- and β-GeS$_2$ (the broken lines) are calculated by the following equation:

$$\chi(E) = x\chi_\alpha(E) + (1 - x)\chi_\beta(E) \tag{5.1}$$

where χ_α and χ_β are the S–K XANES spectra of α- and β-GeS$_2$, respectively, and x is the fraction of α-GeS$_2$. Mean square deviation between the experimental spectra and the calculated spectra was below 0.018.
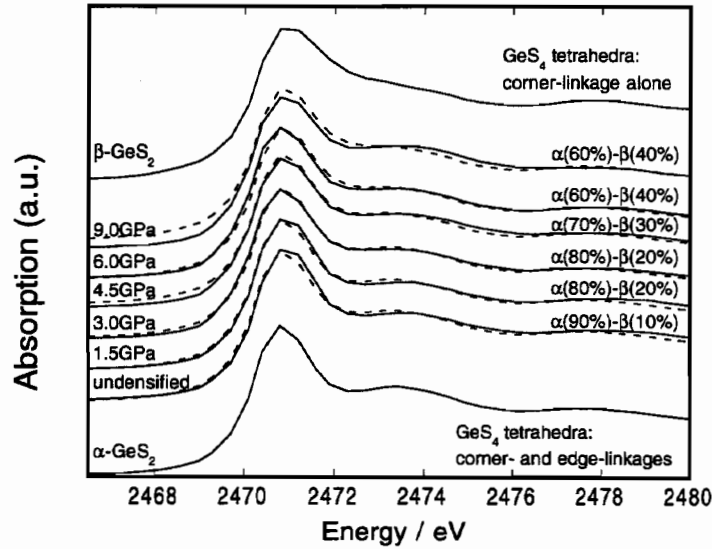
Figure 5.5 Experimental S–K XANES curves (solid lines) of undensified and densified GeS$_2$ glasses and α- and β-GeS$_2$ reference crystals, and S–K XANES curves (broken lines) obtained by combining S–K XANES spectra of α- and β-GeS$_2$ with given ratios.

The Ge–K XANES curves of the undensified and densified GeS$_2$ glasses are shown in Figure 5.6.
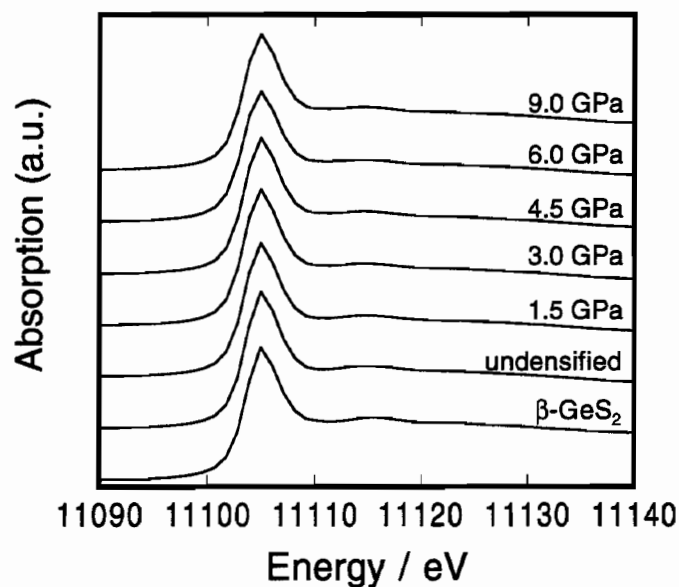
Figure 5.6   Ge–K XANES curves of undensified and densified GeS$_2$ glasses.

5.3.4. X-ray Distribution Functions

Detailed procedures of obtaining radial distribution functions from X-ray diffraction curves have been described elsewhere [10]. The differential radial distribution curves of GeS$_2$ glasses undensified and densified under 1.5 and 6.0 GPa are shown in Figure 5.7.
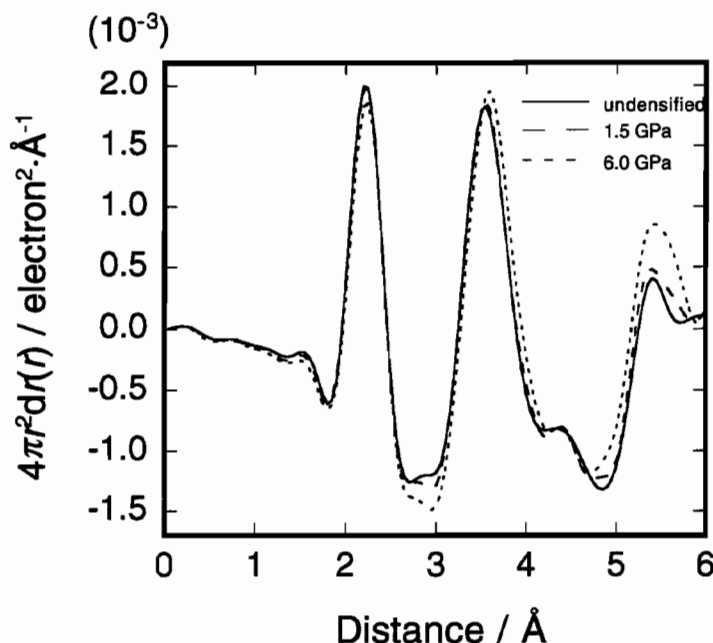
Figure 5.7 Differential radial distribution curves of GeS$_2$ glasses undensified (solid line) and densified under 1.5 GPa (broken line) and 6.0 GPa (dotted line).

5.3.5. Raman Scattering Spectra

The Raman scattering spectra of the undensified and densified GeS$_2$ glasses are shown in Figure 5.8. As indicated in the Raman scattering spectrum of the undensified GeS$_2$ glass in the figure, all the Raman bands are composed of four peaks which are attributed to the totally symmetric stretching and asymmetric stretching vibrations of a GeS$_4$ tetrahedron and the asymmetric bending vibration of Ge–S–Ge [8]. Therefore the peak deconvolution of the respective Raman peaks was performed using four Gaussian functions, as illustrated in the figure.

The peak position and the full width at half maximum (FWHM) of the totally symmetric stretching vibration peak obtained by peak deconvolution are plotted against the applied pressure in Figure 5.9.
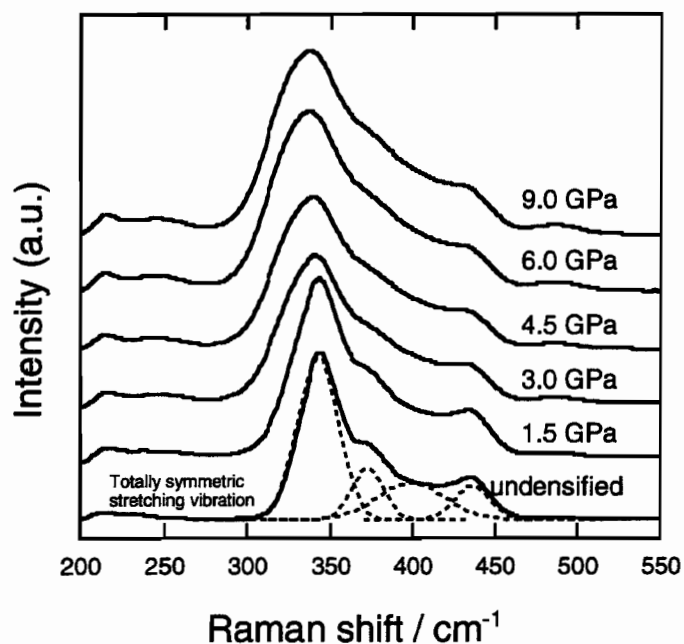
Figure 5.8   Raman scattering spectra of undensified and densified GeS$_2$ glasses.
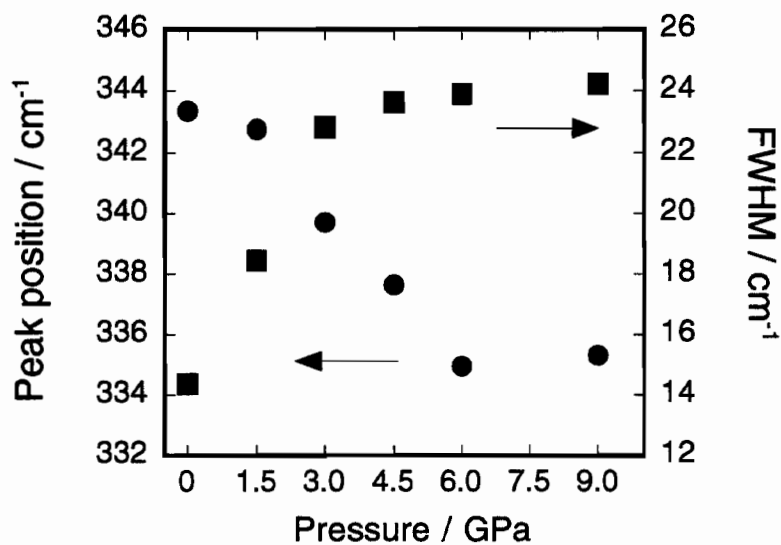
Figure 5.9   Pressure dependences of position (closed circles) and FWHM (closed squares) of totally symmetric stretching vibration peak in undensified and densified GeS$_2$ glasses.

5.3.6. Optical Absorption Edge

Figure 5.10 shows the color change of GeS_2 glass with densification. The optical absorption spectra of the undensified and densified GeS_2 glasses are shown in Figure 5.11. The optical absorption-edge energy of each glass was obtained according to a manner illustrated in the figure. The obtained values are plotted against the applied pressure in Figure 5.12.
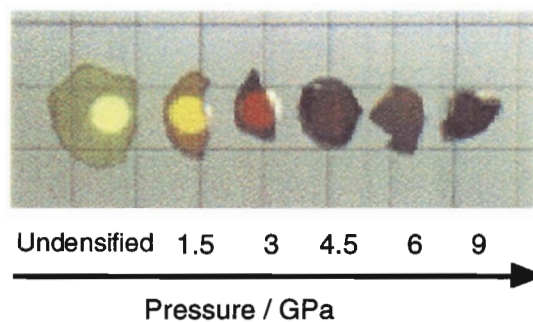
Figure. 5.10   Color change of GeS_2 glass with densification.
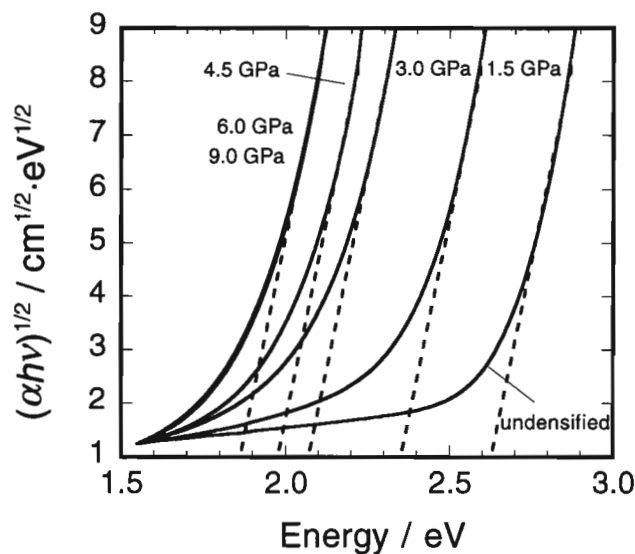
Figure 5.11   Optical absorption spectra of undensified and densified GeS_2 glasses.
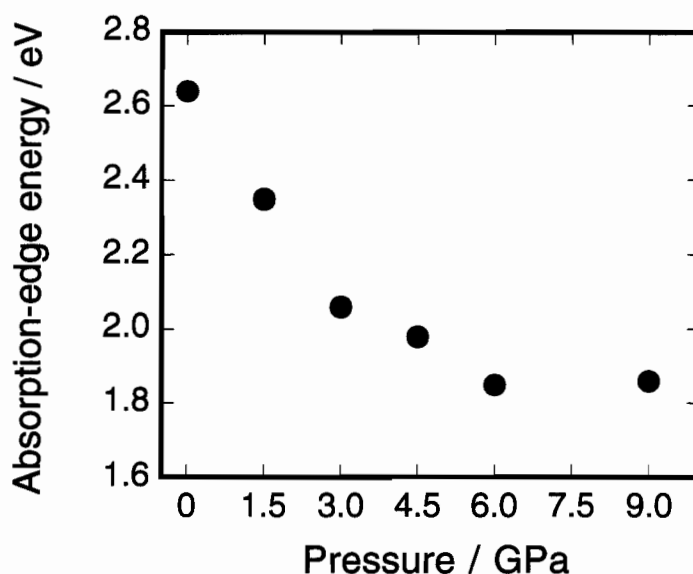
Figure 5.12   Pressure dependence of optical absorption-edge energies in undensified and densified GeS₂ glasses.

5.4. Discussion

Before entering discussion, the structural features of α-, β-, and II-GeS$_2$ crystals are summarized, together with the structure of GeS$_2$ glass at atmospheric pressure, which has been proposed based on various experimental results.

A high-temperature modification of GeS$_2$, α-GeS$_2$, has a two-dimensional network structure (layer structure) with a monoclinic unit cell of a = 6.720 Å, b = 16.101 Å, c = 11.436 Å, and β = 90.88° [13], as shown in Figure 5.13. The layer structure in α-GeS$_2$ consists of chains formed by edge-sharing of corner-linked GeS$_4$ tetrahedra and cross-linked GeS$_4$ tetrahedra to form a two-dimensional network. The presence of edge-shared tetrahedra means that there are pairs of Ge connected by two S

bridging exist. The two kinds of linkage manners produce both six- and four-member ring-structures in a ratio of 2:1.

A low-temperature modification of GeS$_2$, β-GeS$_2$, has a three-dimensional network structure with a monoclinic unit cell of a = 6.875 Å, b = 22.55 Å, c = 6.809 Å, and β = 120.45° [14], as shown in Figure 5.14. In the structure, there are no edge-shared GeS$_4$ tetrahedra like that of SiO$_2$. This three-dimensional network structure is notable in containing large hollows surrounded by twenty-four-member rings composed of corner-shared GeS$_4$ tetrahedra, together with six-member rings.

A high-pressure modification of GeS$_2$, II-GeS$_2$, has a three-dimensional network structure with a tetragonal unit cell of a = 5.420 Å and c = 9.143 Å [12], as shown in Figure 5.15. The network structure consists of six-member rings composed of corner-linked GeS$_4$ tetrahedra only. This structure is analogous to that of a BPO$_4$ crystal with a silica-like structure.
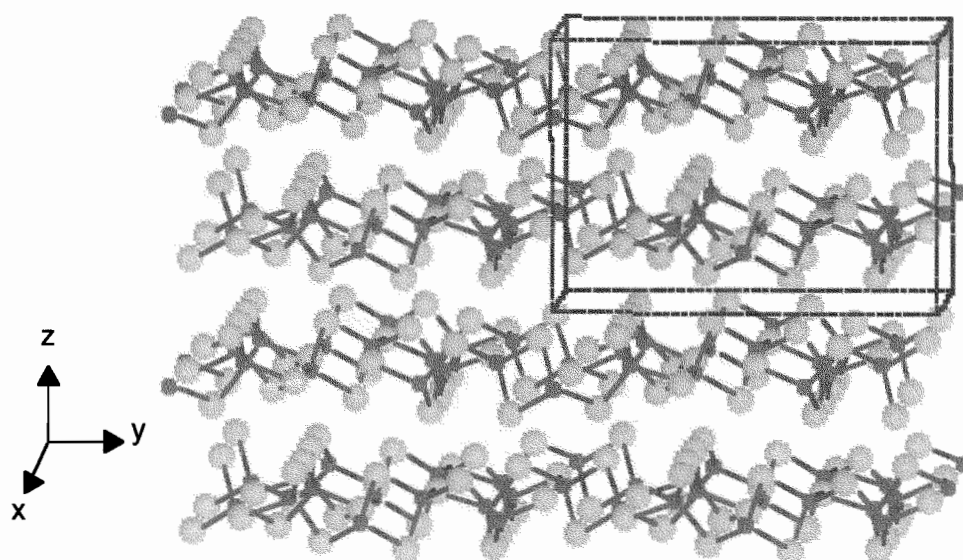
Figure 5.13   Crystal structure of α-GeS$_2$ (high-temperature modification).
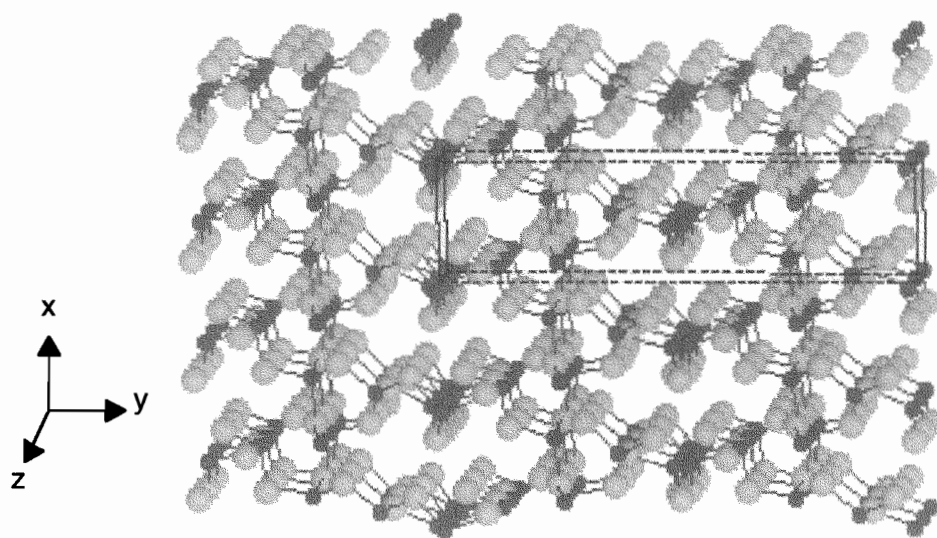
Figure 5.14   Crystal structure of β-GeS₂ (low-temperature modification).
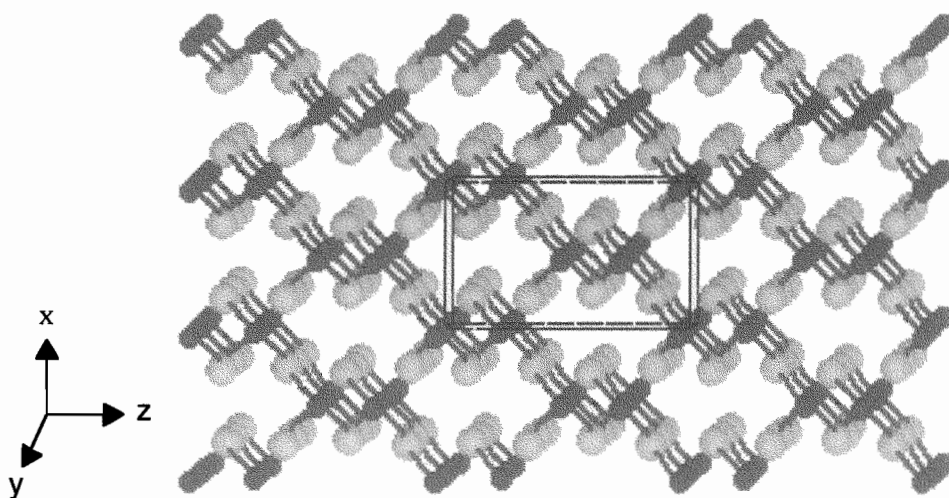
Figure 5.15   Crystal structure of II-GeS₂ (high-pressure modification).

100

The Ge–S, S–S, and Ge–Ge average distances and the S–Ge–S and Ge–S–Ge average bond angles in the α-, β-, and II-GeS$_2$ crystals are summarized in Table 5.1.

At the present stage, on the other hand, the structure of GeS$_2$ glass at atmospheric pressure has been concluded to be an intermediate between the structures of α-GeS$_2$ and β-GeS$_2$. In more detail, the structure is closer to the α-GeS$_2$ structure, judging from a variety of experimental results performed so far [6–11].

Table 5.1   Ge–S, S–S, and Ge–Ge average distances and S–Ge–S and Ge–S–Ge average bond-angles in α-, β-, and II-GeS$_2$ crystals.

Distance or bond angle	α-GeS$_2$	β-GeS$_2$	II-GeS$_2$
Ge–S (Å)	2.21$_7$	2.22$_4$	2.21$_2$
S–S (Å)	3.71$_1$	3.63$_1$	3.61$_3$
Ge–Ge (Å)	2.91$_9$ (in edge-sharing) 3.39$_9$ (in corner-sharing)	3.44$_4$	3.56$_8$
S–Ge–S (°)	109.5	109.4	111.7
Ge–S–Ge (°)	95.7	101.5	107.5

5.4.1. Pressure Dependence of Density

As can be seen from Figure 5.1, the density of GeS$_2$ glass increases monotonously with increasing applied-pressure until 6.0 GPa. Above 6.0 GPa, however, the density appears to approach a constant value in a pressure range from 6.0 to 9.0 GPa. Here it is noteworthy that a tie-line connecting the densities of α- and/or β-GeS$_2$ crystals and that of a II-GeS$_2$ crystal has roughly the same slope as that in the pressure-density dependence in densification of GeS$_2$ glass.

5.4.2. Changes in GeS$_4$ Tetrahedra with Permanent Densification

The pressure dependences of the Ge–S bond length and the S coordination number of Ge in Figure 5.4 indicate the following facts: The Ge–S bond length increases very slightly but definitely with increasing applied-pressure. On the other hand, the S coordination number of Ge seems to be almost constant and four, judging from the inherent uncertainty in coordination number evaluation by EXAFS analysis. A slight increase in the Ge–S bond length is supported by the results of X-ray radial distribution analysis and Raman scattering spectra. In the differential radial distribution functions in Figure 5.7 the first peaks around 2.2 Å are due to the Ge–S pairs. As can be seen from the figure, the peak positions shift very slightly to longer distance sides with densification. The pressure dependence of the peak position of totally symmetric stretching vibration in a GeS$_4$ tetrahedron in Figure 5.9 indicates that the force constants of Ge–S bonds become weaker with densification, proving that the Ge–S bond length becomes longer with increasing applied-pressure.

On the other hand, the FWHM of totally symmetric stretching vibration peak in a GeS$_4$ tetrahedron may be regarded as an indication of an increase in the distribution of Ge–S bond length and/or Ge–S–Ge bond angle. The pressure dependence of FWHM in Figure 5.9 indicates that the distribution of Ge–S bond length and/or Ge–S–Ge bond angle increases with increasing applied-pressure.

From the experimental facts mentioned above, it may be concluded that, in the permanent densification of GeS$_2$ glass, the tetrahedral GeS$_4$ structures are kept, though they are slightly distorted. However the linkage manner of GeS$_4$ tetrahedron may be considered to change with densification.

5.4.3. Changes in Linkage Manner of GeS₄ Tetrahedra

In the linkage of a GeS_4 tetrahedron there are two kinds of manners; corner-sharing (linkage by one S bridge) and edge-sharing (linkage by two S bridges), as mentioned at the beginning of Discussion. The former linkage exists in all GeS_2 modifications; α-, β-, and II-GeS_2, while the latter one is present only in α-GeS_2. As given in Table 5.1, the corner-sharing gives the Ge–Ge average distance of about 3.40Å and the edge-sharing gives that of about 2.92Å.

In the differential radial distribution curves in Figure 5.7, small peaks around 2.9 Å arise from Ge–Ge pairs between two GeS_4 tetrahedra edge-shared by two S bridges. As can be seen from the figure, the magnitude of peak height of 2.9 Å decreases in the order of glass at atmospheric pressure, glass densified under 1.5 GPa and glass densified under 6.0 GPa. This fact indicates that, in the two linkage manners of two GeS_4 tetrahedra, the fraction of edge-sharing decreases with increasing densification, implying a decrease in the α-GeS_2-like structural region. As can be seen from Figure 5.5, the S–K XANES spectral profile changes from almost α-GeS_2 like one to mixed α- and β-GeS_2 like one, indicating that the local symmetry around S changes from α-GeS_2 like one to mixed α- and β-GeS_2 like one, that is, a decrease in the fraction of edge-sharing. This result supports the above consideration. As can be seen from Figure 5.6, on the other hand, changes in Ge–XANES spectral features with densification are hardly discernible, indicating that the GeS_4 tetrahedra structural units are tightly kept and the linkage manners of two GeS_4 tetrahedra give no effects to Ge–XANES spectra.

5.4.4. Changes in Network Structure Composed of GeS$_4$ Tetrahedra

In the differential radial distribution curves in Figure 5.7, peaks at around 3.5 and 5.5 Å increase in both peak-height and peak-area with increasing densification. Such a phenomenon clearly discloses that structural densification in intermediate-range proceeds in high-pressure treatments, causing an increase in density with densification.

Then a possibility of the structural densification in intermediate-range is considered. As mentioned in Section 5.4.3, the short-range structures of densified GeS$_2$ glasses are suggested to progressively change from a mixed α-GeS$_2$-like and β-GeS$_2$-like structure to a β-GeS$_2$-like structure. However the density of β-GeS$_2$ is only about 0.055 g·cm^{-3} higher than that of α-GeS$_2$ [13,14]. This density difference gives no explanation for densification from 2.76 g·cm^{-3} in GeS$_2$ glass at atmospheric pressure to 3.16 g·cm^{-3} in GeS$_2$ glass densified under 9.0 GPa. Here it should be remembered that the structure of β-GeS$_2$ has large hollows surrounded by twenty four-member rings composed of corner-shared GeS$_4$ tetrahedra, together with six-member rings. If these large hollows are collapsed (reorganized to smaller ring structures) and, at the same time, the two-dimensional network structure composed of GeS$_4$ tetrahedra approaches a three-dimensional network structure, then the density of glass of such a structure would be close to that (3.30 g·cm^{-3}) of II-GeS$_2$ of a network structure consisted by six-member rings of corner-linked GeS$_4$ tetrahedra. In order to confirm this speculation, the crystallization behavior of GeS$_2$ glass under the treatment of 6.0 GPa and 600°C was examined. Consequently the GeS$_2$ glass was found to be phase-transformed to a II-GeS$_2$ crystal. This fact supports the above explanation for a change in differential radial distribution curve of GeS$_2$ glass with densification.

5.4.5. Changes in Optical Absorption Edge

As shown in Figure 5.12, the optical absorption edge in the visible region in GeS₂ glass shifted toward lower energies with increasing densification. A similar phenomenon has been observed in optical reflection band in the densification of amorphous SiO_2 [18]. Xu et al. have investigated a relationship between the optical reflection band and the Si–O bond length, Si–O–Si bond angle, and molar volume in several SiO_2 polymorphs. They have concluded that there is a correlation between the optical reflection band and the Si–O bond length and molar volume, but there is no correlation between the optical reflection band and the Si–O–Si bond angle [19]. In the present GeS₂ glass, successive elongation of the Ge–S bond in a GeS₄ tetrahedron with densification was demonstrated, as mentioned in Section 5.4.2. It is noted that the pressure dependence of the optical absorption-edge energy is the same as that observed for density. Therefore the same explanation may be given for the red shift of optical absorption edge of GeS₂ glass with densification. However, the shift with densification in GeS₂ glass is much larger than that of SiO_2 glass. Thus it is doubtful whether the structural changes such as the change in Ge–S bond length induces such a large shift in absorption-edge energies, i.e. bandgap energies, or not. Ar the present stage, therefore, the following mechanism is presumed: The electronic states at the bottom of the conduction band and the top of the valence band in GeS₂ glass are the Ge–S anti-bonding states and the S lone-pair electrons states, respectively [20]. However, it has been known that there exists an imperfection such as E'-center in a GeS₂ glass structure [21], though the electronic state has been cleared yet. By taking into consideration that the imperfection is much affected by pressure treatment, the electronic state of imperfection may be strongly related to the large energy shift with densification in absorption spectra.

5.5. Conclusion

Germanium disulfide glass, GeS_2 glass, was densified under 1.5, 3.0, 4.5, 6.0, and 9.0 GPa at 270°C for 30 min using a 6–8 multi-anvil-type high-pressure apparatus. The densities of permanently densified glasses increased monotonously with increasing applied-pressure until 6.0 GPa and reached a constant value in the pressure range from 6.0 to 9.0 GPa. The structures of undensified and permanently densified GeS_2 glasses were examined by Raman scattering spectroscopy, an X-ray radial distribution analysis, Ge–K EXAFS and XANES spectroscopies and S–K XANES spectroscopy. The structural changes in GeS_2 glass with densification were analyzed from the above experimental results and the structures of α-, β-, and II-GeS_2 crystals.

The following facts were derived: All the densified GeS_2 glasses are composed of GeS_4 tetrahedral units and the Ge-S bond length in the GeS_4 tetrahedra becomes long, though the magnitude is very slight. The structure of GeS_2 glass at atmospheric pressure is situated between that of α-GeS_2 and that of β-GeS_2. With increasing densification the glass structures progressively converted into a II-GeS_2-like structure in which large hollows in β-GeS_2 are collapsed by reorganization of ring-structure.

In densification the red shift of optical absorption edge in the visible region was observed. Changes in both Ge–S bond length and the molar volume are considered to relate to a change in the optical absorption edge. Consequently the mechanism related to an effect of imperfection with densification in GeS_2 glass structure was also presumed.

References

[1] P. W. Bridgman and I. Simon, *J. Appl. Phys.*, **24**, 405 (1953).

[2] S. Sakka and J. D. Mackenzie, *J. Non-Cryst. Solids*, **1**, 107 (1969).

[3] G. Parthasarathy and E. S. R. Gopal, *Bull. Mater. Sci.*, **3&4**, 271 (1985).

[4] R. Zallen, B. A. Weinstein and M. L. Slade, *J. Phys.*, **42**, C4-241 (1981); B. A. Weinstein, R. Zallen, M. L. Slade and J. C. Mikkelsen Jr., *Phys. Rev. B*, **25**, 781 (1982).

[5] Y. Kawamoto and S. Tsuchihashi, *J. Am. Ceram. Soc.*, **52**, 626 (1969); Y. Kawamoto and S. Tsuchihashi, *J. Am. Ceram. Soc.*, **54**, 131 (1971).

[6] W. H. Zachariasen, *J. Chem. Phys.*, **4**, 618 (1936).

[7] S. C. Rowland, S. Narasimhan and A. Bienenstock, *J. Appl. Phys.*, **43**, 2741 (1972).

[8] G. Lucovsky, J. P. deNeufville and F. L. Galeener, *Phys. Rev. B*, **9**, 1591 (1974).

[9] Y. Kawamoto and C. Kawashima, *Mater. Res. Bull.*, **17**, 1511 (1982).

[10] X. Zhao, H. Higuchi and Y. Kawamoto, *Phys. Chem. Glasses*, **39**, 98 (1998).

[11] A. Ibanez, E. Philippot, S. Benazeth and H. Dexpert, *J. Non-Cryst. Solids*, **127**, 25 (1991); P. Armand, A. Ibanez, H. Dexpert and E. Philippot, *J. Non-Cryst. Solids*, **139**, 137 (1992); P. Armand, A. Ibanez and E. Philippot, Nul. Instrum. Meth. *Phys. Res. B*, **97**, 176 (1995).

[12] C. T. Prewitt and H. S. Young, *Science*, **149**, 535 (1965).

[13] G. Dittmar and H. Schäfer, *Acta Crystallogr.*, **B 31**, 2060 (1975).

[14] G. Dittmar and H. Schäfer, *Acta Crystallogr.*, **B 32**, 1188 (1976).

[15] W. Viaene and G. H. Moh, *N. Jb. Miner. Abh.*, **119**, 113 (1973); W. Viaene and G. H. Moh, *N. Jb. Miner. Abh.*, **116**, 283 (1970).

[16] N. Kawai, M. Togaya and A. Onodera, *Proc. Jpn. Acad.*, **49**, 623 (1973).

[17] H. Sakane, T. Miyanaga, I. Watanabe, N. Matsubayashi, S. Ikeda and Y. Yokoyama, *Jpn. J. Appl. Phys.*, **32**, 4641 (1993).

[18] N. Kitamura, K. Fukumi, K. Kadono, H. Yamashita and K. Suito, *Phys. Rev. B*, **50**, 132 (1994).

[19] Y. Xu and W. Y. Ching, *Phys. Rev. B*, **44**, 11048 (1991).

[20] K. Hachiya, *J. Non-Cryst. Solids*, **312-314**, 566 (2002).

[21] K. Arai and H. Namikawa, *Solid State Commun.*, **13**, 1167 (1973).

Chapter 6

High-Energy X-ray Diffraction Study of Permanently Densified GeS₂ Glass

6.1. Introduction

Because an X-ray diffraction study is one of the powerful tools to obtain information on the structure and properties of non-crystalline materials, a number of studies have been performed by many researchers so far. The structures of binary chalcogenide glasses including GeS_2 glass also have been extensively investigated in the 1970's and 1980's using various diffraction techniques [1–3]. However, the resolution in real space of conventional diffraction methods was not sufficient because of a limited range of scattering vectors, Q. To obtain a reliable structural model, diffraction data of high quality in a wide Q range is required, especially for X-rays. In recent years, high-resolution neutron diffraction on a spallation source, anomalous wide-angle X-ray scattering, and high-energy X-ray diffraction on the third generation synchrotron source allow more structural features to be distinguished. Over the past ten years, the structural studies for stoichiometric chalcogenide glasses were carried out using these light sources [4–7].

Structural study on permanently densified GeS_2 glass was carried out by several techniques including a conventional X-ray diffraction method, as described in Chapter 5. As a result it was found that further high-resolution in real space is required

in order to clarify the structure of densified glass in more detail.

In the present study, therefore, measurements of high-energy X-ray diffraction for the undensified and densified GeS_2 glasses are carried out and the structure of each glass are revealed. Then, the mechanism of permanent densification of GeS_2 glass by high-pressure treatment is proposed based on the structural changes.

6.2. Experimental Procedures

6.2.1. Sample Preparation

Germanium disulfide glass, GeS_2, was prepared from metallic Ge (5N purity) and elementary S (JIS special reagent grade) as starting materials. The 5-g batch was melted in an evacuated silica ampoule at 1000°C for 10 h using a rocking furnace and then it was rapidly quenched in air. Detailed procedure was described elsewhere [8]. The prepared glass was annealed at the glass-transition temperature (about 490°C) determined by a DTA analysis.

Permanent densification of the GeS_2 glass was carried out with a 6–8 multi-anvil-type high-pressure apparatus [9]. The specimen was compressed up to 6 GPa with a 0.033 GPa·min^{-1} ascending rate at room temperature. Subsequently the glass was heated up to 270°C within 5 min under 6 GPa and was kept at this temperature for 30 min. After the heating treatment the glass was cooled to room temperature and then the applied pressure was released with a 0.033 GPa·min^{-1} descending rate.

6.2.2. X-ray Diffraction Measurements and Data Analyses

X-ray diffraction measurements were performed with the approval of the Japan Synchrotron Radiation Research Institute (Proposal No. 2002AB0351-ND1-np).

In order to obtain X-ray radial distribution functions of the undensified and densified GeS₂ glasses, the X-ray diffraction measurements were performed with a horizontal two-axis diffractometer installed at SPring-8 bending magnet beamline BL04B2, operated at 8 GeV electron energy. The measurements were carried out in transmission geometry and with an X-ray energy of 61.7 keV obtained by Si(220) reflection. The collected data were corrected using standards programs. In the corrections and normalizations, Ref. 10, 11, 12, and 13 were used for the absorption cross-sections, the incoherent scattering functions, the atomic scattering factors, and the anomalous scattering factors, respectively. Fully corrected data were normalized to Faber–Ziman total structure factor $S(Q)$ [14].

6.3. Results and Discussion

Normalized X-ray scattering intensities $I(Q)$ of GeS₂ glasses undensified and densified under 6 GPa are shown in Figure 6.1. Both of the scattering intensities exhibit significant oscillation that the maximum Q values of approximately 25 Å^{-1} reaches. This value is 9 Å^{-1} larger than that of conventional diffraction carried out in Chapter 5. The coherent scattering intensity of independent atom, $\langle |f(Q)|^2 \rangle$, which was calculated based of the atomic scattering factor, is also shown in the figure.
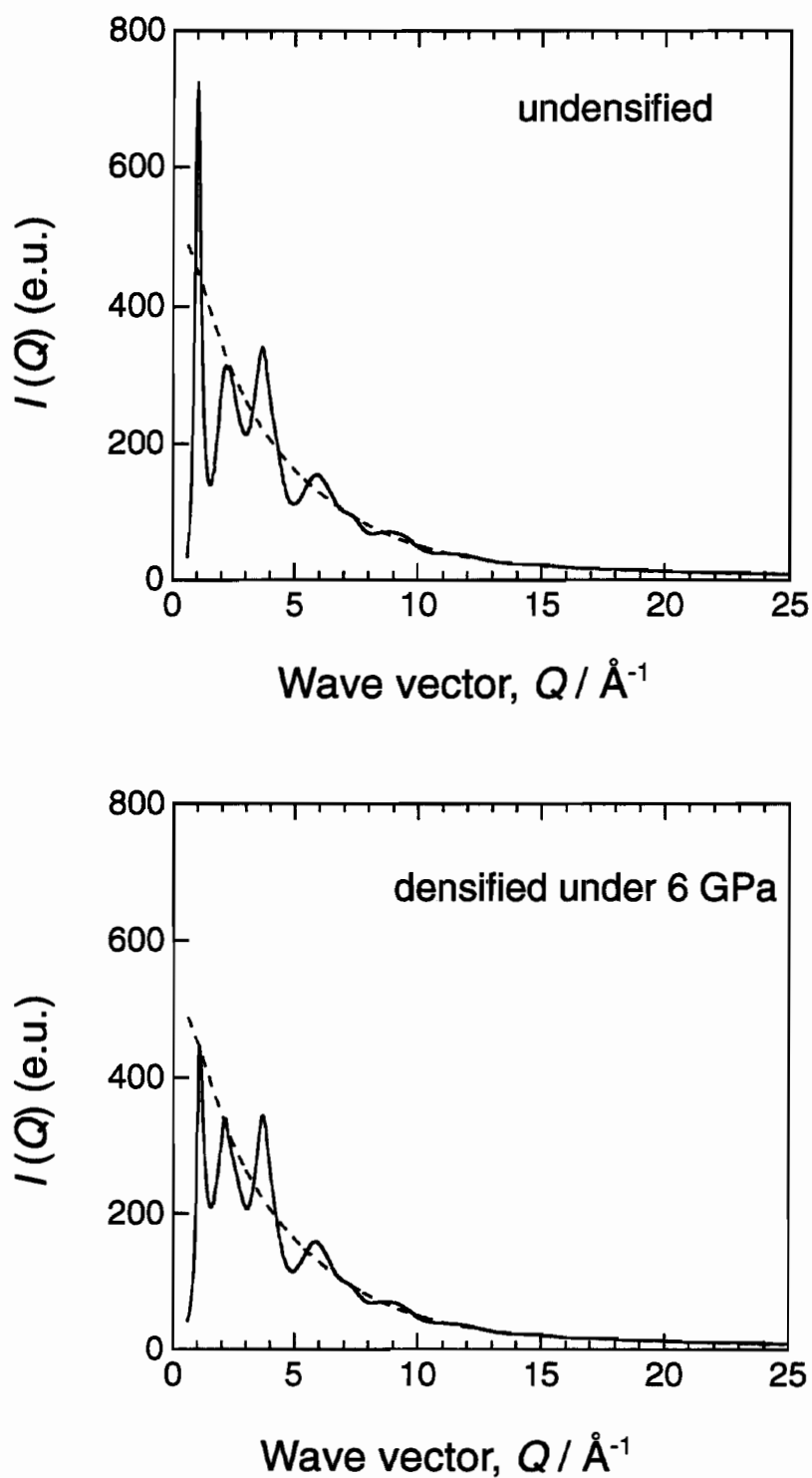
Figure 6.1   Normalized X-ray scattering intensities, $I(Q)$, (solid lines) of undensified and densified GeS_2 glasses and coherent scattering intensities of independent atom, $<|f(Q)|^2>$, (broken lines)

Total structure factors, $Q(S(Q) - 1)$, for GeS$_2$ glasses undensified and densified under 6 GPa are shown in Figure 6.2. As can be seen from the figure, distinct oscillations in the S(Q) can be observed up to 25 Å^{-1}. A remarkable decrease in intensity of the first diffraction peak (FSDP) at 1.03 Å^{-1} occurred. This peak is indicative of a significant intermediate-range order mainly caused by Ge–Ge correlations at 6 – 7 Å [15]. This result is agreed with the structural change model proposed in the previous chapter, that is, the reorganization from large hollows composed of GeS$_4$ tetrahedra to smaller ring-structures. The high Q-range oscillation is similar to each other, compared with low Q-range oscillation, indicating that the intermediate-range structure is largely changed with densification, while the short-range structure is similar to each other.

The X-ray total correlation function, $T(r)$, which is obtained through the Fourier transformation, is

$$T^{X,N}(r) = 4\pi\rho r + \frac{2}{\pi} \int_{Q_{min}} Q \, | \, S^{X,N}(Q) - 1 \, | \sin(Qr) dQ \qquad (6.1)$$

where r is the total number density.

The X-ray total pair-correlation function, $g(r)$,

$$g^{X,N}(r) = T^{X,N}(r) / 4\pi\rho r \qquad (6.2)$$

for each glass is shown in Figure 6.3. The effective radial distribution functions, $N(r)$, derived from

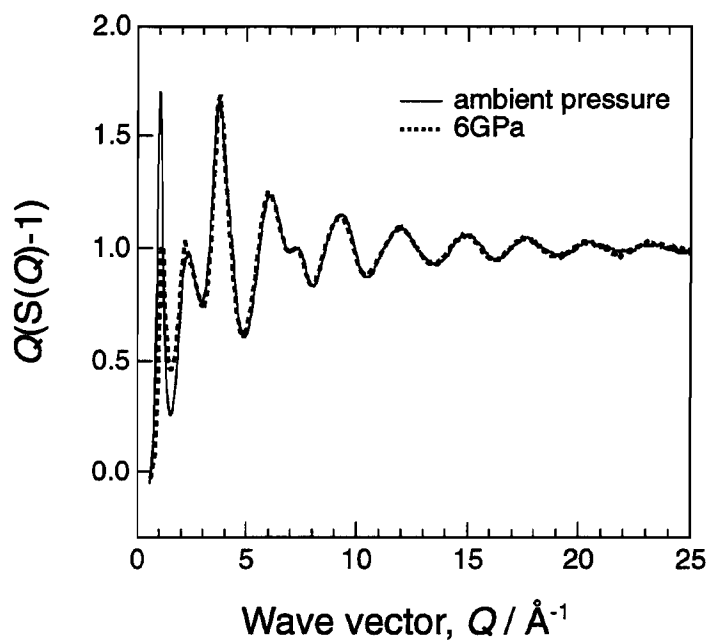$$N^{X,N}(r) = r T^{X,N}(r) \qquad (6.3)$$

are shown in Figure 6.4.

Figure 6.2   Total structure factors, $Q(S(Q) - 1)$, for GeS_2 glasses undensified (solid line) and densified under 6 GPa (dashed line).
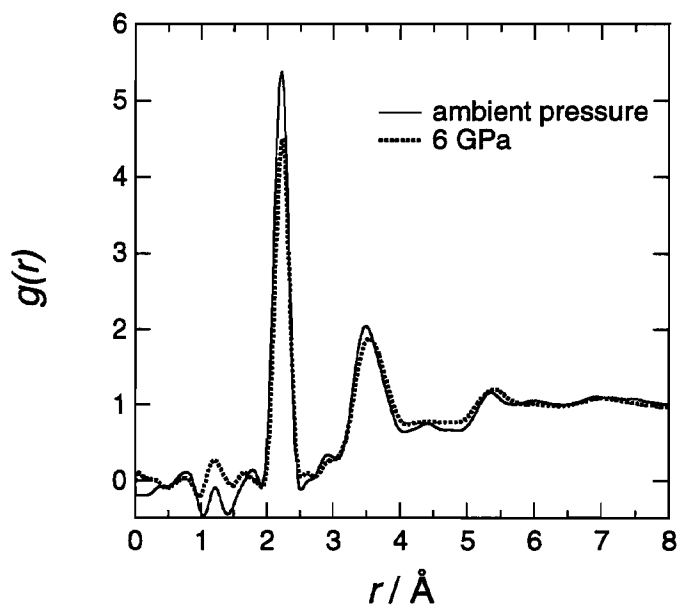

Figure 6.3   X-ray total pair-correlation functions, $g(r)$, for GeS_2 glasses undensified (solid line) and densified under 6 GPa (dashed line).
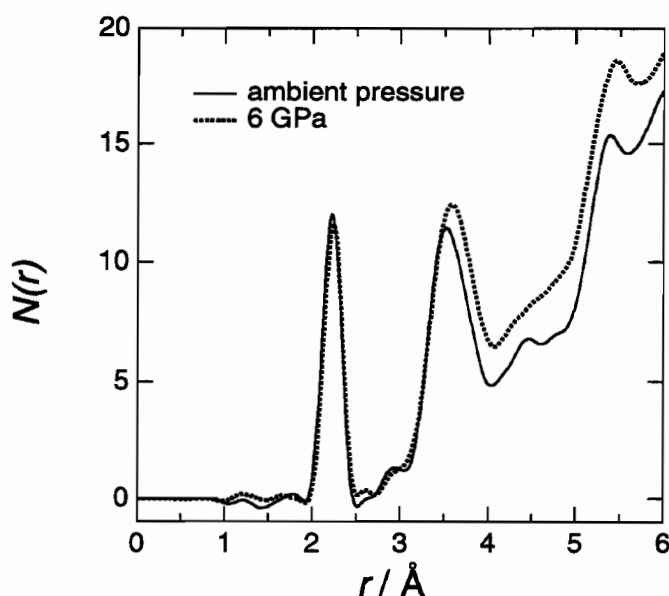
Figure 6.4   Effective radial distribution functions, $N(r)$, for GeS_2 glasses undensified (solid line) and densified under 6 GPa (dashed line).

In the Figure 6.4, the peak at 2.22 Å corresponds to the Ge–S first neighbor correlation in a GeS_4 tetrahedron. This peak position shifted longer side with densification, indicating that the Ge–S bond becomes longer with densification. This result agrees with the results obtained from the Ge–K EXAFS analyses in Chapter 5. The second peak at 2.9 Å corresponds to the Ge–Ge correlation connecting edge-shared GeS_4 tetrahedra. The peak decreased in intensity and becomes broad with densification, indicating that the correlation between Ge–Ge becomes weak. This means that the linkage manner in edge-shared GeS_4 tetrahedra becomes disorder with densification. The third broad peak at 3 – 4 Å corresponds to the Ge–Ge and S–S second neighbor correlations in the corner-shared GeS_4 tetrahedra. This peak is composed of two correlations, but it can be considered to be attributed to be mainly Ge–Ge correlation because the atomic scattering factor of Ge is two times larger than that of S [16]. Therefore, the peak shift indicates that the Ge–Ge distance in corner-shared GeS_4

tetrahedra becomes long. The elongation between the Ge–Ge distances can be considered to occur due to a increase of Ge–S–Ge bond angle. This result also agrees with that of the S–K XANES analysis performed in Chapter 5.

From the above results, it seems that the structure of densified GeS_2 glass has open-structure compared with undensified one. Although this seems a little strange, it can be explained based on the GeS_2 crystal structures. As mentioned in Chapter 5, a GeS_2 crystal has three modifications, i.e., high-temperature modification (α-GeS_2), low-temperature modification (β-GeS_2), and high-pressure modification (II-GeS_2). The structural features of each crystal are summarized in Table 6.1.

Table 6.1   Structural features of GeS_2 crystals.

	α-GeS_2	β-GeS_2	II-GeS_2
Crystal system	Monoclinic	Monoclinic	Tetragonal
Density $(g \cdot cm^{-3})$	2.95	2.99	3.30
S coordination number of Ge	4	4	4
Ge coordination number of S	2	2	2
Ge–S bond length $(Å)$	2.219	2.223	2.212
Ge–Ge distance $(Å)$	3.39 / 2.91	3.44	3.56
Linkage manner	Corner and edge	Corner	Corner
Number of tetrahedron composing ring structures	4 and 6	6 and 24	6
Ge–S–Ge bond angle $(°)$	95.7	101.5	107.5
S–Ge–S bond angle $(°)$	109.5	109.4	111.7

The structure of GeS$_2$ glass is considered to be a random structure of mixing α- and β-GeS$_2$ crystals and the densities of GeS$_2$ glass undensified glass and densified under 6 GPa are 2.76 g·cm^{-3} and 3.15 g·cm^{-3}, respectively. As given in Table 6.1, the Ge–Ge distance of the II-GeS$_2$ crystal is longer than those of the α- and β-GeS$_2$ crystals. On the other hand, the Ge–S–Ge bond angle of II-GeS$_2$ crystal is larger than those of the α- and β-GeS$_2$ crystals. Nevertheless, the II-GeS$_2$ crystal is a dense structure composed of only six-members ring structure, while the α- and β-GeS$_2$ crystals are open-structures due to the two-dimensional layer and the large hollows composed of twenty-four-member ring structure, respectively. These facts mean that, in case of GeS$_2$ compounds, the short-range structure including the linkage of tetrahedral GeS$_4$ should be somewhat open when the network structure is reorganized to dense structure.

In order to clarify the intermediate structural changes such as the reorganization of ring structure, the computer simulation experiments (reverse Monte Carlo method) using both the present diffraction data and the neutron diffraction data is required. Therefore the neutron diffraction measurements are now proceeding.

6.4. Conclusion

The high-energy X-ray diffraction study was carried out in order to investigate the structural change with densification on GeS$_2$ glass using third generation synchrotron radiation as a light source. The total structure factors, $Q(S(Q) - 1)$, for GeS$_2$ glasses undensified and densified under 6 GPa were obtained up to 25 Å^{-1} in the Q-range. The intensity of the first sharp diffraction peak, which corresponds to the Ge–Ge correlation at around 6 – 7 Å in real space, largely decreased with densification, assuming that the reorganization of the ring structures composed of GeS$_4$ tetrahedra

occurs.

The X-ray total pair-correlation functions, $g(r)$, and the effective radial distribution functions, $N(r)$, for GeS_2 glasses undensified and densified under 6 GPa were derived from the total structure factors, $Q(S(Q) - 1)$, of each glass. From these functions, the following facts were found: (1) The first neighbor Ge–S bond length becomes long with densification. (2) The linkage manner in edge-shared GeS_4 tetrahedra becomes disorder with densification. (3) The Ge–Ge distance in the corner-shared becomes long, indicating that the Ge–S–Ge bond angle increased with densification.

The densification mechanism in GeS_2 glass by high-pressure treatment was proposed based on the present results and the structures of three modifications of GeS_2 crystal.

References

[1] Y. Kawamoto and S. Tsuchihashi, *J. Amer. Cera. Soc.*, **54**, 131 (1971).

[2] S. C. Rowland, S. Narasimhan and A. Bienenstock, *J. Appl. Phys.*, **43**, 2741 (1972).

[3] N. Fueki, T. Usuki, S. Tamaki, H. Okazaki and Y. Waseda, *J. Phys. Soc. Jpn*, **61**, 2814 (1992).

[4] S. Susman, K. J. Volin, D. G. Montague and D. L, Price, *J. Non-Cryst. Solids*, **125**, 168 (1990).

[5] P. Armand, A. Ibanez and E. Philippot, *J. Solid State Chem.*, **104**, 308 (1993).

[6] A. C. Hannon and B. G. Aitken, *J. Non-Cryst. Solids*, **256-257**, 73 (1999).

[7] I. Petri, P. S. Salmon and H. E. Fisher, *Phys. Rev. Lett.*, **84**, 2413 (2000).

[8] Y. Kawamoto and S. Tsuchihashi, *J. Amer. Cera. Soc.*, **52**, 626 (1969).

[9] N. Kawai, M. Togaya and A. Onodera, *Proc. Jpn. Acad.*, **49**, 623 (1973).

[10] S. Sasaki, *KEK Report*, National Laboratory for High Energy Physics, Japan, 90-16 (1991).

[11] J. H. Hubbell, Wm. J. Veigele, E. A. Briggs, T. T. Brown, D. T. Cromer and R. J. Howerton, *J. Phys. Chem. Ref. Data*, **4**, 471 (1975).

[12] D. Waasmaier and A. Kirfel, *Acta Crystallogr. A*, **51**, 416 (1995).

[13] S. Sasaki, *KEK Report*, National Laboratory for High Energy Physics, Japan, 83-22 (1984): 88-14 (1989).

[14] T. E. Faber and J. M. Ziman, *Philos. Mag.*, **11**, 153 (1965).

[15] S. C. Moss and D. L. Price, in *"Physics of Disordered Materials"*, edited by D. Adler, H. Fritzsche and S. R. Ovshinsky, (Plenum, New York, 1985), p. 77.

[16] *"International Tables for X-ray Crystallography"*, **4**, 71, (Kynoch Press).

Chapter 7

In-situ EXAFS Study on GeS$_2$ Glass under High-Pressure

7.1. Introduction

In general, when glasses are treated by high-pressure at room temperature or at high temperature, densities of the glasses increase and some extents of the increased densities are kept even after removal of the applied-pressure. Bridgman and Simon found this permanent densification phenomenon of glass for the first time in 1953 [1]. The phenomenon is of great interest from the viewpoint of glass science and technology because changes in glass structure are permanently kept and consequently the optical, electrical, mechanical, and magnetic properties of the glass are largely changed without changing glass composition. So far the phenomenon has been investigated on various kinds of oxide and chalcogenide glasses to develop vitreous materials with new functions and also to elucidate the mechanism of permanent densification. A variety of studies have been carried out to elucidate the mechanism of permanent densification. For example, the structure analyses of permanently densified glasses and of glasses under high-pressure have been performed by means of X-ray diffraction, neutron diffraction, Raman scattering spectroscopy, infrared absorption spectroscopy, and so on [2–4].

More recently the present author et al. have clarified the mechanism of permanent densification behavior of GeS_2 glass by the structural analyses of densified glass, as described in Chapters 5 and 6. However, some ambiguous features have been still remained on the local structural-change around Ge. That is, the Ge–S bond length in GeS_2 glass elongates with permanent densification. However, Perakis et al. [5] have reported that the Ge–S bond length becomes short under high-pressures by *in-situ* Raman scattering spectroscopy.

In the present study the local structural-changes around Ge in GeS_2 glass in the compression and decompression processes are examined by *in-situ* EXAFS method, and the mechanism of densification under high-pressure is investigated.

7.2. Experimental Procedures

7.2.1. Sample Preparation

Germanium disulfide, GeS_2, glass was prepared by using metallic Ge (5N purity) and elementary S (JIS special reagent grade) as starting materials. The batch was melted in an evacuated silica ampoule at 1000°C for 10 h using a rocking furnace and then it was rapidly quenched in air. The prepared glass was annealed at the glass-transition temperature, 490°C, determined by a DTA analysis. No precipitation of crystalline GeS_2 was confirmed by powder X-ray diffraction.

7.2.2. Compression and Heating Treatments

A cubic-type multi anvil press, SMAP 180, installed on BL14B1 at Super Photon ring-8, SPring-8, was used for compression experiments. The prepared GeS_2 glass was powdered and mixed thoroughly with BN powder of pressure-transmission medium. The mixture pressed into pellet was put in a container made of BN. Then the container was put in a high-pressure *in-situ* cell made of amorphous B and epoxy resin. An Au foil, which works as a pressure marker, was also put in the cell separately. Generated pressures were estimated from the Au–Au distances determined by Au L_{III}–edge EXAFS analyses based on the equation of state of Au [6]. Two pieces of graphite plates (0.2 mm thick) were used as a heater. The temperature was measured with a chromel-alumel thermocouple. The construction of high-pressure cell is schematically illustrated in Figure 7.1.
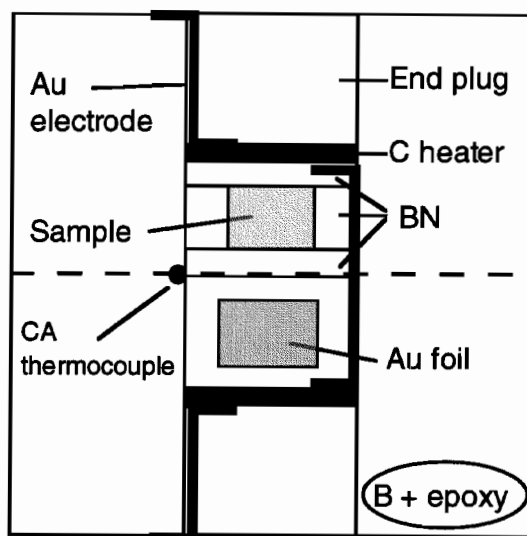

Figure 7.1   Schematic diagram of high-pressure *in-situ* EXAFS cell.

7.2.3. Measurements of X-ray Absorption-Edge Spectra

X-ray absorption measurements were performed with the approval of the Japan Synchrotron Radiation Research Institute (Proposal No. 2001B0473-NX-np).

In order to obtain the EXAFS spectra of Ge K–edge and Au L_{III}–edge, the X-ray absorption spectra of Ge K–edge (11.1 keV) and Au L_{III}–edge (11.9 keV) were measured at a high-pressure station on a bending magnet line, BL14B1, at the SPring-8. X-ray beam was monochromatized using Si(111) reflection. The second mirror vertically focused the X-ray beam. The size of the X-ray beam was reduced to 0.3(H) × 0.3 or 0.05(V) mm² by slits in the experimental station. The intensities of the incident and transmitted X-rays were measured by ionization chambers with flowing gases of N_2 and Ar, respectively. The Ge K–edge and Au L_{III}–edge absorption data were collected in the energy ranges of 10.91 – 12.09 and 11.71 – 12.91 keV, respectively. A β-GeS₂ crystal was used as a reference crystal.

7.2.4. Data Analyses of EXAFS spectra

Analyses of collected EXAFS data were performed using the 'Xanadu' program [7]. After the subtraction of Victoreen-type baselines from the pre-edge regions, EXAFS oscillations, $\chi(k)$, were extracted using cubic spline functions. Fourier transformation was carried out for the normalized $\chi(k)$ spectra in the region of $k = 3 – 14$ Å⁻¹ for each spectrum. Absolute parts, $|\phi(r)|$, of the Fourier transformations are shown in Figure 7.2. The prominent peaks located at around 2.2 Å are assigned to Ge–S bonds. These peaks were filtered in the region from 1.90 to 2.57 Å and inversely Fourier-transformed into k-space. The least-squares fittings in the k-space were carried out for the inversely Fourier-transformed curves using the following single scattering EXAFS formula:

$$\chi(k) = \sum_j \frac{N_j}{R_j^2 k_j} \mid f_j(k_j) \mid \exp\left[-2\left(\sigma_j^2 k_j^2 + \frac{R_j}{\lambda}\right)\right] \sin\{2k_j R_j + \delta_j(k)\} \qquad (7.1)$$

where N_j, R_j, σ_j, and λ_j are the coordination number, the interatomic distance, the Debye-Waller factor, and the mean free path of photoelectron of the jth coordination shell, respectively; $f_j(k)$ and $\delta_j(k)$ are the theoretically calculated backscattering amplitude and the total phase shift, respectively [8]. The photoelectron wave vectors, k and k_j, are defined by

$$k = \left\{\frac{2m_e}{h^2}\left(E - E^{\text{exp}}\right)\right\}^{1/2} \qquad (7.2)$$

and

$$k = \left(k^2 - \frac{2m_e}{h^2}\Delta E_j\right)^{1/2} \qquad (7.3)$$

where m_e and h are the mass of the electron and the Plank constant, respectively, and E and E^{exp} are the X-ray photon and experimental threshold energies, respectively.

The curve-fitting analyses were performed using a one-shell model with σ, λ, and ΔE as variable parameters for reference crystal, β-GeS$_2$. For glasses, N, R, and σ were used as variable parameters and ΔE and λ were kept fixed at the values determined in the least-squares curve-fitting of the reference crystal. Figure 7.3 shows the inversely Fourier-transformed curves and the results of the least-squares curve-fitting for a GeS$_2$ glass at ambient pressure.
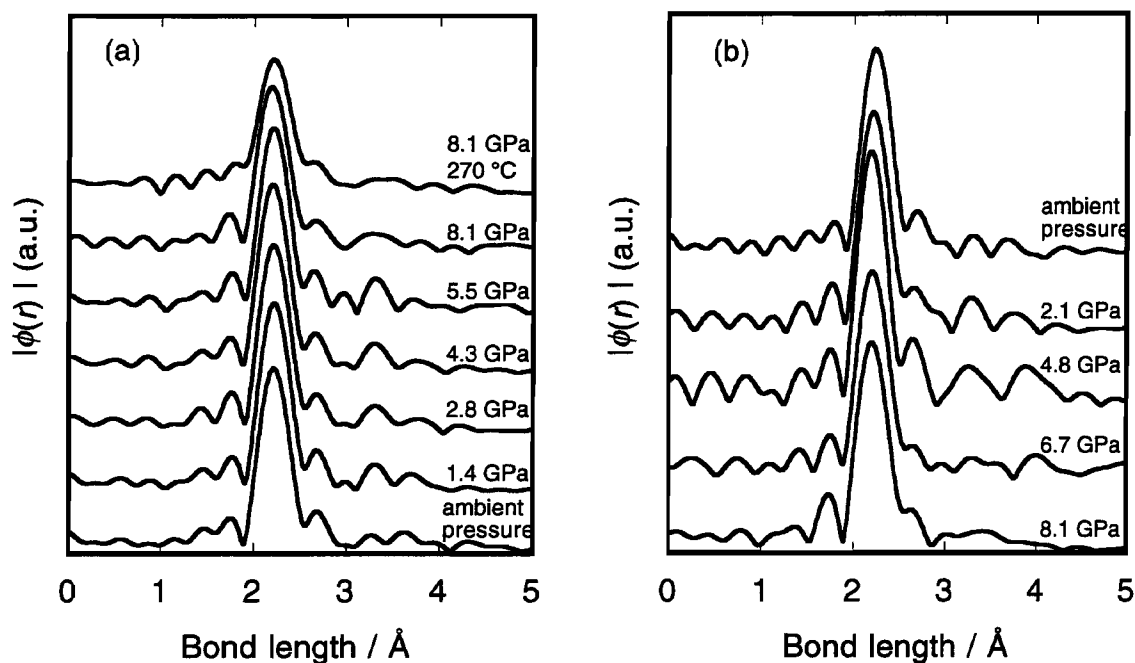
Figure 7.2   Absolute parts, $|\phi(r)|$, of Fourier-transformed $\chi(k)$ curves of GeS₂ glass in compression (a) and decompression (b) processes.
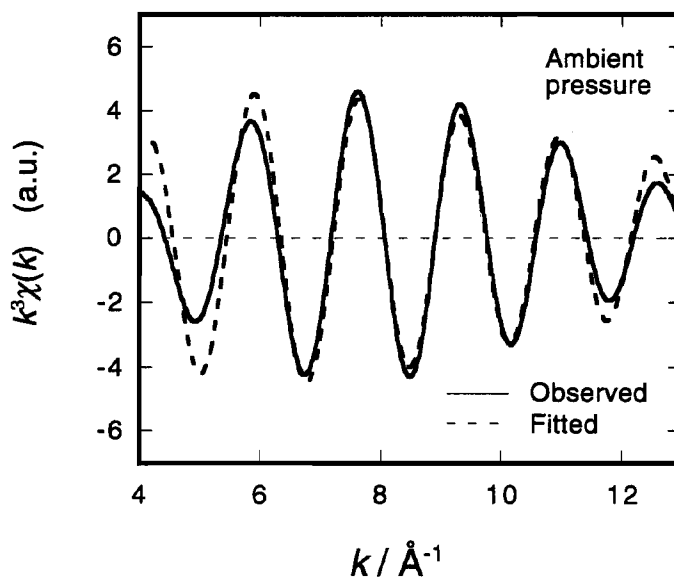

Figure 7.3   Inversely Fourier-transformed curve, $k^3\chi(k)$, (solid line) and least-squares fitted curve (dashed line) for GeS₂ glass at ambient pressure.

7.3. Results and Discussion

The S coordination numbers of Ge under the respective applied-pressures are plotted in Figure 7.4. As can be seen from the figure, large changes such as a 4–6 coordination transition were not found in the present pressure region. The coordination numbers were almost constant values around four, though these became significantly small in heating up to 270°C under 8 GPa. From this result the structural unit in the GeS_2 glass, a GeS_4 tetrahedron, is considered to be tightly maintained during compression and decompression processes.
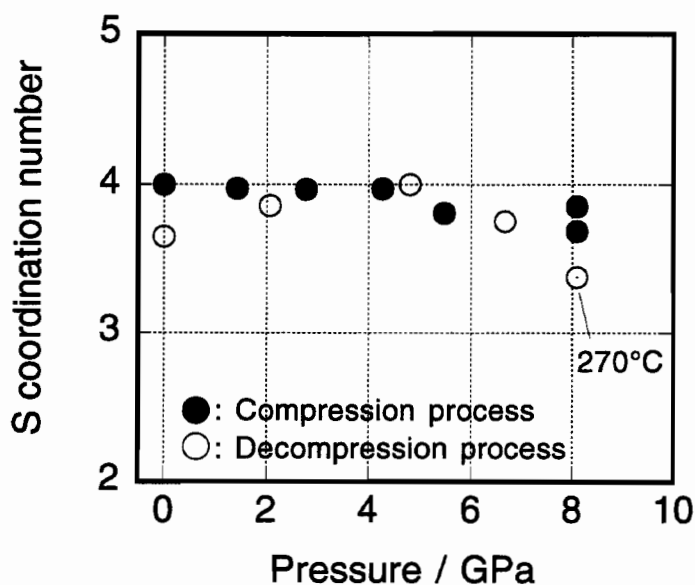

Figure 7.4   Pressure dependence of S coordination number of Ge in GeS_2 glass.

The pressure dependence of Debye-Waller factor, σ, is shown in Figure 7.5. The σ value is related to the thermal vibration and distortion of geometrical structure around absorption atom [9]. As can be seen from the figure, the σ value slightly increased with applied-pressure above 6 GPa and then largely increased at 270°C under 8 GPa. However, this change was reversible after releasing applied-pressure. This indicates that the GeS_4 tetrahedra are slightly distorted above 6 GPa and the distortion of tetrahedral is released with releasing applied-pressure. The large increase of σ at 270°C under 8 GPa may be explained by thermal effect.
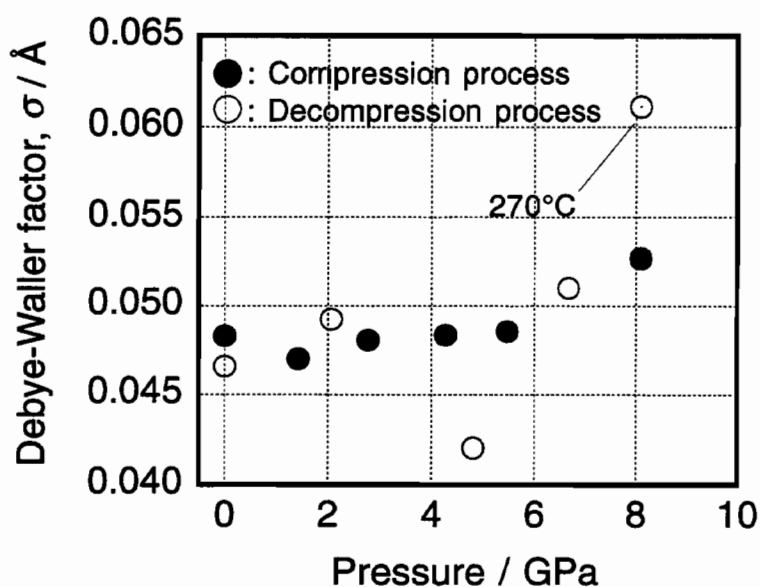
Figure 7.5 Pressure dependence of Debye-Waller factor, σ, in GeS_2 glass.

Figure 7.6 shows the pressure dependence of the Ge–S bond length during the compression and decompression processes. As can be seen from the figure, the bond length became monotonously short with increasing applied-pressure up to 8 GPa. In heating up to 270°C under 8 GPa, the bond length became slightly long. The elongated bond length was almost kept even after the sample was cooled down to room temperature. In decompression process, the bond length became gradually long with releasing applied-pressure down to 2 GPa, following the change in the compression process. However, it largely elongated below 2 GPa, and the final bond length, 2.234 Å, was longer than the initial one, 2.225 Å.
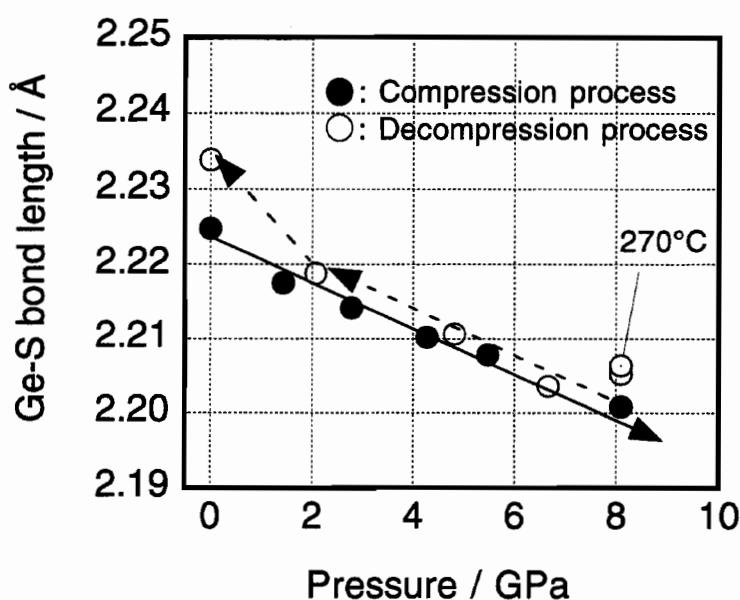

Figure 7.6   Pressure dependence of Ge–S bond length in GeS₂ glass. Lines are guides for eyes.

The fact that the Ge–S bond length elongates after releasing applied-pressure agrees with the previous results described in Chapters 5 and 6. Two types of structural-changes, i.e. elastic and inelastic structural-changes, may be considered to occur due to high-pressure treatment. In the case of GeS_2 glass, the structural-change in GeS_4 tetrahedra is an elastic one, and the structural-change in intermediate-range network structure (the collapse of large ringed-hollows composed of corner-linked GeS_4 tetrahedra) is an inelastic one. When pressure is applied, the GeS_4 tetrahedra are compressed, making the Ge–S bond length short, and at the same time, intermediate-range structure is also compressed, making the Ge–S bond length long. The reason why the latter change occurs is because the structures of densified GeS_2 glasses have much more geometrical restriction than that of an undensified GeS_2 glass and resulting that the GeS_4 tetrahedron is affected by structural-change around itself. Consequently the balance between these two opposite effects decides the Ge–S bond length. In the compression process, the two effects occur at the same time and the Ge–S bond length becomes short due to a strong compression effect. In the decompression process, however, a compression effect becomes weaker with releasing applied-pressure, while the effect of intermediate-range change is retained without structural relaxation. As a result, the elongation of the Ge–S bond length occurs after releasing applied-pressure.

7.4. Conclusion

The local structural-changes around Ge in GeS_2 glass were investigated under high-pressures up to 8 GPa by an *in-situ* EXAFS method. No significant change of S coordination number of Ge was found through compression and decompression processes up to 8 GPa, indicating that the structural unit, a GeS_4 tetrahedron, was tightly

maintained during compression and decompression processes. The Ge–S bond length monotonously decreased with applied-pressure during compression process. In the decompression process, it gradually elongated with releasing pressure down to 2 GPa, following a change in compression process. However, it largely elongated below 2 GPa, being longer than the initial one. This change was explained by a combined effect of elastic and inelastic structural-changes against the applied pressure.

References

[1] P. W. Bridgman and I. Simon, *J. Appl. Phys.*, **24**, 405 (1953).

[2] J. Arndt, *Phys. Chem. Glasses*, **24**, 104 (1983).

[3] B. A. Weinstein, R. Zallen, M. L. Slade and J. C. Mikkelson Jr., *Phys. Rev. B*, **25**, 781 (1982).

[4] R. M. Kimmel and D. R. Uhlmann, *Phys. Chem. Glasses*, **10**, 12 (1983).

[5] A. Perakis, I. P. Kotsalas, E. A. Pavlatou and C. Raptis, *Phys. Status Solidi*, **b 211**, 421 (1999).

[6] J. C. Jamieson, N. N. Fritz and M. H. Manghnani, in *"High Pressure research in Geophysics"*, edited by S. Akimoto and M. H. Manghnani, (Center for Academic Publication, Tokyo, 1982), p. 27.

[7] H. Sakane, T. Miyanaga, I. Watanabe, N. Matsubayashi, S. Ikeda and Y. Yokoyama, *Jpn. J. Appl. Phys.*, **32**, 4641 Prat I (1993).

[8] A. G. McKale, B. W. Veal, A. P. Paulikas, S. K. Chan and G. S. Knapp, *J. Am. Chem. Soc.*, **110**, 3763 (1988).

[9] B. K. Teo, in *"EXAFS: Basic Pronciples and Data Analysis"*, (Springer, Berlin, 1986).

Chapter 8

High Pressure Densification and Thermal Relaxation Behavior of GeS₂ Glass

8.1. Introduction

When a glass is treated under high pressures at high temperatures or at room temperature, the density increases and the densified state is permanently kept even after removal of the applied pressures. This permanent densification phenomenon of glass, which was demonstrated for the first time by Bridgman and Simon in 1953 [1], is of great interest from the viewpoint of glass science and technology, because the changes in glass structure are permanently kept at ambient pressure, and consequently the physicochemical properties of the glass, e.g. the optical, electrical, and mechanical properties, can be changed without changing glass composition. In addition, treating the glass under appropriate pressures and temperatures can control the properties of glass [2,3]. So far this phenomenon has been investigated on various kinds of oxide and chalcogenide glasses to develop vitreous materials with new functions and to elucidate the mechanism of permanent densification. Several kinds of studies have been carried out to elucidate the mechanism of permanent densification, for example, the structural analyses of the permanently densified glasses and of the glasses under high pressure by means of X-ray diffraction, neutron diffraction, Raman scattering spectroscopy and

infrared absorption spectroscopy [4–6]. The relaxation behavior analyses of permanently densified glasses in thermal annealing have been also carried out [7–9].

Recently the present author et al. have clarified the structure of permanently densified GeS_2 glass as described in Chapters 5 and 6, and the structural changes through compression and decompression processes have also examined, as described in Chapter 7. The purpose of this study is to elucidate the mechanism of permanent densification phenomenon of GeS_2 glass by examining the relaxation behavior in thermal annealing.

8.2. Experimental Procedure

Germanium disulfide, GeS_2, glass sample was prepared from metallic Ge (5N purity) and elementary S (JIS special reagent grade) in an evacuated silica ampoule at 1000°C for 10 h using a rocking furnace. The melt of the elements was rapidly quenched in air. Then the prepared glass was annealed at the glass-transition temperature, 490°C, determined by a DTA analysis. No precipitation of GeS_2 crystal was confirmed by powder X-ray diffraction.

Permanent densification of the GeS_2 glass was carried out under 6 GPa at 270°C with a 6–8 multi-anvil-type high-pressure apparatus [10]. Detailed procedures of the high pressure and high temperature treatments have been described in Chapter 2.

Thermal relaxation treatments of the permanently densified GeS_2 glasses were carried out at 100°C, 125°C, 150°C, 200°C, and 300°C *in vacuo* for a total time of 128 h.

The densities of glasses were measured by the Archimedes method using CCl_4 as an immersion liquid. The experimental error in density measurements was about

$\pm 0.005 \text{ g·cm}^{-3}$.

Raman scattering spectra of the permanently densified GeS₂ glass, which was thermally annealed at 100°C, were measured in the wavenumber range from 200 to 600 cm⁻¹ at room temperature in a back-scattering geometry using a Perkin-Elmer 2000NIR FT-Raman spectrometer. A Nd:YAG laser ($\lambda_{emission}$ = 1064 nm) with 500 mW incident power and an InGaAs crystal were used as an excitation source and a detector, respectively.

In order to obtain the EXAFS spectra of Ge–K, the X-ray absorption spectra near the Ge K–edge were measured at Beam Line 10B in Photon Factory, the National Laboratory for High Energy Physics (Tsukuba). The measurements were performed under the approval of the Photon Factory Program Advisory Committee (Proposal No. 99G054). In the measurements, two flat Si(311) crystals were used as monochromators, and absorption data were collected in the energy range from 10859 to 12409 eV. The measurements were made for the permanently densified GeS₂ glass, which was thermally annealed at 100°C, and also for β-GeS₂ crystal as a reference.

Optical absorption spectra of the permanently densified GeS₂ glass, which was thermally annealed at 100°C, were measured at room temperature with a HITACHI U-3500 spectrophotometer in the wavelength range from 400 to 1200 nm. Prior to the measurements the samples were polished to optical quality with 0.9 mm in thickness.

8.3. Results and Discussion

8.3.1. Densities

The density of undensified GeS_2 glass was 2.759 g·cm^{-3}. The density increased about 14.2% ($\Delta\rho/\rho$) after the treatment under 6 GPa at 270°C.

Figure 8.1 shows the relationship between the density-relaxation and the annealing-time in isothermal annealing of the permanently densified GeS_2 glass at several different temperatures. As can be seen from the figure, the density of each sample rapidly decreases at the early stage of the thermal annealing and then gradually decreases toward given values depending on the annealing temperature. These non-exponential decays of density against the annealing time can not be fitted by a normal relaxation function. This type of decay is satisfactorily expressed by the following stretched exponential relaxation function [8,9]:

$$\Phi(T, t) = \exp\{-(t/\tau_{\text{eff}})^{\beta}\}, \tag{8.1}$$

where $\Phi(T, t)$ is the relaxation function defined by

$$\Phi(T, t) = (\rho(T, t) - \rho_{\infty})/(\rho_0 - \rho_{\infty}), \tag{8.2}$$

where ρ_{∞} and ρ_0 are the densities of an undensified (or fully relaxed) glass and an unrelaxed glass before thermal annealing, respectively. The $\rho(T, t)$ is the density after annealing at T K for t hours, and β is a constant value associated with the relaxation process and the τ_{eff} is an effective relaxation time.

Double logarithm of the relaxation function, $\ln(-\ln\Phi)$, is plotted against annealing time in Figure 8.2. As can be seen from the figure, the samples thermally treated below 150°C were fitted by two straight lines with different slopes. This means that the thermal relaxation process of permanently densified GeS_2 glass has two

relaxation processes with different activation energies. For convenience, these two relaxation processes are referred to as the fast relaxation process and the slow relaxation process, respectively. The fast relaxation process occurred at first and then the slow relaxation process proceeded. For the samples treated above 200°C, the fast relaxation process has been already completed on this time scale.

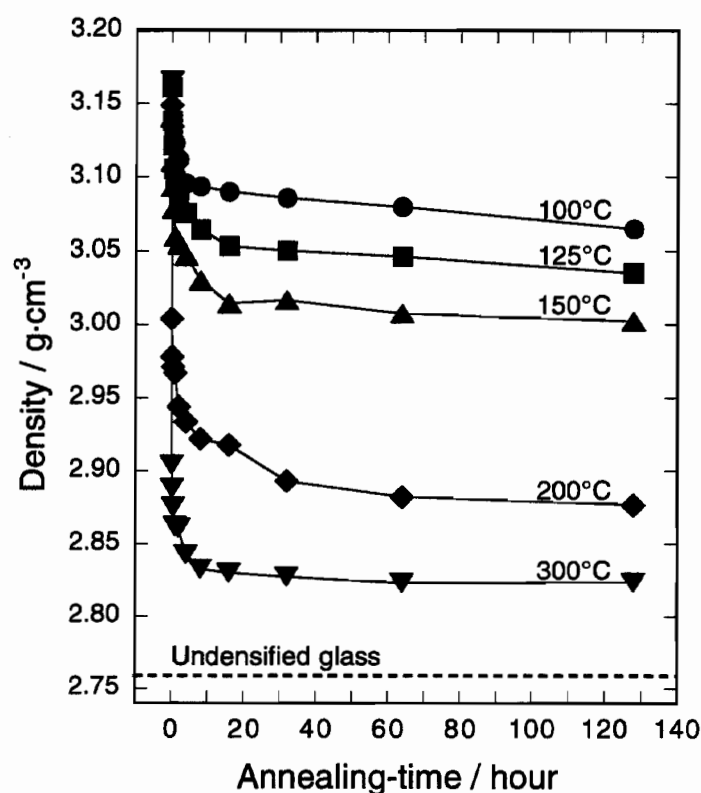

Figure 8.1. Relationship between density-relaxation and annealing-time in isothermal annealing of densified GeS_2 glasses at several different temperatures. Broken line indicates density value of undensified GeS_2 glass.
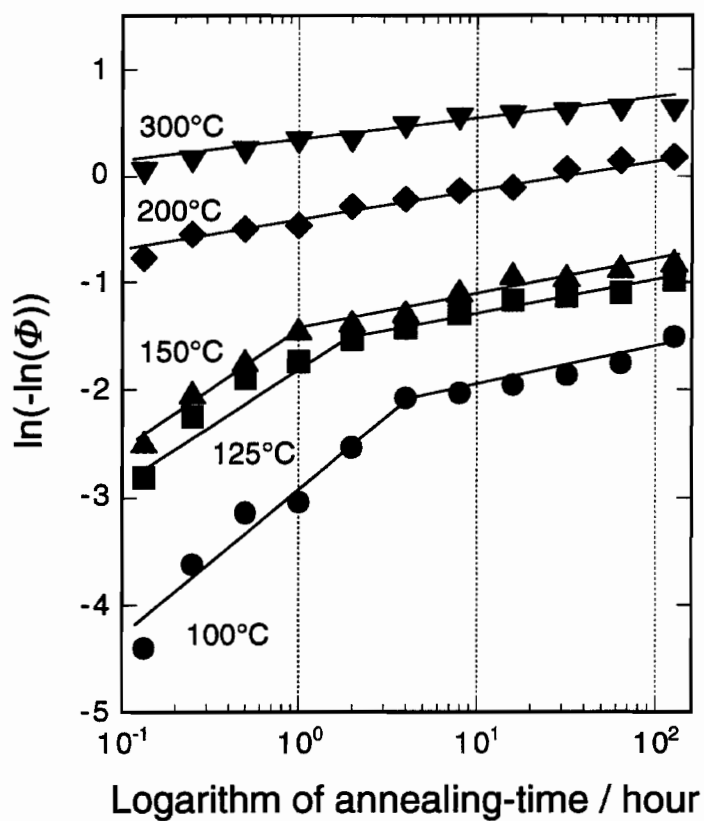
Figure 8.2   Double logarithm of relaxation-function, $\ln(-\ln\Phi)$, vs. annealing-time for densified GeS_2 glass.

8.3.2. Activation Energies

The optimized parameters, β and τ_{eff}, which were obtained by fitting the data using Equation 8.1, are listed in Table 8.1. As given in the table, the β values of both relaxation processes are independent of annealing temperature and keep constant values in each relaxation process. On the other hand, the τ_{eff} values satisfy the Arrhenius equation:

$$\tau_{eff} = \tau_0 e^{E/RT} \tag{8.3}$$

where E and R are an activation energy and the gas constant, respectively, and τ_0 is a constant. The effective relaxation times for the fast and slow relaxation processes are plotted against the annealing temperature in Figure 8.3. Equation 8.3 was fitted to the data points by the least-squares method. The activation energies obtained for the fast and slow relaxation processes were about 51 and 165 kJ·mol^{-1}, respectively. This indicates that the activation energy of the slow relaxation process is larger than that of the fast one, and these values are small compared with the bond energies between the constituent elements, i.e. Ge–S: 285 kJ·mol^{-1}, Ge–Ge: 192 kJ·mol^{-1}, S–S: 282 kJ·mol^{-1} [11]. Therefore, the following three can be assumed: (1) The structural change during the slow relaxation process needs more larger energy than that of the fast one. (2) No breaking of the bonds between constituent elements occurs. (3) Only a release of the strain caused by densification occurs in both the relaxation processes.

Table 8.1. Optimized β and τ_{eff} parameters in stretched exponential relaxation function for permanently densified GeS_2 glasses annealed at several different temperatures.

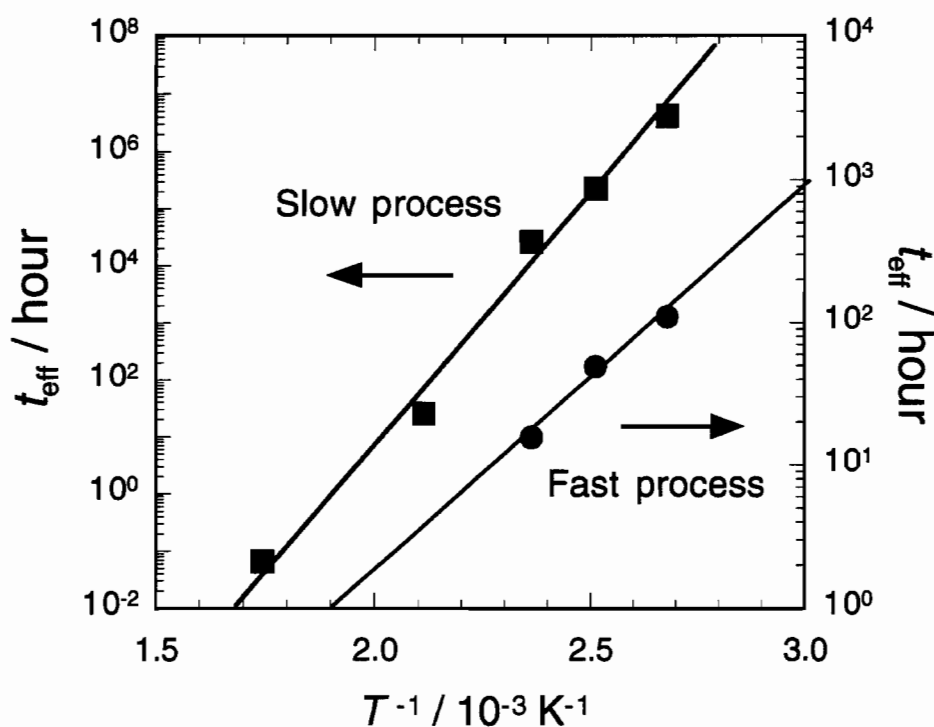| Annealing temperature (°C)	Fast relaxation process		Slow relaxation process	
	β	τ_{eff} (h)	β	τ_{eff} (h)
100	0.62	1.10×10^2	0.15	4.10×10^6
125	0.45	4.93×10	0.13	2.22×10^5
150	0.51	1.56×10	0.14	2.58×10^4
200	-	-	0.13	2.51×10
300	-	-	0.10	6.54×10^{-2}

Figure 8.3. Temperature dependence of effective relaxation time for densified GeS_2 glass in fast and slow relaxation processes.

8.3.3. Structural Relaxation

Here the structural changes of GeS₂ glass caused by densification, which were clarified in the previous studies, are summarized. When a GeS₂ glass is treated by the high-pressure and high-temperature, the following three structural changes occur. (1) Elongation of the Ge–S bond length. (2) Change in the Ge–S–Ge bond angles. (3) Disappearance of the large hollows in the glass network structure, which is accompanied by the transition from the α (high-temperature modification)- and β (low-temperature modification)-GeS₂ like crystal structures to the II (high-pressure modification)-GeS₂ like crystal structure. The disappearance of hollows is considered to be a main reason for densification. The details have been described in Chapters 5 and 6.

As described in Section 8.3.1, the fast and slow relaxation processes are present in the relaxation process of densified GeS₂ glass. In the case of the sample treated at 100°C, the fast relaxation process occurs until 4 h and finished at this point and then the slow relaxation process proceeds. In order to investigate the origin of structural relaxation which occurred during both relaxation processes, the Raman scattering spectra and Ge–K EXAFS measurements were performed on the samples annealed at 100°C. The Raman scattering spectrum of densified GeS₂ glass, i.e. no-annealed glass, is shown in Figure 8.4. As can be seen from the figure, five peaks overlap each other. Therefore, curve-deconvolution was carried out to obtain the accurate peak position and the full width at half maximum (FWHM) of the totally symmetric stretching vibration of GeS₄ tetrahedra, ν_1, which locates around 335 cm^{-1} [12]. The peak positions and the FWHMs of the thermally treated samples are plotted against the annealing time in Figure 8.5. As can be seen from the figure, no changes are occurred in the peak positions during the fast relaxation process, however, these shift to higher energies at the beginning stage of the slow relaxation process and then these keep constant values during the slow relaxation process. The higher-energy shift of the peak

position causes an increase of the force constant of Ge–S bond. Thus it can be deduced that the Ge–S bond length keeps constant during the fast relaxation process and then becomes shorter at the beginning stage of the slow relaxation process and again keeps constant during the slow relaxation process. On the other hand, the FWHM values, which are assigned a variation of the Ge–S–Ge bond angle [13], decrease with the annealing-time. However, the rate of change is different between the fast relaxation process and the slow relaxation process, implying that there are two types in the change of the Ge–S–Ge bond angle.
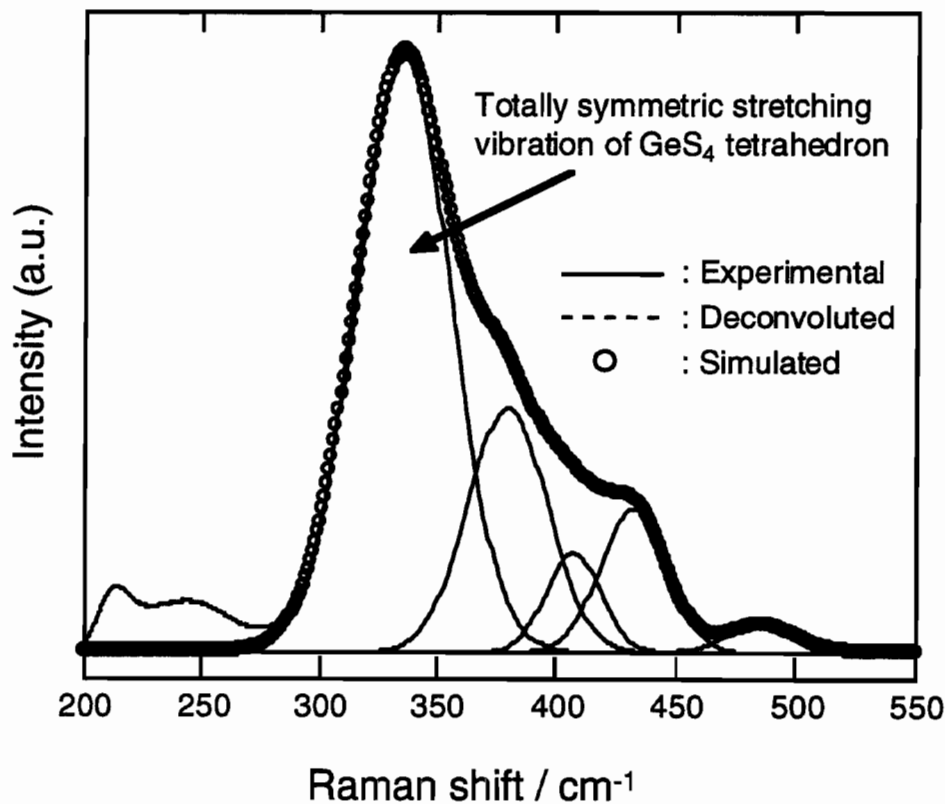

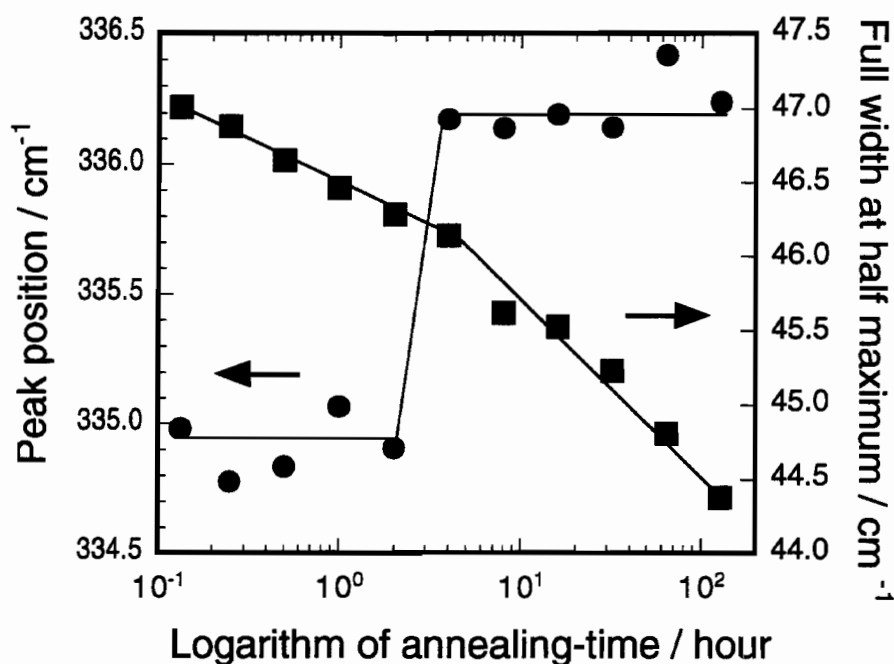Figure 8.4.   Raman scattering spectrum of undensified GeS$_2$ glass.

Figure 8.5. Annealing-time dependences of peak position and FWHM of totally symmetric stretching vibration of GeS$_4$ tetrahedra in thermal relaxation at 100°C.

Figure 8.6 shows the relationship between the annealing-time and the Ge–S bond length obtained by Ge–K EXAFS analyses. The analyses were performed using the XANADU program [14]. Detailed procedures of the data analyses have been described in Chapter 7. As can be seen from the figure, the Ge–S bond length definitely becomes shorter at the beginning stage of the slow relaxation process though its change is very small.

Based on these results, the structural relaxation in thermal annealing is summarized as follows: The Ge–S bond length becomes shorter at the beginning stage

of the slow relaxation process. The recovery of the Ge–S–Ge bond angle occurs during the fast and slow relaxation processes. Taking each activation energy value into account, however, the following is assumed: The recovery of the bond angle, which occurs during the fast relaxation process, accompanies no change of glass network structure, while the recovery of the bond angle, which occurs during the slow relaxation process, accompanies the changes of glass network structure.
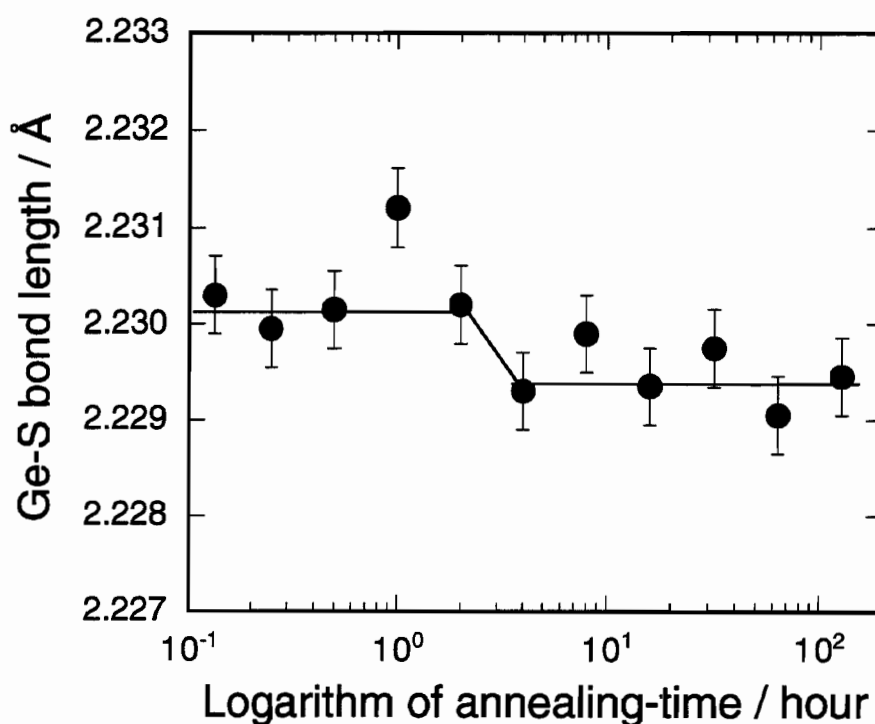

Figure 8.6.   Relationship between annealing-time and Ge–S bond length.

8.3.4. Absorption-Edge Energies in Visible Region

Changes of the absorption-edge energy in the visible region are discussed. According to the previous study, the visible absorption-edge energy largely shifts from 2.64 to 1.85 eV in densification under 6 GPa at 270°C. Figure 8.7 shows the changes of the absorption-edge spectra through thermal annealing. The absorption-edge energies in the visible region were obtained according to a manner illustrated in the figure. The obtained values are plotted against the annealing time, together with the FWHM of v_1 in the Raman spectra analysis in Figure 8.8. As can be seen from the figure, the absorption-edge energies shift toward higher energies in correlation with an increase in the annealing time. However, the rate of change is different between the fast relaxation process and the slow relaxation process. Furthermore this change is similar to that of the FWHM of v_1. Therefore, the changes of the absorption-edge energy and that of the Ge–S–Ge bond angle may be correlated to each other.
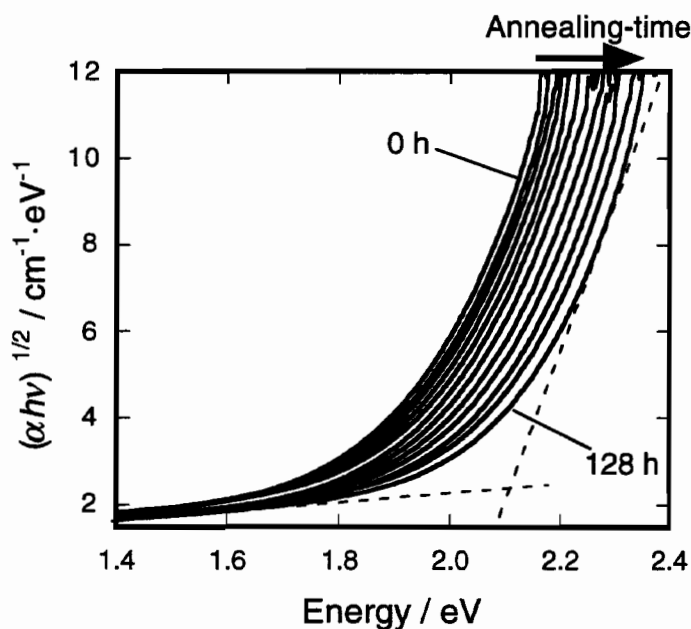

Figure 8.7. Visible absorption-edge spectra of permanently densified GeS₂ glasses thermally annealed for various hours.
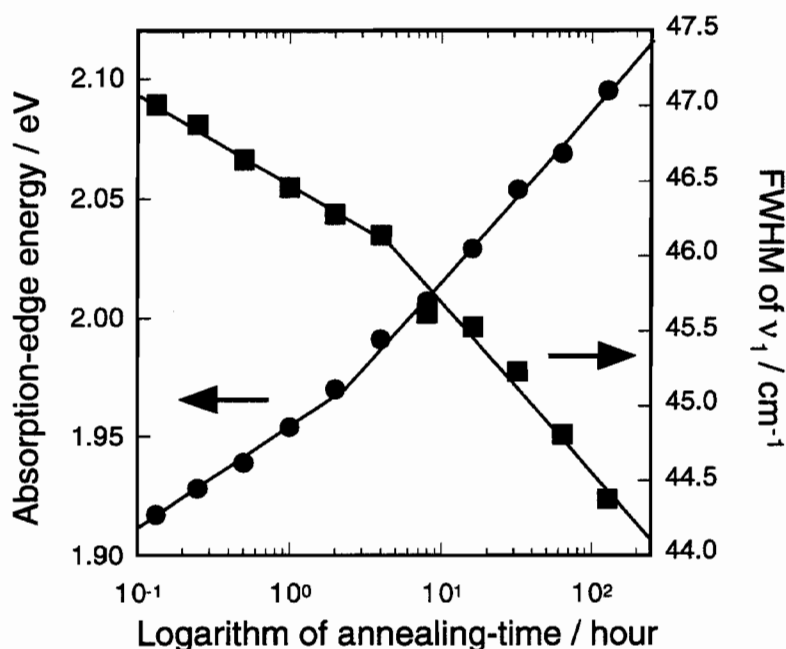
Figure 8.8. Annealing-time dependences of visible absorption-edge energy and FWHM of totally symmetric stretching vibration peak, v_1.

8.4. Conclusion

The permanently densified GeS_2 glass was prepared under 6 GPa at 270°C using a 6–8 multi-anvil-type high-pressure apparatus. The relaxation behavior of the permanently densified GeS_2 glass through thermal annealing was investigated in order to elucidate the mechanism of permanent densification phenomenon of GeS_2 glass. It was found that the fast relaxation process which has an activation energy of 51 kJ·mol^{-1} and the slow relaxation process which has an activation energy of 165 kJ·mol^{-1} were found to occur during thermal relaxation.

The Raman scattering spectra and the Ge–K EXAFS oscillation were

measured on glasses annealed at 100°C for various hours in order to investigate the structural relaxation during both the fast relaxation and slow the relaxation processes. The followings were clarified: The Ge–S bond length becomes shorter at the beginning stage of the slow relaxation process. The recovery of the Ge–S–Ge bond angle occurs during both the fast relaxation and slow relaxation processes. However, the change, which occurs during the fast relaxation process, accompanies no change of glass network structure, while the recovery, which occurs during the slow relaxation process, accompanies changes of glass network structure.

The absorption-edge energy in the visible region shifted toward higher energy in correlation with an increase in the annealing time. It can be assumed that the change of the absorption-edge energy is related to the change of the Ge–S–Ge bond angle by a comparison between the change of the absorption-edge energy and that of the FWHM of v_1.

References

[1] P. W. Bridgman and I. Simon, *J. Appl. Phys.*, **24**, 405 (1953).

[2] D. R. Uhlmann, *J. Non-Cryst. Solids*, **13**, 89 (1973).

[3] J. Arndt and D. Stöffler, *Phys. Chem. Glasses*, **10**, 117 (1969).

[4] J. Arndt, *Phys. Chem. Glasses*, **24**, 104 (1983).

[5] F. A. Seifert, B. O. Mysen and D. Virgo, *Phys. Chem. Glasses*, **24**, 141 (1983).

[6] B. A. Weinstein, R. Zallen, M. L. Slade and J. C. Mikkelsen Jr., *Phys. Rev. B*, **25**, 781 (1982).

[7] J. D. Mackenzie, *J. Am. Ceram. Soc.*, **46**, 470 (1963).

[8] R. M. Kimmel and D. R. Uhlmann, *Phys. Chem. Glasses*, **10**, 12 (1983).

[9] J. Arndt, R. A. B. Devine and A. G. Revesz, *J. Non-Cryst. Solids*, **131-133** 1206 (1991).

[10] N. Kawai, M. Togaya and A. Onodera, *Proc. Jpn. Acad.*, **49**, 129 (1973).

[11] R. L. Myuller, in *"Solid State Chemistry"*, (Consultant's Bureau, New York, 1965), p. 11.

[12] G. Lucovsky, J. P. deNeufville and F. L. Galeener, *Phys. Rev. B*, **9**, 1591 (1974).

[13] J. Sukmanowski, I. Petscherizin, M. Soltwisch and D. Quitmann, *J. Phys.: Conden. Matter*, **2**, 2303 (1990).

[14] H. Sakane, T. Miyanaga, I. Watanabe, N. Matsubayashi, S. Ikeda and Y. Yokoyama, *Jpn. J. Appl. Phys. Part 1*, **32**, 4641 (1993).

Summary

This thesis is composed of two parts. In Part I (Chapters from 1 to 4) is concerned with the peculiar high-pressure behavior in the permanent densification of glass, which was found for the first time in the present work. In the Part, I investigated structural-changes in the densification by high-pressure treatments for several glasses with peculiar permanent densification phenomenon and proposed a mechanism of the phenomenon. In Part II (Chapters from 5 to 8) is concerned with the permanent densification behavior of GeS_2 glass. In the Part, I investigated the properties of densified GeS_2 glasses at first and then examined the structure of permanently densified glasses and the structure under high pressure. Also I examined the relaxation behavior of densified glass due to thermal treatment. I summarized the contents of the respective chapters.

In Chapter 1, I reported the finding of a peculiar permanent densification phenomenon observed in a $60ZrF_4 \cdot 30BaF_2 \cdot 10EuF_3$ fluorozirconate glass. That is, I observed that, in the pressure dependence of density, the densities of permanently densified glasses exhibited a maximum value at the 3.0 GPa and then a marked decreased with further increasing applied-pressure was observed. I investigated the local structures around Zr^{4+} and Eu^{3+} in the densified glasses by means of Raman scattering spectroscopy and Eu^{3+} fluorescence spectroscopy. Based on the results, I proposed the spontaneous structural-relaxation of the F^- coordination environments around Zr^{4+}, Eu^{3+}, and Ba^{2+}, which takes place instantaneously when the applied pressure is released, as a cause of the peculiar permanent densification phenomenon observed in the present fluorozirconate glass.

In Chapter 2, I examined the structural-change with densification in more

detail in a $55ZrF_4 \cdot 17BaF_2 \cdot 23NaF \cdot 10EuF_3$ fluorozirconate glass, which showed a more remarkable peculiar permanent densification phenomenon than a $60ZrF_4 \cdot 30BaF_2 \cdot 10EuF_3$ glass. I investigated the local structural-changes around Zr^{4+}, Eu^{3+}, and Ba^{2+} in undensified and permanently densified glasses by means of Raman scattering spectroscopy, Eu^{3+} fluorescence spectroscopy, and Zr–K, Eu–L_{III}, and Ba–L_{III} EXAFS spectroscopies. I revealed from the EXAFS analyses that the local structure around Ba^{2+} (a network-modifying cation in the glass) remarkably changes with applied pressure, giving a pressure dependence similar to that of density. Also I revealed that the local structures around Zr^{4+} and Eu^{3+} (a network-forming cation in the glass) hardly changed. Therefore, I concluded that the structural change around Ba^{2+}, which is explained by a spontaneous structural-relaxation in the F^- coordination environments around Ba^{2+} under releasing applied pressure, is an origin of a peculiar high-pressure behavior observed in the $55ZrF_4 \cdot 17BaF_2 \cdot 23NaF \cdot 10EuF_3$ fluorozirconate glass.

In Chapter 3, I described the permanent densification experiments on SiO_2–K_2O–CaO–SrO silicate glasses. I found a peculiar behavior in the glasses of lower contents than 50 mol% SiO_2 in permanent densification of $xSiO_2 \cdot 0.4(100 - x)K_2O \cdot 0.4(100 - x)CaO \cdot 0.2(100 - x)SrO$ glasses ($x = 41.2 - 66.7$) in mol% by the high-pressure treatments under 3 and 6 GPa, I investigated the skeleton structures composed of SiO_4 units in the undensified and densified glasses by means of ^{29}Si MAS NMR spectroscopy, that is, examined the Q_n fractions of SiO_4 structural-units, where n ($n = 0 - 4$) means the number of bridging oxygen, from the peak deconvolution of the spectra. At first, I clarified the skeleton structures in the undensified glasses. Then I discussed the skeleton structures of the densified glasses are discussed in comparison with that of the undensified one. I revealed that, irrespective of x value, the fractions of Q_n of small n-values increased with increasing applied-pressure, indicating that some of the Si–O–Si bonds are broken with high-pressure treatments and the changed skeleton-

structures were kept even after releasing applied-pressure. Therefore, I concluded that other causes such as the local structural-changes around network-modifying cations (K^+, Ca^{2+}, and Sr^{2+}) should be considered as an origin of the peculiar behavior observed in the glasses of lower contents than 50 mol% SiO_2.

In Chapter 4, I studied the permanent densification behaviors of ionic ZrF_4-based fluoride glasses, mixed ionic and covalent SiO_2-based oxide glasses, and a covalent GeS_2 sulfide glass from a standpoint of the chemical-bond properties and structure of glasses. This study is summarized as follows: The permanent densification of the respective glasses were performed at temperatures of about three-quarters of their respective glass-transition temperatures under pressures up to 9 GPa in order to compare each other. The densities of GeS_2 glass and silicate glasses of higher contents than 50 mol% SiO_2, which have covalent-bonds and smaller packing densities, increase with increasing applied-pressure. On the other hand, in ZrF_4-based glasses and silicate glasses of lower contents than 50 mol% SiO_2, which have a larger ionicity and larger packing densities, the density increase until around 3 GPa, the density becomes maximum at this pressure, and then the density values decrease with further increasing applied-pressure.

In Chapter 5, I clarified the structure of densified GeS_2 glasses by means of Raman scattering spectroscopy, XAFS spectroscopy, and X-ray radial distribution in order to elucidate the mechanism of densification. I analyzed the experimental results based on the structures of α-GeS_2 (high-temperature modification), β-GeS_2 (low-temperature modification), and II-GeS_2 (high-pressure modification) crystals. I found that, with proceeding of densification the structure of GeS_2 glass, which has a mixed structure of the α-GeS_2 and β-GeS_2 at atmospheric pressure, the undensified glass structure progressively converts to a II-GeS_2-like dense structure. I also measured the optical absorption spectra in the visible region and found that the large red shift of

optical absorption-edge in the visible region is observed with densification.

In Chapter 6, I investigated the structures of GeS_2 glasses undensified and densified under 6 GPa in more detail with high-energy X-ray diffraction measurements using third generation synchrotron radiation as a light source. I found the followings: The intensity of the first sharp diffraction peak, which corresponds to the Ge–Ge correlation at around 6 – 7 Å in real space, largely decreases with densification. This is because of the reorganization of the ring structures composed of GeS_4 tetrahedra, which was proposed mechanism in the Chapter 5. I clarified the structural-changes with densification by the analyses of the X-ray total pair-correlation function, $g(r)$, and the effective radial distribution function, $N(r)$, for each glass. Then I proposed the densification mechanism on GeS_2 glass by high-pressure treatment based on the results and the structures of three modifications of GeS_2 crystal.

In Chapter 7, I described the local structural-changes around Ge in GeS_2 glass during compression and decompression processes, i.e. densification process, which was clarified by means of an in-situ EXAFS analyses. The contents is as follows: "The Ge–S bond length becomes monotonously short with increasing applied-pressure up to 8 GPa at room temperature. When the specimen is heated to 270°C under 8 GPa, however, the bond length becomes slightly long. The elongated bond length is almost kept even after the specimen is cooled to room temperature. In decompression process, the bond length becomes gradually long with releasing applied-pressure down to 2 GPa, following a change in compression process. Below 2 GPa, however, the Ge–S bond length is largely elongated, being longer than the initial one. No significant change of coordination number is found in the compression and decompression processes up to 8 GPa." I explained this change as a combined effect of elastic and inelastic structural-changes and obtained an important information for elucidation of permanent densification mechanism.

In Chapter 8, I examined the thermal relaxation behavior of densified GeS$_2$ glass in order to obtain the information about mechanism of densification. I performed thermal relaxation analyses using a stretched exponential relaxation function and revealed that the fast and slow relaxation processes, of which the activation energies were 51 kJ·mol^{-1} and 165 kJ·mol^{-1}, respectively, are present in thermal relaxation of denified GeS$_2$ glass. The. I revealed the structural relaxation during the fast and slow relaxation processes by the analyses of the Raman scattering spectra and Ge–K EXAFS oscillation. Also I discussed the relationship between the absorption-edge in the visible region and the structural-change was also discussed.

Acknowledgments

First of all, I would like to express special thanks to Professor Yoji Kawamoto of Kobe University, who supervised the present work, for his helpful guidance and continuous encouragement.

I wish to express my sincere acknowledgment to Dr. Naoyuki Kitamura of National Institute of Advanced Material Science and Technology for the collaboration and valuable advice.

Sincere acknowledgments are expressed to Professor Takashi Uchino of Kobe University for his helpful suggestions to carry out the present work.

I express grateful appreciation to Dr. Masanori Shojiya of Nippon Sheet Glass Co. for his helpful discussions all through the duration of the present work.

I would like to thank Dr. Kohei Kadono and Dr. Kohei Fukumi of National Institute of Advanced Material Science and Technology for their support of the EXAFS measurements and analyses.

I wish to express their appreciation to Professor Osamu Ohtaka of Osaka University and Dr. Yoshinori Katayama of Japan Atomic Energy Research Institute for their valuable comments and cooperation in the *in-situ* EXAFS measurements.

Thanks are due to Dr. Shinji Kohara of Japan Synchrotron Radiation Research Institute for the experiments of the high-energy X-ray diffraction using synchrotron radiation.

Helpful suggestions with Dr. Jianbei Qiu of Japan Advanced Institute of Science and Technology are greatly acknowledged. Many thanks are made to all the students of Kawamoto's Laboratory of Kobe University for their help.

<div align="right">

Koichi MIYAUCHI

Kobe, winter 2003

</div>

List of Publications

Part I

Chapter 1

K. Miyauchi, J. Qiu, M. Shojiya, Y. Kawamoto and N. Kitamura, "Peculiar High-Pressure Behavior in Permanent Densification of Fluorozirconate Glass", *Mater. Res. Bull.*, **34**, 1383 (1999).

Chapter 2

K. Miyauchi, M. Shojiya, Y. Kawamoto and N. Kitamura, "Structural Study on Peculiar High-Pressure Behavior of Fluorozirconate Glass in Permanent Densification", *J. Phys. Chem. Solids*, **62**, 2039 (2001).

Chapter 3

S. Sakida, K. Miyauchi, Y. Kawamoto and N. Kitamura, "Permanent Densification Behavior and ^{29}Si MAS NMR of SiO_2–K_2O–CaO–SrO Glasses", *J. Non-Cryst. Solids*, **271**, 64 (2000).

Chapter 4

Y. Kawamoto, K. Miyauchi, M. Shojiya, S. Sakida and N. Kitamura, "High-Pressure Densification of Fluoride, GeS_2 and Silicate Glasses", *J. Non-Cryst. Solids*, **284**, 128 (2001).

Part II

Chapter 5

K. Miyauchi, J. Qiu, M. Shojiya, Y. Kawamoto and N. Kitamura, "Structural Study of GeS_2 Glasses Permanently Densified under High Pressures up to 9 GPa", *J. Non-Cryst. Solids*, **279**, 186 (2001).

Chapter 6

K. Miyauchi, T. Uchino, Y. Kawamoto, N. Kitamura and S. Kohara, "High-Energy X-ray Diffraction Study of Permanently Densified GeS_2 Glass", To be submitted to *J. Non-Cryst. Solids*.

Chapter 7

K. Miyauchi, J. Qiu, M. Shojiya, Y. Kawamoto, N. Kitamura, K. Fukumi, Y. Katayama and Y. Nishihata, "In situ EXAFS Study on GeS_2 Glass under High-Pressure", *Solid State Commun.*, **124**, 189 (2002).

Chapter 8

K. Miyauchi, M. Shojiya, Y. Kawamoto and N. Kitamura, "High Pressure Densification and Thermal Relaxation Behaviour of GeS_2 Glass", *Phys. Chem. Glasses.*, **43C**, 181 (2002).

Other publications not contained in this thesis

1. J. Qiu. K. Miyauchi, Y. Kawamoto, N. Kitamura, J. Qiu and K. Hirao, "Long-Lasting Phosphorescence in Sn^{2+}–Cu^{2+} Codoped Silicate Glass and its High-Pressure Treatment Effect", *Appl. Phys. Lett.*, **81**, 394 (2002).

2. Y. Kawamoto, T. Uchino, J. Qiu, K. Miyauchi, N. Tokura, A. Mukai, Y. Kitai, D. Shibata, H. Hashima, A. Konishi and Y. Tanigami, "Upconversion Glass-Ceramics and its Application", Submitted to *SPIE*.